VOL. 3 No. 2
APRIL 1961

UNIVERSITY OF HAWAII
LIBRARY
JUN 30 '61

URNAL OF THE

LESS-COMMON METALS

AN INTERNATIONAL JOURNAL ON
THEIR CHEMISTRY AND METALLURGY

ORS:
CUTHBERTSON (Nottingham)
AIRBROTHER (Manchester)

ORIAL ADVISORY BOARD:
NARD (Paris)
RICE COOK (Birmingham)
ECROLY (Brussels)
DJINGHEUZIAN (Ottawa)
FLETCHER (Harwell)
GONSER (Columbus, Ohio)
ANSEN (Frankfurt a.M.)
NDELLI (Genoa)
LEMM (Münster)
KROLL (Corvallis, Ore.)
URRAY (Harwell)
OWOTNY (Vienna)
PIDGEON (Toronto)
POWELL (Wembley)
RALSTON (Hyattsville, Md.)
VAN ARKEL (Leyden)
WORNER (Melbourne)
YNTEMA (Menlo Park, Calif.)

ELSEVIER

GENERAL INFORMATION

Types of contributions

(a) Original research work not previously published in other periodicals.
(b) Reviews on recent developments in various fields.
(c) Short communications.
(d) Bibliographical notes and book reviews.

Languages

Papers will be published in English, French or German.

Submission of papers

Papers should be sent to one of the following Editors:

Professor J. W. CUTHBERTSON (*Metallurgy*), Department of Metallurgy, The University, University Park, Nottingham, England.
Professor F. FAIRBROTHER (*Chemistry*), The University of Manchester, Department of Chemistry, Manchester 13, England.

Authors should preferably submit two copies in double-spaced typing on pages of uniform size. Legends for figures should be typed on a separate page. The figures should be in a form suitable for reproduction, drawn in Indian ink on drawing paper or tracing paper, with lettering etc. in thin pencil. The sheets of drawing or tracing paper should preferably be of the same dimensions as those on which the article is typed. Photographs should be submitted as clear black and white prints on glossy paper.
All references should be given at the end of the paper. They should be numbered and the numbers should appear in the text at the appropriate places.
A summary of 50 to 200 words should be included. Authors of papers in French or German are encouraged to supply also a translation of the summary in English.

Reprints

Twenty-five reprints will be supplied free of charge. Additional reprints can be ordered at quoted prices. They must be ordered on order forms which are sent together with the proofs.

Publication

The *Journal of the Less-Common Metals* will have six issues to the volume, approx. 500 pages per volume.
Subscription price: £ 5.7.6 or Dfl. 57.— per volume (post free).
For advertising rates apply to the publishers.

Subscriptions

Subscriptions should be sent to:

ELSEVIER PUBLISHING COMPANY, Spuistraat 110-112, Amsterdam-C., The Netherlands.

OXIDATION OF TITANIUM IN THE TEMPERATURE RANGE 800–1200°C

P. KOFSTAD, P. B. ANDERSON AND O. J. KRUDTAA

Central Institute for Industrial Research, Blindern, Oslo (Norway)

(Received October 27th, 1960)

SUMMARY

Oxidation of titanium in the temperature range 800–1200°C has been studied. In agreement with WALLWORK AND JENKINS[7] the initial approximate parabolic oxidation rate has been shown to be primarily associated with oxygen dissolution in the metal. When the oxygen concentration in the outer layer of the metal reaches a composition $TiO_{0.35}$, heavy oxide formation begins to take place and the oxidation eventually follows a linear oxidation rate. It is suggested that the corresponding oxidation is governed by oxide nucleation and growth of oxide nuclei. Above 950°C recrystallization and sintering of the outer layers of the TiO_2-scale take place.

INTRODUCTION

Oxidation of titanium involves both oxide-scale formation and oxygen dissolution in the metal[1–7]. Above 700°C oxidation rate measurements have shown that the oxidation initially follows an approximate parabolic rate which is followed by an approximate linear oxidation rate[5,7]. This change in kinetics has usually been interpreted in terms of rate-determining diffusion of ions through the TiO_2-scale and a cracking of the oxide scale when it reaches a certain critical thickness. Recently WALLWORK AND JENKINS[7] have proposed that the initial parabolic rate is associated with the establishment of an oxygen diffusion gradient in the metal, while the linear rate is associated with the penetration of a steady oxygen gradient into the metal.

Assuming an oxidation governed by diffusion of ions through the TiO_2-scale most authors favour predominant oxygen ion diffusion. KINNA AND KNORR[8] and HURLEN *et al.*[6,9] propose titanium ion diffusion on the basis of marker studies and structural considerations of TiO_2, respectively.

In the present work oxidation of titanium has been studied in the temperature range 800–1200°C. The studies include oxidation rate measurements, marker studies, X-ray diffraction and metallographic studies on oxidized specimens.

EXPERIMENTAL METHODS

Electron-beam-melted titanium with a hardness of V.H.N. 90 (10 kg) was used. Spectrographic analysis gave the following estimate of impurities: Fe, Mn, Al, Sn, Mg and Cr, each 0.01%; Cu, 0.001%. The specimens (1 × 1.5 × 0.2 cm) were polished with alumina, rinsed in distilled water and acetone. Specimens for marker studies were slightly bent and platinum wire of 30 μ was placed across the convex side of

the specimen. A weight of 1 g was attached to the ends of the wire to press the wire against the metal surface.

Rates of oxidation were measured gravimetrically employing both a micro-torsion balance and a quartz helix type apparatus. The weight gains could be estimated to ± 0.005 mg/cm^2. The measuring units were enclosed in vacuum systems which were evacuated overnight to a pressure of $\leq 10^{-5}$ mm Hg before the start of each run. Commercial tank oxygen which was dried over phosphorus pentoxide was used in the studies.

EXPERIMENTAL RESULTS

Oxidation rate measurements

The results of the oxidation rate measurements in 1 atm oxygen in the temperature range 800–1200°C are shown in Figs. 1–3. The curves represent averages of 3 or 4

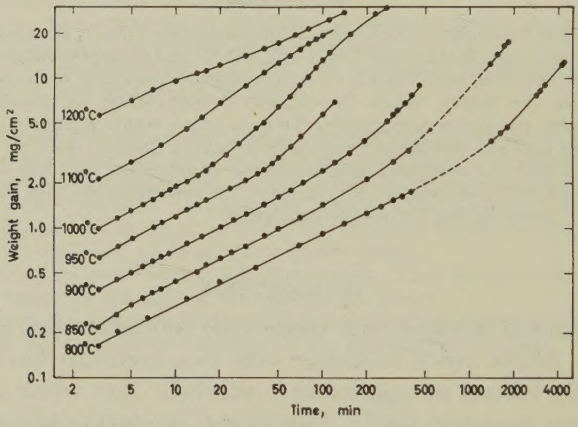

Fig. 1. Double logarithmic plot of oxidation of titanium in the temperature range 800–1200°C at 1 atm oxygen.

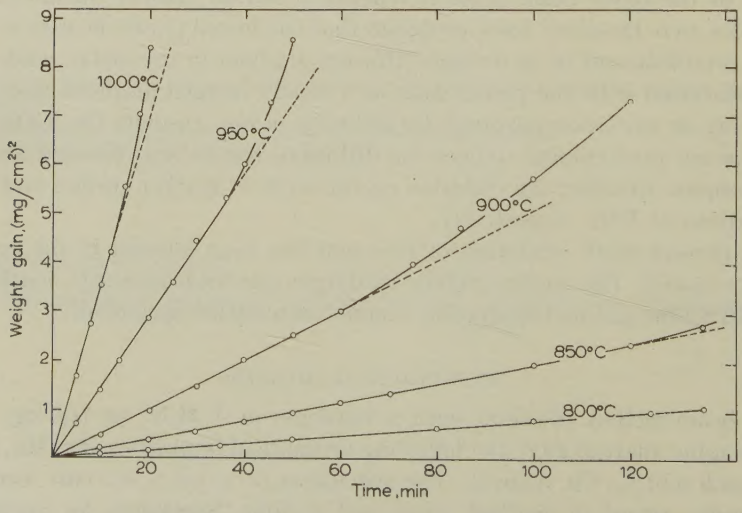

Fig. 2. Parabolic plot of oxidation of titanium at 800–1000°C. The stippled lines are extensions of the straight-line parts of the curves.

runs, which were reproducible to within 10%. As seen in Figs. 1 and 2 the oxidation initially follows an approximately parabolic rate below 1000°C. Furthermore, the duration of the parabolic period decreases with increasing temperature. After the parabolic period, one observes an increase in the rate of oxidation, and as seen in Fig. 3 the oxidation eventually follows an approximately linear oxidation rate.

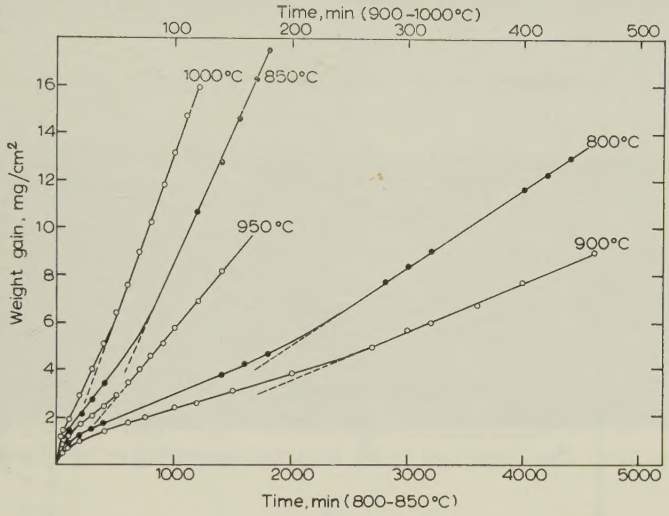

Fig. 3. Linear plot of oxidation of titanium at 800–1000°C. The stippled lines are extensions of the straight-line parts of the curves.

Appearance of oxidized specimens

The specimens had a grey, metallic-like appearance and the oxide films were very thin and extremely adherent to the metal during the parabolic period. The linear period was associated with formation of heavy oxide scales which had poor adherence to the metal. The colour of the oxide changed to white and yellow during the linear period. By means of X-ray diffraction the oxide scales were in all cases found to consist of rutile.

X-ray diffraction and micro-indentation hardness studies

To study the relative importance of oxygen dissolution and oxide-scale formation specimens were oxidized for various lengths of time and subjected to X-ray diffraction and micro-indentation hardness measurements. Oxide-scales were removed from specimens oxidized at 900°C and the change in lattice parameter of the metal next to the metal/oxide interface was determined by X-ray diffraction (Cu radiation). The change in lattice parameter of the (012) reflection and the variation in half-widths of the (012) and (103) reflections are shown in Fig. 4. As may be seen, the half-widths reach an approximately constant value after about 60–70 min of oxidation. The lattice parameter tends towards a limiting value which corresponds to a composition $TiO_{0.35}$[10]. The results of the micro-indentation hardness studies on the same specimens are shown in Fig. 5.

Metallographic and marker studies

After extended oxidation at 800 and 900°C the oxide-scales had a lamellar structure. In the corresponding marker studies the Pt-markers were always found on the surface of the oxide-scale. These features are shown in Fig. 6, which refers to a specimen oxidized for 12 h at 900°C. Above 900°C one observed in addition a recrystallization or sintering of the outer layers of the TiO_2-scales. The time of the first appearance

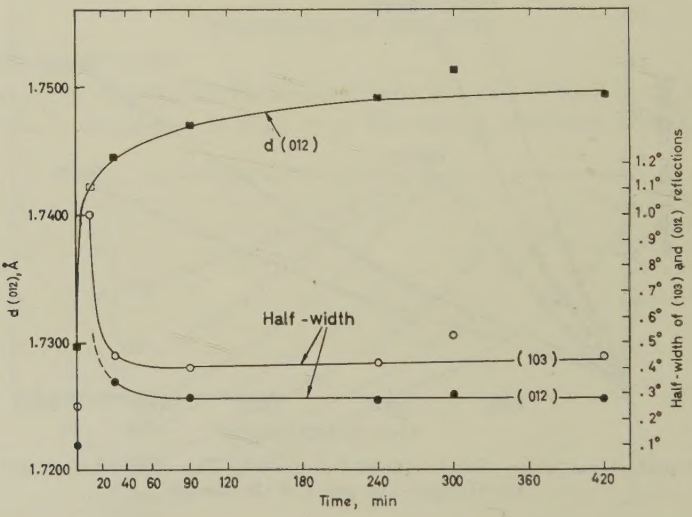

Fig. 4. The change in lattice parameter of the (012) reflection and the variation in half-widths of the (012) and (103) reflections as a function of time of oxidation at 900°C and 1 atm oxygen. Measurements taken on Ti-surface after removal of oxide.

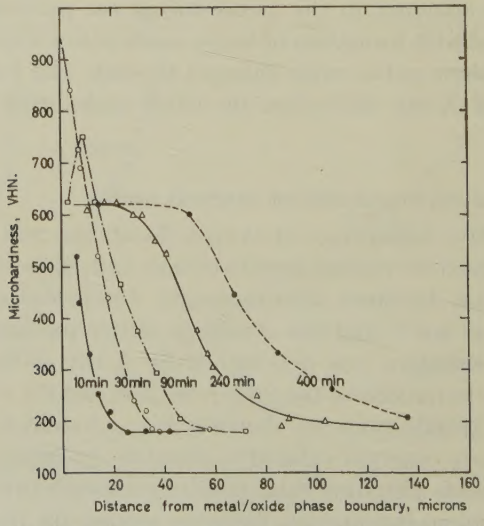

Fig. 5. Micro-indentation hardness measurements on specimens oxidized for various lengths of time at 900°C and 1 atm oxygen. 16.8 g load.

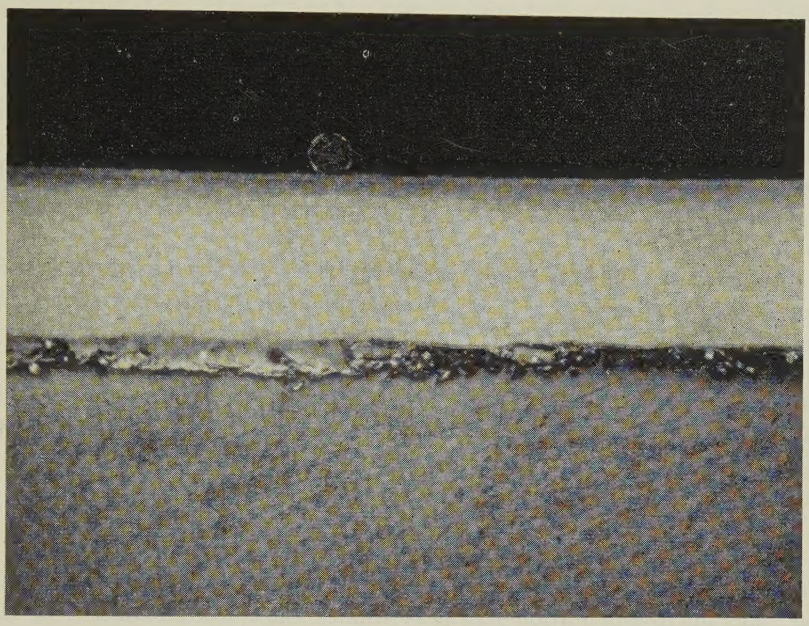

Fig. 6. Pt-marker study on Ti-specimen oxidized for 17 h at 900°C and 1 atm oxygen. (100×)

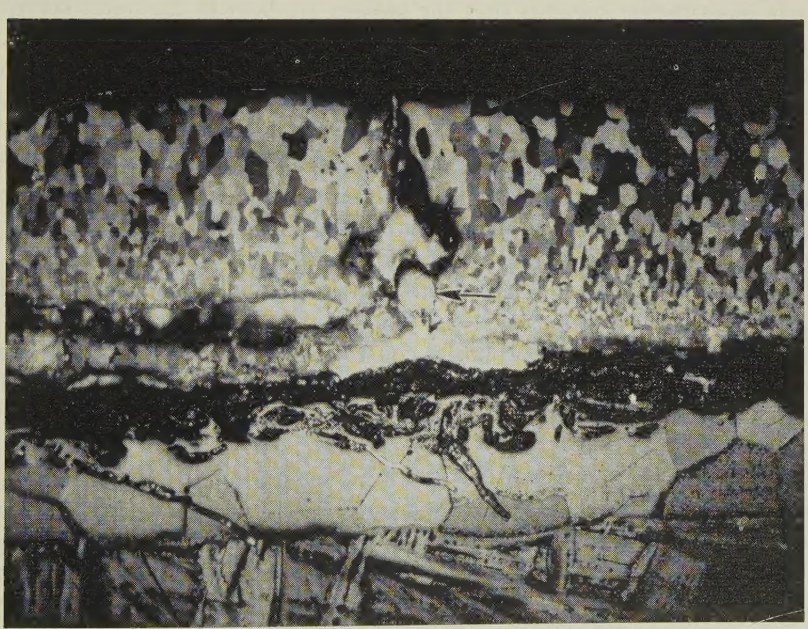

Fig. 7. Pt-marker study on Ti-specimen oxidized for 1 h at 1175°C and 1 atm oxygen. The picture clearly shows the border between the transformed β-titanium and the oxygen-stabilized α-titanium which is next to the oxide scale. (100×)

of this recrystallized layer decreased rapidly with increasing temperature. At 950°C the first recrystallization of the outer layer of the scale appeared after 10–15 h, while at 1200°C the process was so fast that the main part of the scale was recrystallized even after 5 min of oxidation. This process resulted in a two-layered TiO_2-scale: an outer recrystallized layer and an inner apparently porous layer. In the marker studies the Pt-markers were invariably found at or close to the border between the two TiO_2-layers. The position of the marker in a specimen oxidized for 1 h at 1175°C is shown in Fig. 7.

Concurrently with the appearance of the outer recrystallized layer one observed a decrease in the oxidation rate. This feature is evident in the curve for 1000°C in Fig. 1 after about 100 min of oxidation. The colour of the oxide scale became gray after recrystallization took place.

Titanium changes from the α- to β-modification at 883°C. Oxygen has, however, an α-stabilizing effect, and there will thus be an outer layer of α-titanium present during oxidation of titanium above the transition temperature. This feature is clearly shown in Fig. 7.

DISCUSSION

In agreement with previous investigations the present X-ray diffraction, metallographic, and micro-indentation hardness studies show that oxidation of titanium involves both oxide scale formation and oxygen dissolution in the metal. The X-ray diffraction studies (Fig. 4) show that the concentration of oxygen in the outer layers of the metal tends towards a limiting value which corresponds to a composition $TiO_{0.35}$. The fact that the half-widths reach an approximately constant value after 60–70 min of oxidation suggests that the oxygen gradient in the outer layers of the metal remains approximately constant after this time period. As seen in Figs. 1 and 2 the deviation from parabolic behaviour also occurs after 60–70 min, and it thus appears that this change in kinetics is associated with an enrichment of oxygen in the outer layer of titanium up to a concentration of $TiO_{0.35}$.

Assuming to a first approximation that the hardness increases linearly with oxygen content, the data in Figs. 1, 4 and 5 may be used to estimate the relative importance of oxygen dissolution and oxide film formation. The results indicate that after 30 min of oxidation at 900°C more than 80% of the reacted oxygen has dissolved in the metal. This estimate is also in agreement with metallographic studies of oxide films formed under these conditions. On this basis we conclude that during the initial periods, oxidation of titanium primarily constitutes oxygen dissolution in the metal and that the parabolic oxidation behaviour is a result of the rate-determining diffusion of oxygen in titanium. The results are thus in accord with the interpretations of WALLWORK AND JENKINS[7].

In terms of this interpretation the activation energy for the initial parabolic rate may be considered an average activation energy for diffusion of oxygen in titanium–oxygen solid solutions. As seen in Fig. 8 the corresponding activation energy is 51 kcal/mole. Assuming a linear increase in hardness with oxygen content the data in Fig. 5 may be used to evaluate an average diffusion coefficient for diffusion of oxygen in α-titanium–oxygen solid solutions. Neglecting the oxide film formation this yields an approximate value of $D = 0.5 \exp(-51000/RT)$.

If the first deviation from the parabolic rate corresponds to an oxygen enrichment

in the outer layer of the Ti-metal up to a composition $TiO_{0.35}$, the time lag of this effect as a function of temperature should yield an activation energy close to 50 kcal/mole. It is of course difficult to estimate this time lag with any great degree of accuracy. However, as seen in Fig. 9, where the logarithm of the time lag (Fig. 2) is plotted *versus* the reciprocal of the absolute temperature, the results suggest an activation energy close to the expected value.

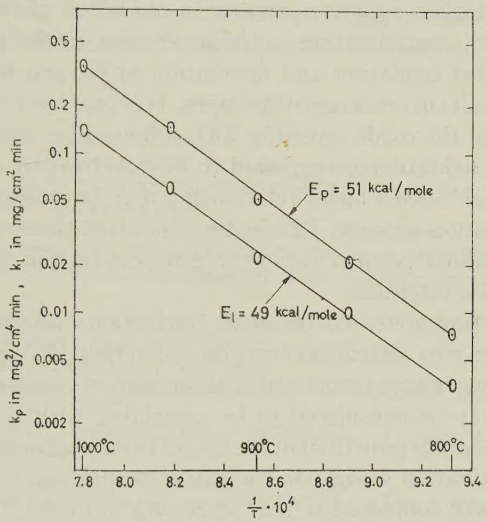

Fig. 8. Logarithm of the parabolic and linear rate constants as a function of reciprocal absolute temperature. Oxidation of titanium in the temperature range 800–1000°C at 1 atm oxygen.

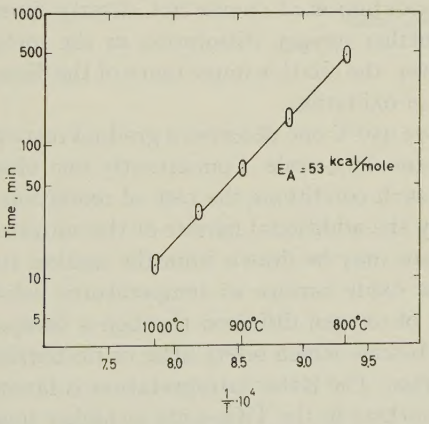

Fig. 9. Logarithm of time of deviation from parabolic behaviour as a function of reciprocal absolute temperature.

On the basis of geometrical considerations one might expect that oxygen diffuses faster in the β-modification (b.c.c. structure) than in the low-temperature α-modification (h.c.p. structure). However, as mentioned above, oxygen has an α-stabilizing

effect and an outer layer of α-titanium will thus always be present during oxidation of titanium. It is believed that the phase change is of minor importance with regard to the oxidation mechanism at temperatures below 1000°C, except during the very initial stages of the oxidation.

Studies of the lattice parameters of titanium as a function of oxygen content by MAGNÉLI *et al.*[10], show that important structural changes occur at $TiO_{0.35}$. At this composition the length of the a-axis goes through a maximum, while the c-axis increases rapidly at higher oxygen contents. In oxidation of titanium it is believed that when the oxygen concentration in the layer next to the metal/oxide interface reaches $TiO_{0.35}$, further oxidation and dissolution of oxygen leads to large stresses and strains which results in cracking of the layer. It is proposed that further oxidation involves nucleation of the oxide (possibly TiO) followed by rapid oxidation to TiO_2.

The linear rate of oxidation is suggested to be governed by oxide nucleation and growth of oxide nuclei. Such a linear relationship may be considered to be a result of a steady-state nucleation process. This in turn involves the assumption of an outer porous oxide-scale which permits rapid oxygen penetration down to the reaction site at the metal/oxide interface.

An oxidation reaction governed by oxide nucleation and growth of oxide nuclei qualitatively involves two activation energies: an activation energy of oxide nucleation and an activation energy associated with growth of oxide nuclei[11,12]. The latter activation energy may be considered to be associated with the diffusion and rearrangement of atoms during growth of oxide nuclei from a saturated solution of oxygen in titanium. The activation energy of nucleation is difficult to evaluate at present, but it is probably small compared to that of growth of nuclei. If such is the case one might expect an activation energy of the linear rate of oxidation which is close to that of the parabolic. As seen in Fig. 8 the activation energy for the linear oxidation rate is 49 kcal/mole.

The linear rate of oxidation is of course not strictly limited to oxide formation. As seen from Fig. 5 further oxygen dissolution in the metal continues during the linear oxidation. However, the relative importance of the dissolution process decreases with increasing length of oxidation.

At temperatures above 950°C one observes a gradual recrystallization and sintering of the outer layers of the TiO_2-scale. Concurrently one observes a decrease in the oxidation rate. Under such conditions the rate of oxidation and the mechanism of oxidation is affected by the additional barrier of the sintered TiO_2 layer.

No definite conclusions may be drawn from the marker studies. The fact that the markers remain on the oxide surface at temperatures below 950°C may either be interpreted as a result of oxygen diffusion through a compact TiO_2-scale or it may be due to a porous TiO_2-scale which offers little or no barrier to oxygen penetration down to the metal surface. The latter interpretation is favoured in the present case. The burial of the Pt-markers in the TiO_2-scale at higher temperatures may be interpreted as a titanium ion diffusion in the scale if one assumes a compact oxide layer. However, in the present case the burial of the markers appears to be directly associated with recrystallization and plastic flow in the outer layers of the scale. The present results serve to emphasize that marker studies are not always directly applicable in deciding the type of ions which diffuse through oxide scales.

With regard to alloying of titanium for better oxidation resistance it appears that

the primary aim must be to reduce oxygen diffusion in the metal. The importance of oxygen dissolution in the metal explains why the semiconductor approach to alloy oxidation is of minor value in the case of titanium.

Oxidation of metals which may dissolve relatively large amounts of interstitial oxygen appears to have many features in common. Niobium and tantalum exhibit incubation periods primarily associated with oxygen dissolution in the metal followed by rapid oxidation associated with heavy oxide formation[13,14]. For niobium and tantalum this behaviour is found at the relatively low temperatures of 300 to 500°C due to the very rapid diffusion of oxygen in these metals.

REFERENCES

1 A. E. Jenkins, *J. Inst. Metals*, 82 (1954) 213.
2 M. Simnad, A. Spilners and O. Katz, *J. Metals*, 7 (1955) 645.
3 P. Kofstad and K. Hauffe, *Werkstoffe u. Korrosion*, 7 (1956) 642.
4 A. E. Jenkins, *J. Inst. Metals*, 84 (1956) 1.
5 P. Kofstad, K. Hauffe and H. Kjöllesdal, *Acta Chem. Scand.*, 12 (1958) 239.
6 T. Hurlen, H. Kjöllesdal, J. Markali and N. Norman, *Oxidation of Titanium*, A.R.D.C. Rept., Central Institute for Industrial Research, Oslo, Norway, April, 1958, to be published in *J. Inst. Metals*.
7 G. R. Wallwork and A. E. Jenkins, *J. Electrochem. Soc.*, 106 (1959) 10.
8 W. Kinna and W. Knorr, *Tech. Mitt. Krupp*, 14 (1956) 99.
9 T. Hurlen, *Acta Chem. Scand.*, 13 (1959) 365.
10 S. Andersson, B. Collén, V. Kuylenstierna and A. Magnéli, *Acta Chem. Scand.*, 11 (1957) 1641.
11 J. H. Hollomon and D. Turnbull, *Progr. Metal Phys.*, 4 (1953) 333; D. Turnbull, *Solid State Physics*, 3 (1956) 226.
12 P. Kofstad, On the role of oxide nucleation and growth of oxide nuclei in oxidation of niobium, *1st International Congress on Metallic Corrosion, London, April, 1960*, to be published.
13 T. Hurlen, H. Kjöllesdal, J. Markali and N. Norman, *Oxidation of Niobium*, A.R.D.C. Rept., Central Institute for Industrial Research, Oslo, Norway, April, 1959, to be published in *J. Inst. Metals*.
14 P. Kofstad, to be published.

THE PILOT PLANT PRODUCTION OF ELECTROLYTIC URANIUM DIOXIDE

J. R. CHALKLEY

Impregnated Diamond Products Ltd., Gloucester (Great Britain)

(Received November 14th, 1960)

SUMMARY

The pilot plant production of uranium dioxide crystals by a fused salt electrolytic process is described. The electrolyte, containing uranyl chloride dissolved in molten NaCl/KCl eutectic, is obtained by the direct chlorination of uranium oxide *in situ* in the fused salt, and electrolysis between graphite electrodes forms a crystalline deposit of UO_2 at the cathode. The deposition is carried out with either horizontally or vertically disposed electrodes, but the latter are preferred from the point of view of simplicity. An alternative process, using uranium ore concentrate as the starting material and involving three electrolytic stages is also described. The bulk of the impurities are removed in the first electrolysis in which anodic chlorination is used to improve the efficiency of the stage. The product, 99% pure, is then treated in the same way as the pure oxide starting material, but a third electrodeposition, in which the UO_2 plated cathode is used as a soluble anode, is necessary to achieve the purity level required for nuclear fuel applications. The impurities found in the product are discussed in the context of their origin and their behaviour in the process, particular reference being made to the rare earths. The process has been found capable of producing oxides within the range of composition UO_2 to $UO_{2.5}$, and the conditions affecting this variation are described.

INTRODUCTION

The ease with which uranium can be electrodeposited as uranium dioxide from fused chloride baths was clearly demonstrated during early attempts to extract uranium metal by electrolysis. To deposit the metal the uranium in the bath should be in the form of the trichloride. Under conditions in which oxygen has access to the melt, either as air or as oxygen-containing impurities, oxidation occurs to give oxychlorides of uranium, principally uranyl chloride, UO_2Cl_2. Electrolysis of this chloride, which is soluble in the electrolyte, yields the crystalline dioxide at the cathode and chlorine at the anode.

The process of electrodepositing uranium dioxide has been studied from the aspect of nuclear fuel applications. The potentiality of this process lies in the production of the oxide in coarse crystalline form which would, for example, have the advantage of retaining the fission gases during irradiation.

Basically, the process consists of a single electrodeposition from a melt prepared by the direct chlorination of a purified uranium oxide in a bath of fused sodium chloride–potassium chloride eutectic. An alternative approach was outlined by GIB-

SON AND WASSELL[1] in the application of a fused salt electrolytic process for the extraction and purification of uranium dioxide using uranium ore concentrate as the starting material. A procedure for this treatment has been developed on the pilot plant scale.

PREPARATION OF THE URANYL CHLORIDE ELECTROLYTE

Direct chlorination of the uranium oxides UO_2, U_3O_8 and UO_3 in a melt of NaCl–KCl eutectic at 800°C in each case yields the yellow UO_2Cl_2, the reaction normally being rapid and going to completion under continued chlorination. The uranyl chloride dissolves in the melt, probably forming double chlorides $K_2(UO_2)Cl_4$, $Na_2(UO_2)Cl_4$. With the higher oxides, oxygen is evolved, although these reactions can be reversed and oxides deposited by passing air or oxygen through the melt.

$$UO_2 + Cl_2 \rightarrow UO_2Cl_2$$
$$U_3O_8 + 3\,Cl_2 \rightarrow 3\,UO_2Cl_2 + O_2$$
$$2\,UO_3 + 2\,Cl_2 \rightarrow 2\,UO_2Cl_2 + O_2$$

Silica pots are satisfactory for pilot plant use throughout this process. Some surface attack occurs in contact with uranium oxides, but over long periods of use this has not led to any serious failures. Preferably, tall, narrow pots should be used to increase the gas–solid contact time, but the electrodeposition stage which follows the chlorination is normally carried out in the same vessel and the factors determining the design of the electrolytic cell are the more important. Lids can be fabricated from alumina cement reinforced with nichrome wire, although pyrophyllite, machined and then fired, is more suitable for smaller applications. The chlorine is passed into the melt through a silica tube leading to the bottom of the pot, and the oxide is added at an even rate to the surface of the melt. Analytical control can be applied to trace the course of the chlorination but the end-point is adequately indicated by a dip sample — obtained by dipping a cold, dry silica rod into the melt — being completely soluble in slightly acidified water. Chlorine efficiencies of up to 70% can be expected. Chlorination of recycled electrolytic UO_2 is difficult due to the physical nature of the oxide, and prior roasting to U_3O_8 should be carried out.

The presence of graphite during this stage leads to the formation of green uranium tetrachloride.

$$UO_2 + 2\,C + 2\,Cl_2 \rightarrow UCl_4 + 2\,CO$$
$$UO_2Cl_2 + 2\,C + Cl_2 \rightarrow UCl_4 + 2\,CO$$

This reaction is appreciable when the chlorine is passed over the graphite surface, but otherwise it has only limited effect, as in the horizontal cell, where chlorination is carried out with the graphite anode resting in the bottom of the cell. Melts containing UCl_4 can be reoxidised by passing oxygen or air through the melt to reform the yellow uranyl chloride. The colour change is normally used to determine the course of this oxidation, and although the reaction can proceed beyond the uranyl state this only occurs to the extent of occasionally causing blockage of the air inlet tube. The only method of ensuring the uranyl state completely is by prolonged chlorination of the oxide in the absence of reducing agents. The melt should then be maintained under an inert atmosphere.

The chlorination of uranium ore concentrate proceeds as rapidly as with the pure oxide. Effervescence occurs due to the moisture present in the concentrate, requiring the addition rate to be more carefully controlled, and the small amount of light coloured insoluble material remaining at the end causes some doubt as to the true end-point.

Melts containing about 20% UO_2 (as UO_2Cl_2) are most suitable for electrodeposition in each of the cells described. Higher starting concentrations can be used, but they lead to prolonged electrolyses at lower efficiencies, and the fall in melt level during electrolysis under such conditions is inconvenient from practical considerations. The capacity of the cathode in terms of the weight of deposit is also a limiting factor.

ELECTROLYTIC DEPOSITION PROCESSES

The direct electrolysis of a uranyl chloride melt between two suitable electrodes leads to the deposition of UO_2 at the cathode and the liberation of chlorine at the anode Evidence points to the following reactions

$$UO_2Cl_2 \rightleftharpoons UO_2^{2+} + 2\,Cl^-$$

Cathode: $UO_2^{2+} + 2\,e \rightarrow UO_2$

Anode: $2\,Cl^- \rightarrow 2\,Cl + 2\,e$

$$2\,Cl \rightarrow Cl_2$$

The anode reaction is complicated by the unavoidable use of graphite as the anode material, which causes the formation of uranium tetrachloride as already indicated. This has two principal effects. Firstly, erosion of the UO_2 deposit takes place (probably by the reaction represented below) causing a low cathode efficiency and a flat, dense form of deposit, and, secondly, the conversion to tetrachloride lowers the concentration of UO_2Cl_2 in the melt causing an increase in cell resistance and a limit to the yield of UO_2 obtainable from a single electrolysis.

$$UO_2 + UCl_4 \rightarrow 2\,UOCl_2$$

Nevertheless, advantage can be taken of these effects in various ways, with the result that more than one type of cell operation can be discussed. Firstly, the build-up of UCl_4 is allowed to occur in order to maintain the bath in a reduced state. Under these conditions, dioxide of low oxygen content ($UO_{2.0}$ to $UO_{2.05}$) and high density (over 10.8 g/cm^3) can be prepared. Without this reducing reaction and under normal atmospheric conditions, oxide of higher oxygen content is formed. Secondly, the anodic reaction is used to dissolve further oxide. Increased deposition efficiency is obtained because of the absence of UCl_4 in the cell, and although the chlorination stage cannot be altogether avoided, the throughput of oxide and the overall chlorine efficiency are greatly improved, and the problem of fume extraction and scrubbing is minimised.

These two methods of operation are both of value. The first method referred to as "direct" deposition, is most easily carried out using vertical electrodes. Electrolysis is allowed to continue until the cell resistance begins to rise rapidly and at this point, which coincides with a falling off in deposition efficiency, the melt is replenished by chlorinating more oxide in it.

The design of the anodic chlorination cell depends largely on the material being treated in the cell. Three main applications have been developed. For the first stage treatment of the concentrate, vertical electrodes may be used in the same way as for direct deposition, but for denser oxides, a horizontal cathode-above-anode design of cell is necessary. The third application which has received practical consideration is one in which the plated cathode from a direct deposition has been used as the soluble anode in a "replating" vertical cell.

Graphite is used as electrode material throughout. No alternative anode material has been found, and although a number of metals may be used as cathodes (*e.g.* nickel, stainless steel) the impurity introduced is less desirable than graphite which is already present in the cell.

TREATMENT OF PURE URANYL CHLORIDE MELTS

The main choice lies between "direct" deposition and the "horizontal" cell which incorporates anodic chlorination. To prepare oxide of low oxygen content, which has been the main consideration in this work, the direct cell is the easier to operate, but for oxide of a less rigid specification, the horizontal cell is the more applicable.

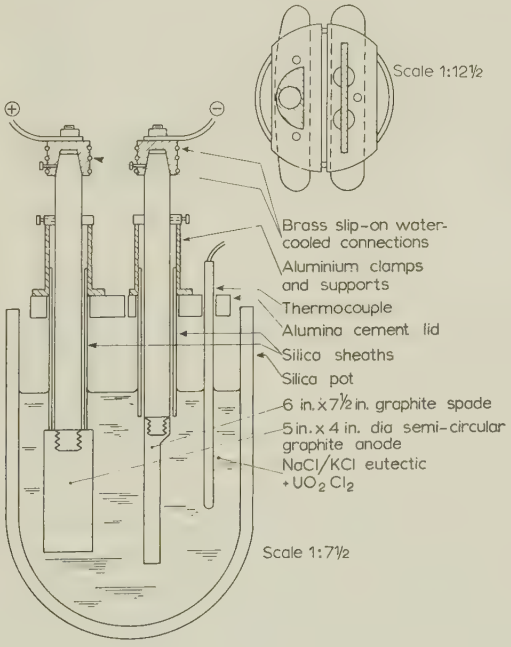

Fig. 1. Direct deposition.

Direct electrodeposition

A scale diagram of the pilot plant cell for direct deposition is shown in Fig. 1. No atmospheric protection is present, the design being based on features which allow the operation to be as simple as possible. Slip-on electrical connections and alumina cement lids incorporating nichrome tape handles are particularly advantageous. The

cathode spade is as large as possible without coming into contact with the walls of the cell during the electrolysis, and the anode is of suitable size to give a reasonable current and current distribution, without presenting an excessive graphite surface to the melt. The anodes have to be replaced every 5–7 runs, so to avoid unnecessary machining it is preferable to choose a convenient shape from this aspect. The cell is operated at 800°C, and currents up to 175 A are obtained, the applied voltage being limited to 3 to avoid the alkali metal deposition which causes breakdown of the graphite cathode.

Uranium dioxide commences to deposit at very low voltages (less than 0.01 V) and there is evidence that crystals form on a graphite rod without an applied voltage, although the part taken by impurities, for example in the graphite, in this deposition has not been investigated.

On average, 1.1 kg UO_2 is extracted in a run lasting 3 h, equivalent to a 50% yield at a current efficiency of about 50–70%. The efficiency in this cell is dependent on the surface oxidation of the melt, which counters the formation of UCl_4, and the best results can be obtained by applying fume extraction directly to the cell, causing a stream of air to pass over the surface. Little advantage is gained by attempting to increase this oxidation. A faster flow of air tends to cause solidification of the melt surface, and bubbling air through the melt gives a lower rate of oxidation due to the very much smaller volume of air involved. It also introduces disadvantages associated with melt agitation. For example, erosion of the deposit is increased due to the readier contact of UCl_4 with it, and problems associated with splashing and solidification round the top of the pot are increased.

Leaching of the deposits is straightforward. A static leaching tank with occasional agitation is satisfactory, using 1% HCl followed by a water wash. The fines (*ca.* 3%) may contain graphite and are recycled to the cell. Normal drying procedures can be adopted.

The general form of the deposit obtained under these conditions can be described as a dense, flat crust adhering to the cathode, forming mainly on the front face and sides and only occasionally as a thin layer of loose, finely-divided deposit on the back. The main deposit forms a columnar growth, its surface at the end of the deposition varying from a matt finish to a surface in which flat crystalline faces of the cubic UO_2 are seen. The deposit is removed as a complete crust and broken up into pieces. In this form its columnar growth is very apparent.

Some variation is obtained with different graphites as cathode material. The fine-grained graphites give very adherent deposits which have advantages under certain conditions, but normally the coarser grades are used for direct deposition to avoid difficulties in separating. Thin crystals of the deposit are red–brown to transmitted light and when ground yield a powder of similar colour. Oxygen contents vary from $UO_{2.0}$ to $UO_{2.05}$ and densities are in the range 10.80 to 10.85 g/cm^3. Impurity levels are discussed in a later section.

Horizontal deposition

A scale diagram of this cell is shown in Fig. 2. UO_2 or U_3O_8 in normal powder form is fed into the cell to cover the anode. Sufficient for each electrolysis is added before inserting the cathode, the batch size being dependent mainly on cathode capacity which in this cell is about 1 kg.

Electrolysis is normally carried out at about 100–120 A with an applied voltage of 2 to 2.5 V, each run lasting about 2 h. The concentration of dissolved UO_2 in the cells falls by about 2% during an electrolysis, indicating an anodic efficiency of near 80% and this necessitates a chlorination stage to be carried out after every four or five electrolyses.

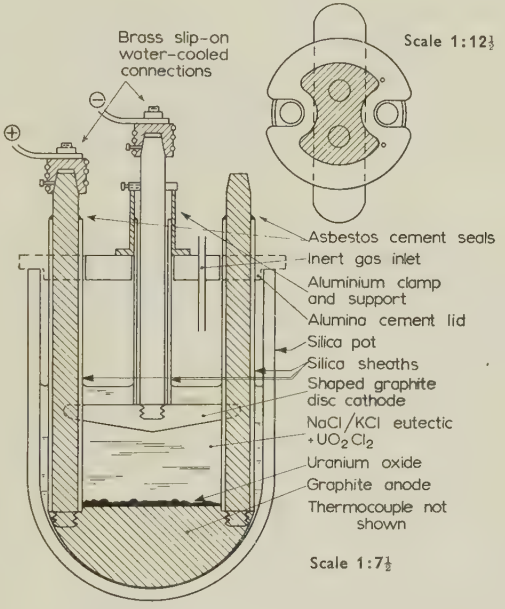

Fig. 2. Horizontal deposition.

Cathode efficiencies vary directly with the oxygen content of the deposit, which is dependent on the degree of atmospheric protection afforded to the cell. The three ways of introducing oxygen, in excess of the oxygen–uranium ratio 2 to 1, are (a) in the oxide added to the cell, (b) in the starting melt prior to electrolysis and (c) by atmospheric oxidation during the deposition. Uranyl chloride melts have been found to be able to pick up oxygen from the air and retain it in a soluble form which on electrolysis gives a deposit which can vary from UO_2 to at least $UO_{2.5}$. This oxygen can be picked up either whilst standing between the chlorinating and electrolytic stages, or during the electrolysis itself. There is little doubt that the evidence points to the presence in the melt, as soluble species, of a compound or compounds such as $U_2O_5Cl_2$ and $U_3O_7Cl_2$ and their equivalent ionic forms $U_2O_5^{2+}$ and $U_3O_7^{2+}$.

These factors can be controlled to vary the oxygen content of the deposit. Complete protection, which in practice is considerably more complicated than direct operation, gives up to 90% deposition efficiency and forms deposits in the range UO_2 to $UO_{2.07}$, whilst the controlled ingress of air gives oxygen contents in the range up to $UO_{2.2}$. The addition of U_3O_8 to the cell has only a limited effect within this range, and the higher contents are most easily obtained by electrolysing at low rates of deposition, when the surface oxidation effect is greatly increased. For example, deposition at 10 A for 15 h or more in the horizontal cell gives a deposit analysing at $UO_{2.5}$.

The form of the deposits obtained in the horizontal cell depends largely on oxygen content. Deposits with low oxygen content resemble closely the direct type deposits, forming a dense layer over the surface of the cathode but tending to break down more easily on leaching. Very little sign of erosion is present and the surface of the layer or crust shows clearly the faces of the oxide crystals. Deposits with higher oxygen content vary from open growths of fine crystals in the range $UO_{2.15}$ to $UO_{2.3}$ to fairly tight growths of coarse crystals formed at low deposition rates in the range $UO_{2.45}$ to $UO_{2.5}$. Ignition of these coarser crystals of higher oxygen content converts them to U_3O_8 but with no change in crystalline form. All other deposits break down to powder on ignition. The colour of the ground deposits varies from red–brown to dark green ($UO_{2.1}$) and black ($UO_{2.2}$ and over) and the density falls from 10.8 to about 9 g/cm^3 with increasing oxygen content.

TREATMENT OF URANIUM ORE CONCENTRATE

A single stage electrodeposition process can be used to produce electrolytic UO_2 crystals from a melt formed by chlorinating uranium ore concentrate, but more than one stage is required to achieve high purity combined with crystalline form. The impurities can be grouped into those dissolved during the chlorination and those remaining insoluble. The possibility of melt filtration is a problem that has not been tackled but which is likely to be solved more easily on a large scale than on the scale considered here. It may be possible that a filtration stage could be used as an alternative to the first stage described below, and this would afford considerable economies in time and effort. However, the proposed first stage removes the bulk of both the soluble and insoluble impurities, and the alternative filtration stage would necessitate modifications to the later stages, particularly with regard to the recycling of the melt and preventing the build-up of impurities in the system.

The first stage deposition is a purification stage which includes aqueous leaching of the deposit. A high throughput to the cell is obtained by taking advantage of anodically chlorinating the concentrate, but the open structure of the deposit causes inclusion of insoluble impurities and melt which can only be separated by leaching and rejecting the fines. The roasted deposit from this stage is sufficiently pure to be treated as the starting material for pure melt electrolysis in a direct-type cell. The product from this cell achieves a fairly high purity but in certain respects, notably the rare earths, it falls short of the purity level required for nuclear fuel. In this case replating electrolysis can be applied as a third electrolytic stage in which the cathode from the direct cell is used as the soluble anode.

First stage: deposition with anodic chlorination

As already mentioned, a vertical design of cell is used, virtually the same as that used for direct deposition, but in order to match the output of this first stage with the cell of the second stage, the cell dimensions are considerably smaller, as shown in Fig. 3. The starting melt prepared using melt recycled from the second stage, contains about 20% UO_2 as UO_2Cl_2, and electrolysis is carried out on this scale at 30 A for 3 h. The applied voltage is in the range 1.1 to 1.8 V and, in all, 400 g concentrate is added evenly during the run. No predrying of the concentrate is necessary. Deposits average about 450 g indicating 100% cathode efficiency, but to make up for the lower anode efficiency it is necessary to carry out a short chlorination between each electrolysis.

Half an hour is convenient for this chlorination, during which a further 200-g concentrate is added.

Cathode efficiencies are, of course, dependent on the rate of concentrate added, and apparent figures over 100% can be achieved. These may be corrected by making allowance for the incomplete reduction to the UO_2 state. Deposits are collected and

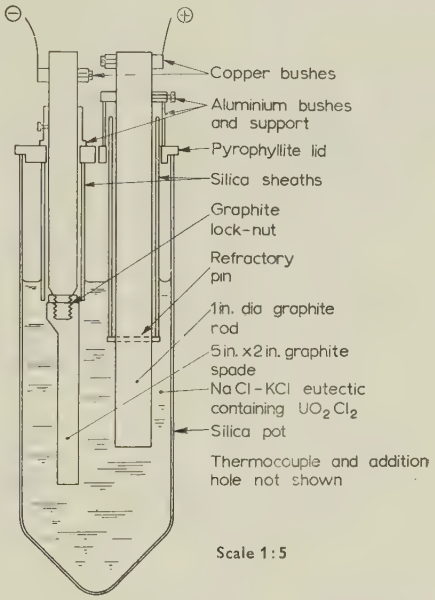

Fig. 3. First stage treatment of concentrate.

leached in 1% HCl and the very fine sludge which is mainly impurities is separated by decantation with the wash liquors. The crystals of UO_2 are then treated in an elutriation column to complete the washing and to separate about 8% of the finer crystals which contain a higher proportion of impurities. This 'float' fraction is returned to the first stage to be mixed with the concentrate additions. The 'sink' fraction, about 99% pure, is passed to the second stage.

A complete cycle for the first stage consists of nine electrolyses, by which time the melt has become too thick and sludgy for continued operation. The uranium content is allowed to fall over the last two electrolyses to leave the final melt with a sufficiently low content for the uranium to be recovered by a simple aqueous leaching. Chlorination of the melt after the last electrolysis, during which the sludge settled from the wash liquors may also be chlorinated, ensures the uranium being water soluble.

Second stage: direct deposition

This stage is identical with that already described for the treatment of pure melts, except that the applied voltage is limited to 2 V to effect further purification. The melt is recycled every 10 to 15 electrolyses and this matches the requirement of the first stage. The starting melt can be prepared from melt recycled from the replating stage or from fresh NaCl–KCl eutectic. No leaching of the deposit is carried out when

a replating stage is included in the process, the cathode and deposit being transferred direct to the replating cell. A cathode spade with angled saw cuts, as shown in Fig. 4, should be used.

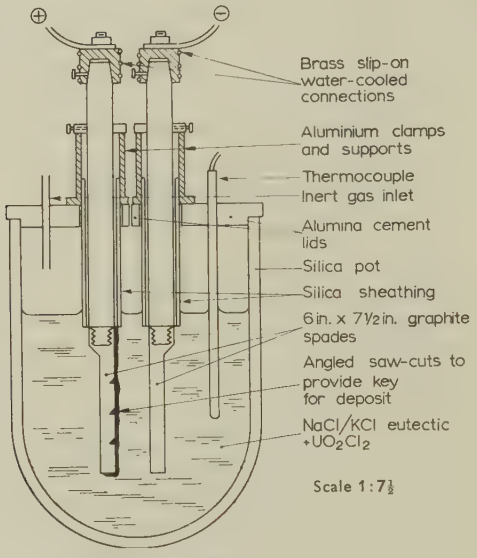

Fig. 4. Replating deposition.

Third stage: replating deposition

The cell is a simple arrangement with two graphite spades close together and facing each other. This cell was associated with early ideas of purifying the deposit by operating with a short anode–cathode distance at low voltage to separate the oxide from the impurities with higher deposition potentials. Although UO_2 has a very low deposition potential, little is gained by only operating at low potential, and in fact, as already mentioned, high oxygen content can result. The principal impurities under consideration at this stage are the rare earths, and the most important single factor controlling their deposition is the oxidising state of the bath. If, therefore, the bath can be maintained under slightly reducing conditions and with an inert atmosphere during operation, satisfactory separation can be effected. Low voltage deposition in addition will improve upon these results and also increase the crystal size of the deposit, but it has the disadvantage of unduly prolonging the electrolysis.

To obtain increased purity, this cell can only be used to prepare oxide of low oxygen content, and an inert atmosphere must be maintained over the melt throughout the operation. Deposition efficiencies are 90% or over, but anodic efficiencies fall short of this (60 to 80%). A major problem is associated with the adhesion of the deposit to the anode spade. The deposit falls off the anode before the end of the run, but the angled saw cuts in the spade help to retain it until about 80% has dissolved. Plating is normally continued beyond this point in order to maintain the uranium balance in the cell. A short chlorination period is required to dissolve the deposit fallen off into the cell and every four or five runs some readjustment of the uranium concen-

tration in the melt may be necessary. The melt is recycled to the direct cell after 10 to 15 electrolyses.

Deposits obtained from the replating cell vary, occasionally showing pronounced dendritic growths but more often, particularly with lower oxygen contents, approaching

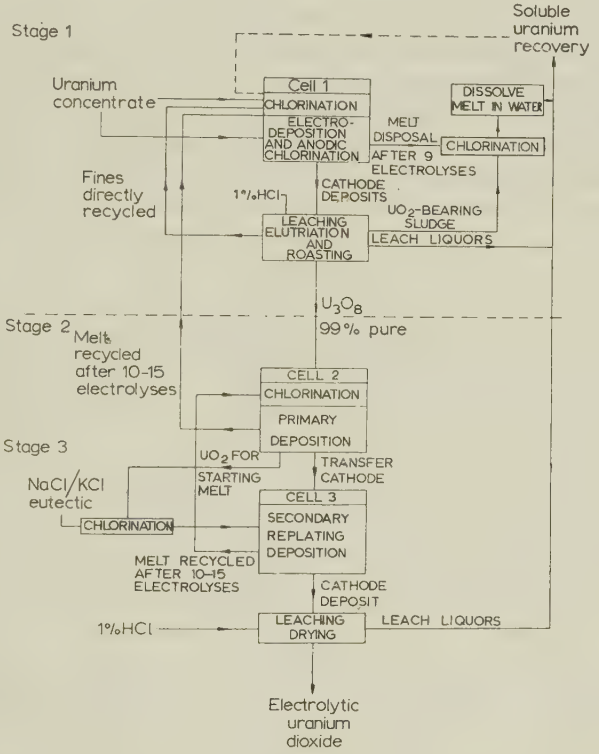

Fig. 5. Flow-sheet for treatment of uranium concentrate.

the flat direct-type deposit. The deposits break down to individual crystals or aggregates on leaching, the crystal size being much larger than that from the horizontal cell. A typical sieve analysis is given in Table I.

TABLE I

SIEVE ANALYSIS OF SECONDARY DEPOSIT

BSS fraction	*Wt.%*
+ 12	7
— 12 + 25	36
— 25 + 52	37
— 52 + 100	15
—100 + 300	4
—300	1

BEHAVIOUR OF IMPURITIES

The impurities present in this process are those which are derived from (a) the starting material and (b) the cell constituents. The second class of impurities include carbon,

silicon, aluminium, sodium, potassium and chlorine and these are present in all electrolytic oxide prepared by this process. In addition to these elements, oxide derived from the ore concentrate has the rare earths (including scandium and yttrium), thorium, calcium, magnesium, titanium and iron in amounts which may give cause for concern.

Carbon contents depend mainly on the form of the deposit. Separating the hard direct deposits from the cathodes tends to produce carbon dust which is carried forward with the deposits, but careful handling can keep the level of contamination down. Silicon and aluminium contents are not high, but both potassium and chlorine are present to the extent of 100 to 200 p.p.m. Sodium levels show a marked variation with the oxygen content of the oxide deposit, varying from below 400 p.p.m. for direct, low oxygen deposits to over 0.2% for some of the higher oxygen deposits within the

TABLE II

SUMMARY OF ANALYTICAL RESULTS

	Uranium ore concentrate		*Concentration treatment (p.p.m.)*			*Deposit from pure oxide treatment (p.p.m.)*
			1st stage product	*2nd stage product*	*3rd stage product*	
	*A**		*B*	*C*	*D*	*E*
U	69.7	%	—	—	—	—
H_2O	9.2	%	—	—	—	—
CO_2	ND		—	—	—	—
Al	1.0	%	1400	100	50	30
Ca	0.6	%	2000	300	60	30
Fe	2.1	%	60	30	15	20
Mg	2.0	%	600	10	5	6
K	0.2	%	250	150	100	150
Si	0.1	%	500	100	50	45
Na	4.0	%	800	350	150	400
V	0.2	%	50	<10	<1	<1
C	ND		50	1000	500	130
Cl	ND		200	200	200	150
Cr	500		40	<5	1	3
Ti	300		90	40	10	3
B	5		0.8	<0.2	<0.2	<0.2
Cd	<0.2		<0.2	<0.2	<0.2	<0.2
Li	2		<0.2	<0.1	<0.1	<0.1
Th	400		300	250	200	10
Sc	550		500	150	20	0.5
Y	700		600	200	20	<0.5
La	800		700	15	3	<0.5
Ce	450		600	20	<5	<2
Pr	<60		<100	<20	<5	<1
Nd	50		50	6	<5	<1
Sm	<80		<100	<15	<5	<1
Eu	<20		<20	<3	<1	<0.2
Gd	20		25	5	<3	<1
Tb	<30		10	4	2	<1
Dy	100		150	40	<10	<0.5
Ho	20		30	8	4	<1
Er	100		100	50	3	<1
Tm	ND		ND	ND	ND	ND
Yb	200		300	70	5	<0.2
Lu	20		30	10	<2	<0.3

ND: not determined

* in p.p.m. unless otherwise indicated

cubic UO_2 range. The results indicate that the increasing accommodation of oxygen in the cubic structure enables an increasing number of sodium atoms to be fitted into the lattice. The ionic radii of U^{4+} and Na^{+} are similar (0.89 and 0.95 Å respectively) whereas the larger potassium ion is not easily accommodated. Leaching tests show no sign that these levels of impurities can be reduced by any normal procedures.

Of the impurities in the concentrate only the rare earths and thorium are of any concern. The successful removal of the rare earths depends more on the reducing nature of the bath than on any other factor. In the first stage, therefore, no separation is achieved, and adequate purification from the rare earths depends entirely on the later stages which are operated in a bath with a deficiency of oxygen. The evidence points to the formation of rare-earth oxychlorides which have low deposition potentials and which, under oxidising conditions, deposit with the uranium oxides. In the presence of uranium tetrachloride or under conditions in which it is formed, the rare-earth oxychlorides are converted to the fully chlorinated form and take no part in the electrolysis. The rare-earth chlorides all have decomposition potentials greater than 2 V. Thorium is thought to behave in a similar way to the rare earths but results are inconclusive. It is possible that the oxychloride of thorium persists in relatively more reducing conditions than those of the rare earths. Analyses give thorium figures between 90 and 300 p.p.m.

Table II lists a summary of the analytical results in this work. The first column (*A*) is the analysis of a batch of uranium ore concentrate used in this work and is followed by typical analyses of the material obtained from the first, second and third stages respectively (*B*, *C* and *D*) in the treatment of the concentrate. Column *E* gives the analysis of electrolytic dioxide obtained by the single stage direct deposition from a pure melt.

CONCLUSION

An electrolytic method has been developed for the production of crystalline uranium dioxide of high density which has potential technical advantages because of its physical form.

The crystals can be prepared either by converting pure uranium oxide or by treating uranium ore concentrate directly. Although reasonable purity can be obtained by the latter method, it cannot be considered economic as a purification process in its own right. For small requirements of the electrolytic oxide, advantage must obviously be taken of using as starting material oxide purified by the present large scale production, but for any future large scale requirement of large crystals, the process using ore concentrate as starting material should be considered as worthy of future development.

ACKNOWLEDGEMENTS

Acknowledgements are due to the Director of the Atomic Energy Authority Establishment, Harwell and the Directors of Impregnated Diamond Products Ltd., Gloucester, for permission to publish paper. The work formed part of a programme of research and development carried out at Gloucester for the United Kingdom Atomic Energy Authority.

REFERENCE

A. R. Gibson and L. L. Wassell, Extraction of uranium and uranium dioxide from an Australian ore concentrate by a chloride route, *A.E.R.E. Rept. M/R 2513*, (1958).

HIGH TEMPERATURE ALLOTROPY AND THERMAL EXPANSION OF THE RARE-EARTH METALS*

F. H. SPEDDING, J. J. HANAK AND A. H. DAANE

Institute for Atomic Research and Dept. of Chemistry, Iowa State University, Ames, Iowa (U.S.A.)

(Received November 17th, 1960)

SUMMARY

By means of high temperature X-ray techniques the crystal structure of lanthanum, cerium, praseodymium, neodymium, ytterbium, and possibly gadolinium was found to be body-centered cubic at temperatures near their respective melting points. For ytterbium a hexagonal close-packed structure was also observed, which was shown to be stabilized by atmospheric impurities. Evidence for possible high temperature crystalline transformations in gadolinium, terbium, dysprosium, holmium, and lutetium was obtained by means of electrical resistance measurements; erbium gave no such evidence. X-ray data were used to derive empirical equations which describe thermal expansion coefficients of scandium, yttrium and the rare-earth metals. Europium exhibits a rapidly decreasing coefficient of expansion with increasing temperature, which may be a consequence of a gradual promotion of one of the 4f electrons into the conduction band. The hexagonal rare-earth metals were found to have nearly the same axial ratio at their respective transformation temperatures.

INTRODUCTION

In recent studies of the physical properties of pure rare-earth metals in this laboratory[1-6] it was found that several of the rare-earth metals exhibit crystalline transformations at temperatures near their melting points. These transformations have been observed in thermal analyses at the following temperatures: lanthanum, 868°C; cerium, 730°C; praseodymium, 798°C; neodymium, 868°C; samarium, 917°C; gadolinium, 1263°C; terbium, 1310°C; and ytterbium, 798°C. Lanthanum undergoes an additional transformation between 250° and 310°C. HABERMANN[3] has recently observed a transformation in yttrium at 1455°C that EASH[7] has also found in his study of the yttrium–magnesium system. On the basis of there ports of BARRETT[8] and SPEDDING *et al.*[9] europium does not exhibit any crystalline transformations.

At room temperature lanthanum, praseodymium, and neodymium have a hexagonal structure (double *c*-axis) in which crystal planes stack in the "*abac* . . ." sequence. Cerium and ytterbium have a face-centered cubic (f.c.c.) structure, samarium a rhombohedral structure, europium a body-centered cubic (b.c.c.) structure, while the remaining stable rare-earth metals, including scandium and yttrium, exhibit a hexagonal close-packed (h.c.p.) structure.

* Contribution No. 940. Work was performed in the Ames Laboratory of the U.S. Atomic Energy Commission.

The only high temperature structures previously reported for the rare-earth metals have been f.c.c. lanthanum (stable above 310°C) and the β-form of yttrium (above 1495°C), which was inferred to be b.c.c. from phase diagram studies reported by EASH[7] and GIBSON AND CARLSON[10].

In the present work a detailed study was made of the structures of the high temperature phases of the rare-earth metals. The possibility of the existence of other crystalline modifications was also investigated by X-ray methods and by electrical resistivity measurements. Since the crystallographic method offers a means of accurate measurement of the lattice dimensions as a function of temperature, the thermal expansion characteristics of the rare-earth metals were also determined in this study.

EXPERIMENTAL

High temperature X-ray techniques

For the high temperature X-ray studies three different techniques were used. In the first two, methods of the type described by BUERGER *et al.*[11] were used with the appropriate modifications described below.

X-ray method applicable up to 1000°C. Wire specimens of rare-earth metals were fitted with tungsten spacers and mounted in silica capillaries in a vacuum. A platinum wound furnace inside the camera heated the samples to the desired temperature, which was measured with a thermocouple. Calibration with silver indicated an accuracy in temperature measurement of ± 7°C in the range 20° to 950°C. The details of this method are given elsewhere[13].

X-ray method applicable up to 2200°C. Wire specimens of rare-earth metals were mounted in a slotted copper holder which provided space for the entering and diffracted X-ray beams. The ends of the sample were mounted so that current from a 6 V battery heated the specimen to the desired temperature by its own resistance heating. The exterior of the copper holder was treated with a plastic spray and then wrapped with "Saran Wrap" which permitted evacuation of the sample chamber to pressures as low as $1 \cdot 10^{-6}$ mm, and also provided a very transparent window for the X-rays. The temperature of the specimen was determined by optical pyrometric and electrical resistivity measurements. The details have been described in more detail[13].

In the third method a high temperature X-ray diffractometer previously described by CHIOTTI[12] was used to substantiate some observations made on ytterbium by the first method.

Determination of phase transformations by electrical resistance measurements

To determine the existence of crystalline transformations by electrical resistance measurements the apparatus described by CHIOTTI[14] was used. In this method cylindrical samples 8 cm long and 0.5 cm in diameter were heated by passing alternating current through them. The electrical resistance of the sample was determined by measuring the voltage across the samples by alternating current potentiometric methods. The temperature of the samples was measured by an optical pyrometer focussed on a small sight hole drilled into the metal, or by a thermocouple imbedded in the metal.

Methods of calculation

The determination of the lattice constants was done by COHEN's least-squares

method[15] on an IBM-650 computer. For cubic lattices, a program was used requiring only the Bragg angles and the Miller indices as input data. For hexagonal lattices a program was written which indexed the diffraction patterns and then calculated the lattice constants by the least-squares method. For this program a prior knowledge of the approximate lattice constants was required (to within 0.01 Å). The indexing was performed by synthesizing the allowed reflections on the basis of these lattice constants and comparing them to the observed reflections. When a poor guess of the approximate lattice constants was made, the new lattice constants used in the subsequent iteration generally gave rise to the proper indexing of the pattern.

The quality of the diffraction patterns of the rare-earth metals deteriorated with increasing temperature. For temperature ranges where back-reflection lines appeared it was possible to determine the lattice constants with an accuracy of ± 0.005 to ± 0.0005 Å. In such cases the lattice constants and related data were fitted to empirical equations of the type

$$R = A + Bt + Ct^2 + Dt^3 \quad (1)$$

or

$$R = A + Bt \quad (2)$$

where R is a lattice constant or a related property, t the temperature in °C and A, B, C and D the coefficients of t^n. The linear equation was used in cases where data of inferior accuracy were obtained or for data available for only short temperature ranges.

Source and quality of materials

Most of the metals were prepared by metallothermic reduction of the trifluorides with calcium metal as described by SPEDDING AND DAANE[1]. Europium and ytterbium were prepared by vacuum distillation of these metals from a heated mixture of the respective sesquioxides and lanthanum metal, as described by SPEDDING *et al.*[9] and by DAANE *et al.*[16]. Scandium, dysprosium, holmium, erbium and thulium samples were vacuum distilled prior to use, with the exception of the erbium metal used for the electrical resistance measurements.

All of the metals studied were analyzed spectrographically for other rare earths and other common impurities. The neighboring rare earths, calcium, magnesium and silicon were usually present in hundredths of a per cent. The main metallic impurity was tantalum, which in lutetium amounted to more than 1%; in yttrium, about 0.4%; in other metals cast in tantalum crucibles, less or equal to 0.1%; and was not detected in the distilled metals. The tantalum was present in dendritic form, and could be recovered as an acid-insoluble residue of pure tantalum.

Chemical analyses revealed the presence of 50 to 250 p.p.m. of carbon and 20 to 450 p.p.m. nitrogen in most of these metals. Yttrium, praseodymium, and neodymium were also analyzed by vacuum fusion, which showed hydrogen to be present in the amounts 130, 10 and 40 p.p.m., and oxygen in 480, 800 and 1900 p.p.m. respectively.

RESULTS AND DISCUSSION

Diffraction patterns of the rare-earth metals generally yielded back-reflection lines and, hence supplied accurate data up to 400 to 700°C with the light rare earths and 650 to 1000°C with scandium, yttrium, and the trivalent heavy rare earths. At ap-

proximately 600°C the metals began recrystallizing, giving rise to spotted diffraction lines, which could be easily distinguished from the full lines caused by surface impurities formed at higher temperatures by the reaction of the metals with residual gases. The patterns of the high temperature phases contained only front reflection lines which were also spotted hence limiting the precision of the lattice constants to hundredths of an Ängstrom unit. Although the spotted lines gave a reliable indication that a pattern of a high temperature structure was that of a metal, an additional assurance of this fact was gained by cooling the sample below the transformation point and obtaining the familiar pattern of the lower temperature form.

High temperature allotropy

Below 292°C lanthanum was found to exhibit a mixture of h.c.p. (double *c*-axis) and f.c.c. structures, the amounts of which varied sporadically for different samples. The presence of surface impurities seemed to stabilize the f.c.c. structure below 293°C. The patterns of both structures were diffuse, indicating lattice defects. Above 293°C only the f.c.c. phase was present, yielding sharp lines in the diffraction pattern. The transformation of the h.c.p. (double *c*-axis) form to the f.c.c. form was accompanied by a decrease of 0.5% in volume. Above 868°C the latter form transformed into a b.c.c. form for which the pertinent crystallographic data appear in Tables I and II. The atomic volumes of the three solid phases of lanthanum are shown in Fig. 1.

TABLE I

X-RAY DIFFRACTION DATA FOR b.c.c. La, Ce, Pr, Nd AND Yb

hkl	$\sin^2\theta$					
	La	*Ce*	*Pr*		*Nd*	*Yb*
			K_α	K_β		
110	0.0661	0.0710	0.0705	0.0576	0.0703	0.0604
200	0.1325	0.1414	0.1403	0.1147	0.1406	0.1212
211	0.1976	0.2119	0.2098	0.1715	0.2104	0.1806
220	0.2637	0.2810	0.2794	0.2286	0.2802	0.2407
310	0.3282	0.3528	0.3482	—	0.3490	0.3013
222	0.3945	0.4249	—	—	0.4194	0.3620
321	0.4604	0.4941	0.4888	—	0.4888	0.4214
400		0.5642	—	—		—
411,330			—	—		0.5432
420			0.6963	0.5680		0.6012

TABLE II

LATTICE CONSTANTS AND RELATED DATA FOR b.c.c. La, Ce, Pr, Nd AND Yb

Metal	*Number of experimental points*	*Average temperature (°C)*	*Lattice constant (Å)*	*Atomic volume (cm³/mole)*	*Density (g/cm³)*	*Change in volume on transformation to b.c.c. (%)*
La	3	887	4.26	23.2	5.98	+1.3 ± 0.4
Ce	8	757	4.12	21.0	6.67	+0.1 ± 0.7
Pr	6	821	4.13	21.2	6.64	+0.5 ± 0.7
Nd	4	883	4.13	21.2	6.80	+0.1 ± 0.6
Yb	5	774	4.44	26.5	6.54	—0.1 ± 0.4[a]

[a] The change of volume from the f.c.c. or the h.c.p. structure to the b.c.c. structure is the same

Cerium, praseodymium, and neodymium retained their room temperature structures up to the reported transformation temperatures of 730, 798 and 868°C, respectively, and above these temperatures they all exhibited a b.c.c. structure. In one sample, surface impurities lowered the transformation temperature of neodymium to at least 850°C. The details concerning the high temperature structure of these metals are given in Tables I and II.

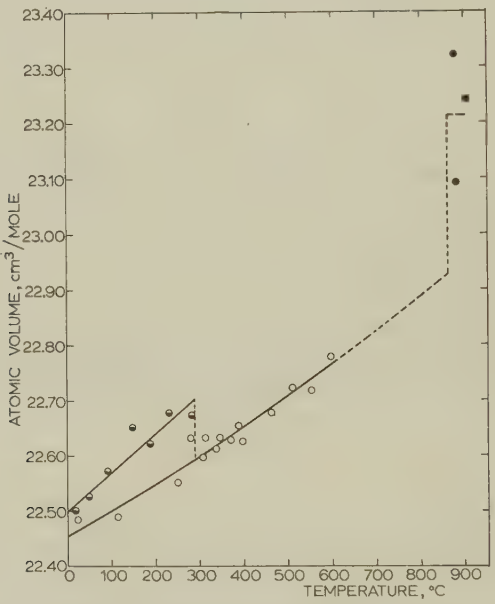

Fig. 1. Atomic volume *vs.* temperature plot for lanthanum, showing the three crystallographic forms: ◒, h.c.p. lattice; ○, f.c.c. lattice; ●, b.c.c. lattice.

Europium was investigated crystallographically from room temperature up to 450°C and it was found to be b.c.c. in this temperature range. Above this temperature extensive vaporization of the metal prevented further attempts to obtain diffraction patterns, even though the samples were kept in an atmosphere of argon. A similar difficulty was encountered in the case of samarium. Thermal analyses indicate europium to have no crystallographic transformations in the solid state.

Ytterbium, being about as volatile as europium, presented similar problems. It was found, however, that by sealing an ytterbium specimen in a silica capillary filled with air (about 2 mm³ of air, which is only about 4% of the amount necessary to completely convert the sample to YbO and YbN) and heating it, a tight transparent coating was formed which prevented the metal from evaporating, and contributed an easily identified f.c.c. pattern to the composite pattern. Thus it was possible to obtain X-ray patterns of the metal to above 800°C. These patterns indicated that the metal retained its f.c.c. structure up to at least 732°C. Above this temperature ytterbium exhibited a b.c.c. structure, the details of which are given in Tables I and II. The presence of the atmospheric impurities lowered the transformation temperature to as low as 720°C.

When one sample of ytterbium in the b.c.c. form was cooled to below 700°C, instead of the expected f.c.c. form, a h.c.p. form appeared which persisted to about 260°C, when it transformed into the original f.c.c. form. The h.c.p. and the b.c.c. structures reappeared when the sample was heated above 260° and 720°C, respectively. The crystallographic data for the h.c.p. structure are given in Table III. The atomic volumes of the three phases may be seen in Fig. 2.

TABLE III

X-RAY DIFFRACTION DATA FOR h.c.p. YTTERBIUM

$a = 3.911 \pm 0.003$ Å; $c = 6.403 \pm 0.003$ Å; $c/a = 1.637$; $t = 268$°C; atomic volume = 25.54 cm³/mole; density = 6.775 g/cm³; change of volume on transformation from f.c.c. to h.c.p. = +0.7%.

hkl	$\sin^2\theta_{obs.}$	$\sin^2\theta_{calc.}$	$\sin^2\theta_{obs.} - \sin^2\theta_{calc.}$
001	—	0.0145	—
100	0.0513	0.0517	—0.0004
002	0.0582	0.0579	+0.0003
101	0.0662	0.0662	—0.0000
102	0.1105	0.1096	+0.0009
003	—	0.1302	—
110	—	0.1552	—
103	0.1818	0.1820	—0.0002
200	—	0.2069	—
112	—	0.2130	—
201	0.2216	0.2213	+0.0003
004	0.2304	0.2316	—0.0012
202	0.2658	0.2648	+0.0010
104	0.2836	0.2833	+0.0003
203	0.3386	0.3371	+0.0015
005	—	0.3618	—
210	0.3628	0.3620	—0.0008
211	0.3771	0.3765	+0.0006
114	0.3848	0.3867	—0.0019
105	0.4147	0.4135	+0.0012
212	0.4199	0.4199	—0.0000
204	0.4363	0.4384	—0.0021
300	—	0.4654	—
213	0.4918	0.4923	—0.0005
006	0.5206	0.5210	—0.0004
302	—	0.5242	—
205	0.5710	0.5687	+0.0023
106	0.5710	0.5727	—0.0017
214	0.5925	0.5936	—0.0011
220	—	0.6216	—
310	0.6740	0.6723	+0.0017
116	—	0.6761	—
222	—	0.6785	—
311	0.6891	0.6868	+0.0023
304	—	0.6970	—
007	—	0.7091	—
215	0.7254	0.7238	+0.0016
215	0.7249	0.7238	+0.0011
206	0.7287	0.7274	+0.0013
206	0.7282	0.7274	+0.0008
312	—	0.7302	—
107	0.7629	0.7608	+0.0021
107	0.7628	0.7608	+0.0020
313	0.8038	0.8026	+0.0012
313	0.8046	0.8026	+0.0022

TABLE III (Continued)

hkl	$sin^2\theta_{obs.}$	$sin^2\theta_{calc.}$	$sin^2\theta_{obs.} - sin^2\theta_{calc.}$
400	—	0.8275	—
401	—	0.8419	—
224	—	0.8521	—
216	0.8844	0.8830	+0.0014
216	0.8844	0.8830	+0.0014
402	—	0.8854	—
314	0.9047	0.9039	+0.0008
314	0.9048	0.9039	+0.0009
207	0.9169	0.9160	+0.0009
207	0.9164	0.9160	+0.0004
008	—	0.9262	—
403	—	0.9577	—
108	0.9786	0.9779	+0.0007
108	0.9777	0.9779	−0.0002

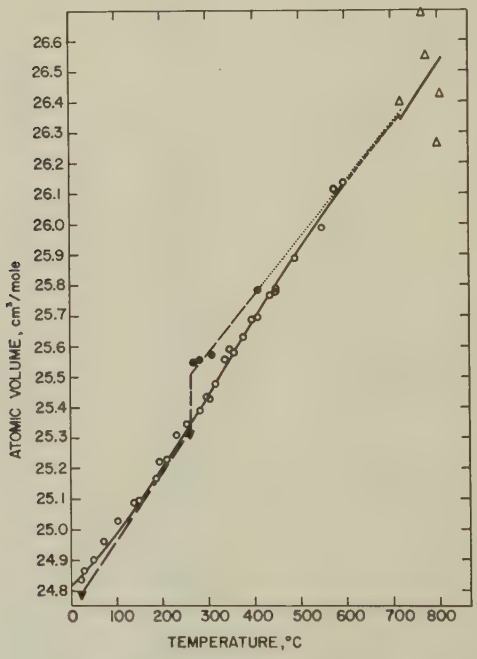

Fig. 2. Atomic volume *vs.* temperature plot for ytterbium, showing h.c.p. phase stabilized by impurities: ○, f.c.c. lattice; △, b.c.c. lattice; ●, h.c.p. lattice; ▼, f.c.c. lattice after h.c.p. → f.c.c. transformation.

In order to determine which of the two ytterbium structures appearing above 260°C was stable, a massive sample measuring 2.5 × 1.25 × 0.5 cm was studied using a high temperature diffractometer. The sample was heated under a vacuum and was thermally cycled at least two times above the f.c.c.–b.c.c. transformation temperature to duplicate the thermal history of the sample which exhibited the h.c.p. structure. The massive sample failed to exhibit the h.c.p. structure; the extensive vaporization of this sample which took place at high temperatures apparently minimized the for-

mation of a surface film. Since, on the other hand, the wire specimen was in intimate contact with intentionally deposited surface impurities which could easily diffuse into the sample, it was concluded that the h.c.p. structure was not a stable form of pure ytterbium, but was merely stabilized by these impurities.

Calcium exhibits an allotropic behavior similar to that of ytterbium. According to SMITH *et al.*[17], 99.96% pure calcium exists only in f.c.c. and b.c.c. forms, the transformation temperature being 464°C. However, calcium samples of inferior purity show the presence of a h.c.p. phase and an additional complex phase, the h.c.p. phase being stabilized by small amounts of hydrogen, as reported by SMITH AND BERNSTEIN[18]. The lattice dimensions of h.c.p. calcium and ytterbium are strikingly similar, the lattice constants of calcium being $a = 3.97$ Å and $c = 6.49$ Å with $c/a = 1.63$.

Gadolinium was investigated by the second high temperature X-ray technique described above and was found to retain its room temperature structure (h.c.p.) up to at least 1200°C. Above 1262°C some evidence was obtained for the existence of a b.c.c. structure. Of the first four possible reflections two were observed as plainly visible spots and two as rather faint spots. The approximate lattice constant obtained was 4.06 Å, yielding a value of the atomic volume 2% smaller than the extrapolated atomic volume of the h.c.p. phase.

Lutetium was also found to be h.c.p. to at least 1400°C. Vaporization of the sample in the camera above this temperature interfered with further X-ray investigation.

The remaining rare-earth metals including scandium and yttrium and excluding samarium were investigated up to about 1000° C. They were all found to retain their h.c.p. room temperature structure up to at least the following maximum temperatures: Sc, 1009°C; Y, 957°C; Tb, 950°C; Dy, 970°C; Ho, 966°C; Er, 917°C; and Tm, 1004°C.

The changes in volume occurring during the crystalline transformations described above are small in comparison to the volume change for the transformation in cerium from the normal f.c.c. form to the collapsed f.c.c. form, which has been attributed to an electronic transition between tri- and tetravalent cerium. Therefore, it appears that in the phase transformation described here the metals retain their original valence.

Detection of phase transformations by means of electrical resistance

Electrical resistance measurements were performed on gadolinium, terbium, dysprosium, holmium, erbium and lutetium from 900°C to their melting points. To prevent the samples from evaporating at high temperatures they were kept under an atmosphere of helium. This provision was not sufficient for the more volatile dysprosium, holmium and erbium metals, and these metals had to be enveloped in a 0.063 mm tantalum foil; in these samples, the sight hole drilled into the metal to simulate black-body conditions was lined with a 0.013 mm tantalum foil. The tantalum envelope conducted approximately 10% of the total current through the sample, so that discontinuities in the electrical resistance of the rare earth metals were not masked out by tantalum.

The plots of electrical resistivity as a function of temperature for gadolinium, terbium, and lutetium are shown in Figs. 3, 4 and 5, respectively. Gadolinium and terbium exhibit similar discontinuities at 1262 ± 14°C and at 1316 ± 10°C, respectively, both agreeing quite well with the previously reported transformation temperature of 1263°C[2] and 1310°C[3], respectively. The rather large ranges of temperature in which the transformations occurred were apparently caused by temperature gradients in

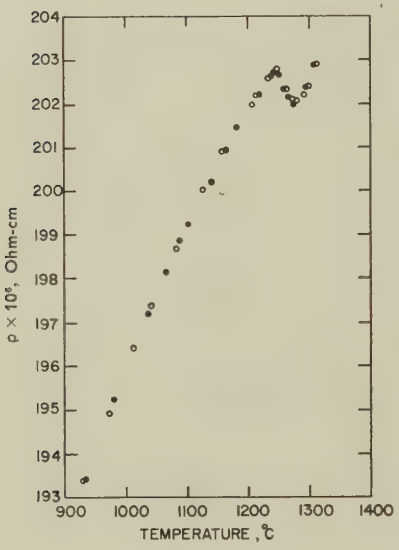

Fig. 3. Electrical resistivity *vs.* temperature plot for gadolinium: ○, heating; ●, cooling.

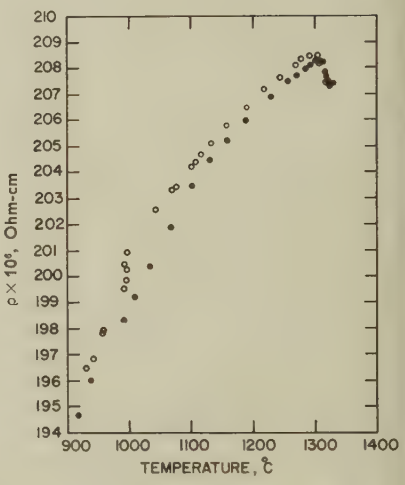

Fig. 4. Electrical resistivity *vs.* temperature plot for terbium: ●, heating; ○, cooling.

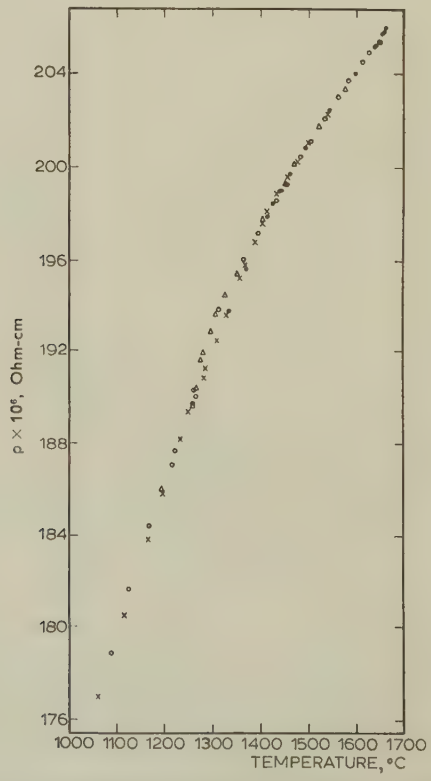

Fig. 5. Electrical resistivity *vs.* temperature plot for lutetium: ○, cooling; ×, heating; △, cooling; ●, heating.

the samples arising from the samples' ends being fastened to water-cooled copper electrodes.

An evidence of a second possible transformation was observed in terbium, appearing as a hysteresis loop between 1115°C on heating and 995°C on cooling. The anomaly on heating occurred instantly, whereas on cooling, the apparent isothermal break was completed in about 20 min. Subsequent thermal cycling showed that all the anomalies were reproducible, with the exception that the discontinuity observed at 995°C took place at 1016°C and lasted about 15 min. It is apparent that the phase existing above 1115°C in terbium has a tendency to supercool.

In lutetium a hysteresis loop in the electrical resistivity was observed between 1407°C on heating and 1260°C on cooling. Neither of the anomalies seemed to be time dependent.

The absolute values of the electrical resistivity of dysprosium, holmium and erbium could not be obtained conveniently because these samples were enveloped in tantalum. For dysprosium a discontinuous increase in resistivity occurred at 1392 ± 8°C, being reproducible for several heating and cooling cycles. In holmium a slight discontinuous increase in resistivity occurred at 1442 ± 8°C. The resistivity–temperature curve of erbium did not exhibit any anomalies indicative of crystalline transformations.

Thermal expansion of the rare-earth metals

The lattice constants of the rare-earth metals were determined at approximately 50°C intervals, except in the case of ytterbium where about thirty patterns were taken

TABLE IV

COEFFICIENTS OF EMPIRICAL EQUATIONS RELATING THE RARE-EARTH METAL PROPERTIES DETERMINED BY X-RAY STUDIES TO TEMPERATURE

M	*R*	*S*	*T*	σ	*Equation coefficients*			
					A	*B* ($\times 10^5$)	*C* ($\times 10^8$)	*D* ($\times 10^{11}$)
La	*a*	h.c.p.	293	0.002	3.770	1.7	—	—
La	*c*	h.c.p.	293	0.02	12.13	33.0	—	—
La	*v*	h.c.p.	293	0.03	22.50	70.	—	—
La	*d*	h.c.p.	293	0.008	6.174	—19.1	—	—
La	*a*	f.c.c.	598	0.002	5.303	3.4	1.0	0.0
La	*v*	f.c.c.	598	0.02	22.46	44.	13.	0.
La	*d*	f.c.c.	598	0.005	6.186	—12.0	—3.8	0.8
Ce	*a*	f.c.c.	619	0.0005	5.1604	3.28	—0.59	1.37
Ce	*v*	f.c.c.	619	0.006	20.695	38.3	—3.2	13.4
Ce	*d*	f.c.c.	619	0.001	6.771	—12.6	1.5	—4.5
Pr	*a*	h.c.p.	449	0.0008	3.6702	1.66	—	—
Pr	*c*	h.c.p.	449	0.004	11.828	13.3	—	—
Pr	*v*	h.c.p.	449	0.008	20.778	42.4	—	—
Pr	*d*	h.c.p.	449	0.003	6.782	—13.7	—	—
Nd	*a*	h.c.p.	696	0.0008	3.6582	3.18	—3.96	4.92
Nd	*c*	h.c.p.	696	0.004	11.802	16.6	—14.1	17.8
Nd	*v*	h.c.p.	696	0.01	20.60	65.	—70.	88.
Nd	*d*	h.c.p.	696	0.003	7.004	—21.9	23.2	—28.7
Eu	*a*	b.c.c.	352	0.001	4.578	17.4	—28.2	31.0
Eu	*v*	b.c.c.	352	0.02	28.91	309.	—439.	457.

TABLE IV (Continued)

M	R	S	T	σ	Equation coefficients			
					A	B (×10⁵)	C (×10⁸)	D (×10¹¹)
Eu	*d*	b.c.c.	352	0.004	5.259	—56.6	84.5	—86.8
Gd	*a*	h.c.p.	644	0.0009	3.631	4.26	—5.49	5.05
Gd	*c*	h.c.p.	644	0.001	5.777	4.8	5.4	—3.5
Gd	*c/a*	h.c.p.	644	0.0004	1.590	—0.27	3.02	—2.36
Gd	*v*	h.c.p.	644	0.01	19.88	49.	3.	3.
Gd	*d*	h.c.p.	644	0.005	7.895	—25.0	17.0	—17.5
Tb	*a*	h.c.p.	852	0.0009	3.5990	3.37	—0.72	1.03
Tb	*c*	h.c.p.	852	0.001	5.696	6.9	3.8	0.6
Tb	*c/a*	h.c.p.	852	0.0006	1.5827	0.43	1.38	—0.31
Tb	*v*	h.c.p.	852	0.009	19.245	59.2	5.5	13.7
Tb	*d*	h.c.p.	852	0.004	8.272	—25.4	—1.8	—5.3
Dy	*a*	h.c.p.	685	0.0004	3.5923	2.73	—3.53	3.69
Dy	*c*	h.c.p.	685	0.0009	5.6545	8.74	1.43	3.34
Dy	*c/a*	h.c.p.	685	0.0004	1.5741	1.24	1.93	—0.68
Dy	*v*	h.c.p.	685	0.005	19.032	58.7	—33.0	51.1
Dy	*d*	h.c.p.	685	0.002	8.536	—26.3	15.0	—22.1
Ho	*a*	h.c.p.	708	0.0007	3.5761	2.64	—2.55	2.42
Ho	*c*	h.c.p.	708	0.0008	5.6174	11.13	—3.78	4.71
Ho	*c/a*	h.c.p.	708	0.0004	1.5708	1.95	0.05	0.25
Ho	*v*	h.c.p.	708	0.008	18.742	61.6	—32.4	37.0
Ho	*d*	h.c.p.	708	0.003	8.803	—30.4	18.7	—18.9
Er	*a*	h.c.p.	917	0.0003	3.5590	2.95	—2.99	4.37
Er	*c*	h.c.p.	917	0.001	5.592	11.9	—4.1	4.9
Er	*c/a*	h.c.p.	917	0.0002	1.5711	2.06	0.13	—0.56
Er	*v*	h.c.p.	917	0.006	18.473	70.2	—45.8	63.5
Er	*d*	h.c.p.	917	0.003	9.051	—33.8	20.9	—28.3
Tm	*a*	h.c.p.	853	0.0006	3.5372	3.19	—1.41	1.19
Tm	*c*	h.c.p.	853	0.0007	5.5619	12.51	—3.89	3.27
Tm	*c/a*	h.c.p.	853	0.0003	1.5723	2.15	—0.55	0.43
Tm	*v*	h.c.p.	853	0.007	18.151	73.7	—26.7	23.1
Tm	*d*	h.c.p.	853	0.004	9.332	—37.4	14.0	—11.2
Yb	*a*	f.c.c.	598	0.001	5.481	14.1	7.0	—6.2
Yb	*v*	f.c.c.	598	0.02	24.80	191.	103.	—85.
Yb	*d*	f.c.c.	598	0.004	6.977	—54.1	—23.0	23.4
Lu	*a*	h.c.p.	956	0.0007	3.5050	.77	4.83	—2.17
Lu	*c*	h.c.p.	956	0.0006	5.5486	11.50	—4.55	3.16
Lu	*c/a*	h.c.p.	956	0.0002	1.5831	2.90	—3.44	1.86
Lu	*v*	h.c.p.	956	0.008	17.779	45.0	34.1	—11.1
Lu	*d*	h.c.p.	956	0.005	9.842	—24.7	—18.4	6.9
Sc	*a*	h.c.p.	1009	0.0008	3.3080	2.46	0.78	0.01
Sc	*c*	h.c.p.	1009	0.0009	5.2653	8.06	—0.52	0.79
Sc	*c/a*	h.c.p.	1009	0.0003	1.5917	1.23	—0.51	0.22
Sc	*v*	h.c.p.	1009	0.009	15.028	45.5	5.7	2.7
Sc	*d*	h.c.p.	1009	0.002	—2.992	—9.1	—0.9	—0.4
Y	*a*	h.c.p.	897	0.0007	3.6451	2.76	—1.92	2.16
Y	*c*	h.c.p.	897	0.0009	5.7305	12.40	—3.13	2.92
Y	*c/a*	h.c.p.	897	0.0002	1.5722	2.21	—0.09	—0.09
Y	*v*	h.c.p.	897	0.01	19.86	73.	—32.	34.
Y	*d*	h.c.p.	897	0.002	4.478	—16.8	8.1	—7.9

in the temperature range of 20 to 600°C, and in the case of the high temperature structures, where usually several patterns were taken in small temperature intervals. As mentioned above, the more accurate data were related to temperature by means of empirical equations. The coefficients A, B, C and D (eqns. (1) and (2)) are given in Table IV, where the following symbols were used: M, the metal studied; R, the physical property; S, the crystal structure; T, the maximum temperature in °C at which the equation applies; σ, the standard deviation of the experimental points from the calculated curves (in the same units as the given property); a and c, the lattice constants (in Å); c/a, the axial ratio; v, the atomic volume (in cm³/mole); d, the density (in g/cm³). The lowest temperature at which these equations apply is 20°C, except in the case of gadolinium, where the lowest temperature is 88°C. The lattice constants c of gadolinium between 20 and 50°C exhibited an anomalous increase of about 0.002 Å over that at 88°C, this phenomenon probably being due to the onset of ferromagnetism at 16°C.

By the use of these equations the coefficients of expansion were obtained. A comparison of these results with the dilatometric data obtained by BARSON *et al.*[5] and by BORN[19] showed the best agreement at the mid-range temperature (approximately 400°C). The average deviation of the two sets of data was less than $\pm 5\%$ at this temperature, the maximum deviation being 13%. At the two extreme temperatures the average deviations were about 20%, although the values obtained in the present work were in most cases somewhat higher than the dilatometric data. When using the equations in Table III to derive the approximate coefficients of expansion, the reader should be aware of these deviations.

In Table V are given the values of the thermal expansion coefficients of the rare earth metals at 400°C. For europium, to point out its rather unusual behavior, the data are given at 50°C and 300°C. Data for samarium were not obtained.

TABLE V

THERMAL EXPANSION COEFFICIENTS OF THE RARE-EARTH METALS AT 400°C

Metal	*Structure*	*Thermal expansion coefficient* ($°C^{-1}$)		
		a-axis	*c-axis*	*average linear*
La	f.c.c.	—	—	7.9
Ce	f.c.c.	—	—	6.7
Pr	h.c.p.(2-*c*)	4.5	11.3	6.8
Nd	h.c.p.(2-*c*)	6.5	11.7	8.3
Eu	b.c.c.	—	—	32.2[a]
Eu	b.c.c.	—	—	19.2[b]
Gd	h.c.p.	6.3	13.0	8.9
Tb	h.c.p.	9.1	17.9	12.1
Dy	h.c.p.	4.7	20.3	9.9
Ho	h.c.p.	4.9	18.4	9.5
Er	h.c.p.	7.5	19.5	11.5
Tm	h.c.p.	7.5	19.7	11.6
Yb	f.c.c.	—	—	30.6
Lu	h.c.p.	10.2	16.9	12.5
Sc	h.c.p.	9.3	15.2	11.4
Y	h.c.p.	6.2	19.7	10.8

[a] Value for 50°C.
[b] Value for 300°C.

The large values of the thermal expansion coefficients of europium and ytterbium can be attributed to the fact that these metals are divalent, whereas the rest of the rare-earth metals are considered trivalent. An unusual effect in europium is that this property decreases in magnitude at a rapid rate with increasing temperature. A possible explanation of this anomalous behavior is that one of the 4f electrons is being gradually promoted to the conduction band, the extent of this promotion being governed by the Boltzmann distribution law. The increase of the number of electrons in the conduction band tends to enhance bonding and, hence, to shrink the lattice, thereby diminishing the expansion of the lattice caused by thermal vibrations. The promotion of the 4f electron into the conduction band is not unlikely, since the 4f band and the conduction band in europium metal must be close in energy, judging from the fact that the element exhibits di- and tri-valence in its compounds, where trivalence is preferred.

Relationship between axial ratios and phase transformations

The axial ratios as a function of temperature for the h.c.p. heavy rare-earth metals are shown in Fig. 6 where the heavy lines represent the experimental data fitted to

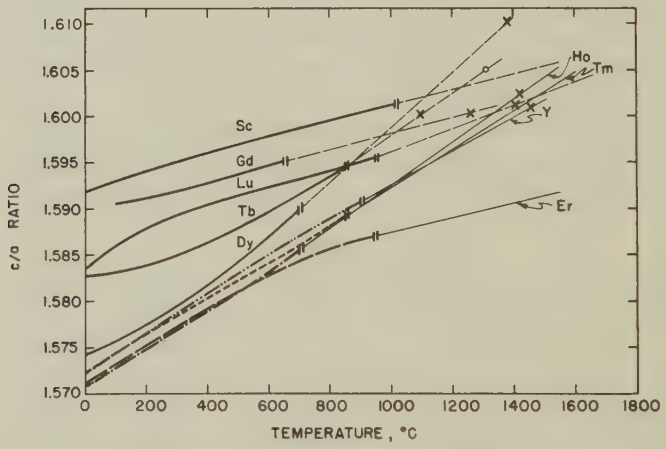

Fig. 6. c/a axial ratios of normal h.c.p. rare-earth metals *vs.* temperature.

empirical equations and the light lines represent the linear extrapolation of the axial ratios up to the melting points of these metals. Two short vertical lines on each curve signify points from which the extrapolations were made, and the points marked as "x" are the observed transformation temperatures. In the case of terbium, the second transformation is marked by "o".

An observation of interest is that the axial ratios tend to converge to a nearly constant value at the transformation temperatures. In the case of yttrium, gadolinium, terbium, holmium, and lutetium, the transformations were observed when the values of the axial ratios lay between 1.600 and 1.602. The value not falling in this range at the transformation temperature was 1.610 for dysprosium; however, this

discrepancy might have been due to the excessively long temperature range over which the extrapolation was carried out. The second transformation in terbium is not considered a discrepancy, since the metal probably is not h.c.p. above the first transformation.

Erbium, which did not give evidence of any crystalline transformation, failed to attain this limiting value of the axial ratio, thus giving support to the observation that a limiting axial ratio is required for a solid phase transformation to take place in these metals.

Data on the existence of crystalline transformations in scandium and thulium are lacking. However, if the axial ratio criterion holds, one can expect to find transformations in these metals in the temperature ranges of 1009 to 1140°C and 1370 to 1480°C, respectively. (Since this manuscript was prepared, BEAUDRY[20] has observed a transformation in scandium at 1335°C.)

Lanthanum, cerium, praseodymium, and neodymium also exhibit a limiting value of the axial ratio, the individual values of $1/2\ (c/a)$ being 1.619, 1.618, 1.619 and 1.621, respectively, as shown in Fig. 7. The value of the axial ratio of cerium is that reported by MCHARGUE *et al.*[21].

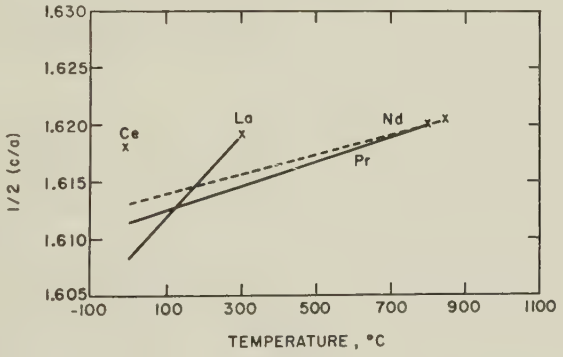

Fig. 7. c/a axial ratios of the light rare earths *vs.* temperature.

The impurity stabilized h.c.p. structure of ytterbium has a slightly greater than ideal axial ratio at lower temperatures. With increasing temperature this axial ratio approaches the ideal value.

ACKNOWLEDGEMENTS

The authors wish to express their appreciation to Messrs. G. WAKEFIELD and C. HABERMANN for preparing most of the metals studied in this work. The authors are also thankful to Dr. CHIOTTI for the use of his electrical resistivity apparatus and for his assistance in the electrical resistivity measurements.

REFERENCES

1 F. H. SPEDDING AND A. H. DAANE, *J. Metals*, 6 (1954) 504.
2 F. H. SPEDDING AND A. H. DAANE, *U.S. Atomic Energy Commission Rept. ISC-484*, Iowa State College, (1954).
3 C. E. HABERMANN, *M. S. Thesis*, Iowa State University, (1960).

[4] F. H. Spedding, A. H. Daane and K. W. Herrmann, *J. Metals*, 9 (1957) 895.
[5] F. Barson, S. Legvold and F. H. Spedding, *Phys. Rev.*, 105 (1957) 418.
[6] F. H. Spedding, J. J. McKeown and A. H. Daane, *J. Phys. Chem.*, 64 (1960) 289.
[7] D. T. Eash, *Ph.D. Thesis*, Iowa State University, (1959).
[8] C. S. Barrett, *J. Chem. Phys.*, 25 (1956) 1123.
[9] F. H. Spedding, J. J. Hanak and A. H. Daane, *Trans. Am. Inst. Mining Met. Engrs.*, 212 (1958) 379.
[10] E. D. Gibson and O. N. Carlson, *Trans. Am. Soc. Metals*, 52 (1960) 1084.
[11] M. J. Buerger, N. W. Buerger and F. H. Chesley, *Am. Mineralogist*, 28 (1943) 285.
[12] P. Chiotti, *Rev. Sci. Instr.*, 25 (1954) 683.
[13] J. J. Hanak, F. H. Spedding and A. H. Daane, *Rev. Sci. Instr.*, in press.
[14] P. Chiotti, *Rev. Sci. Instr.*, 25 (1954) 876.
[15] M. U. Cohen, *Rev. Sci. Instr.*, 6 (1935) 68.
[16] A. H. Daane, D. H. Dennison and F. H. Spedding, *J. Am. Chem. Soc.*, 75 (1953) 2272.
[17] J. F. Smith, O. N. Carlson and R. W. Vest, *J. Electrochem. Soc.*, 103 (1956) 409.
[18] J. F. Smith and B. T. Bernstein, *J. Electrochem. Soc.*, 106 (1959) 448.
[19] H. J. Born, *M. S. Thesis*, Iowa State University, (1958).
[20] B. J. Beaudry, unpublished data, Iowa State University, (1960).
[21] C. J. McHargue, H. L. Yakel, Jr. and L. K. Jetter, *Acta Cryst.*, 10 (1957) 832.

SOME FEATURES OF THE REFRACTORY METALS*

L. NORTHCOTT

War Office, Armament Research and Development Establishment, Fort Halstead (Great Britain)

(Received December 11th, 1960)

SUMMARY

After reviewing all the high melting point metals, it is concluded that for engineering purposes the question of cost and availability limits the field to the four metals niobium, tantalum, molybdenum and tungsten. As these four metals have the b.c.c. structure, the significance of this and the factors affecting the ductile-to-brittle transition are discussed. The study of the alloy behaviour shows these metals to be mutually soluble but intermetallic compounds are formed with other metals. Reference is made to the excellent properties of the 35% rhenium alloys. A brief review of the oxidation properties of the four metals and their alloys suggests that protective coatings will be required where oxidising conditions are present. Reference is made to mechanical properties and ingot preparation and the paper concludes with some comments on future developments.

INTRODUCTION

It may be worth while first of all considering the reasons for having a symposium on these four metals. We know that Ta is in use as a corrosion-resistant lining in chemical plant and a W alloy known as heavy metal has applications dependent on its high density for balance weights and as bomb containers for radioactive metals. Apart from these room temperature applications the four metals have several properties in common and the chief one is that all have a high melting point. In view of the present requirements in the field of metals for high temperature use in engines, high speed aircraft and missiles it is this aspect which renders these four metals of current interest. There are, however, other metals having high melting points and Fig. 1 is a global view of the Periodic Table showing all metals having a melting point

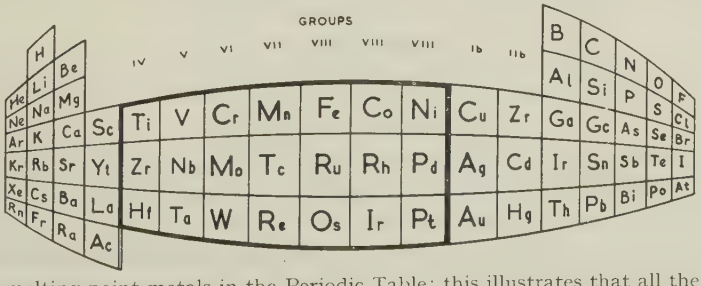

Fig. 1. High melting point metals in the Periodic Table: this illustrates that all the high melting point metals are transition elements; that m.p. increases in each of these groups with increasing at. no.; and that, apart from rare and costly elements, Nb, Ta, Mo and W are profitable subjects for study.

* Prepared by Dr. NORTHCOTT for the Conference on Niobium, Tantalum, Molybdenum and Tungsten held at the University of Sheffield, September, 1960.

approaching 2000°C or above. The metals in Group Va and VIa are the only metals of high melting point having a b.c.c. structure, the remaining metals being in the f.c.c. or h.c.p.

Reference to the Periodic Table shows why the particular order was chosen in the list of metals providing the subject of this symposium, *i.e.* Nb is in the second long series and Ta in the third of Group 5A and similarly Mo and W are in Group 6A also in order of the second and third long series. Fig. 2 shows EPPRECHT's diagram[2] of the

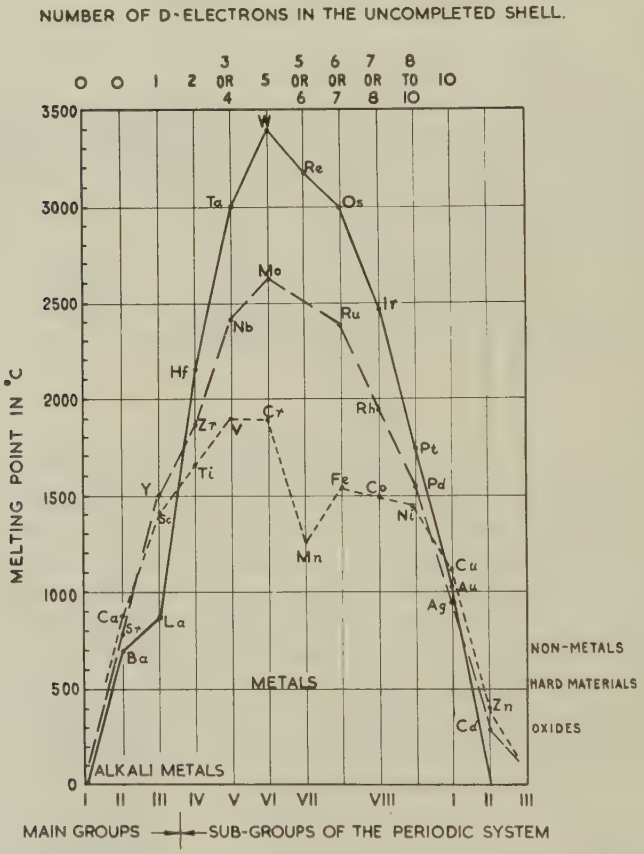

Fig. 2. Melting point of metals and their positions in the Periodic Table of the elements.

variation in melting point among the transition metals in the long series of the Periodic Table, from which it will be seen there are about a dozen metals having quite high melting points. These twelve can be split up into two groups of six on two grounds (a) crystal structure already referred to above and (b) availability and cost. Fig. 3 shows the metals listed in order of decreasing melting point together with their crystal structures, from which it will be seen that six metals, W, Ta, Mo, Nb, V and Cr, *i.e.* the metals in Groups Va and VIa, have the b.c.c. structures whereas the remaining six have either the f.c.c. or h.c.p. structures. Although it is doubtful whether engineers are the least bit interested in this aspect, it is one of fundamental importance

to metallurgists, who have found that the b.c.c. structure brings with it one or two unfortunate metallurgical properties which I propose to refer to at some length later on.

METAL	MELTING POINT °C	CRYSTAL STRUCTURE
TUNGSTEN	3380	b.c.c.
RHENIUM	3170	c.p.h.
TANTALUM	2996	b.c.c.
OSMIUM	2700	c.p.h.
MOLYBDENUM	2620	b.c.c.
NIOBIUM	2468	b.c.c.
RUTHENIUM	2450	c.p.h.
IRIDIUM	2443	f.c.c.
HAFNIUM	2220	c.p.h.
RHODIUM	1960	f.c.c.
VANADIUM	1860	b.c.c.
CHROMIUM	1850	b.c.c.

Fig. 3. Melting points and crystal structures.

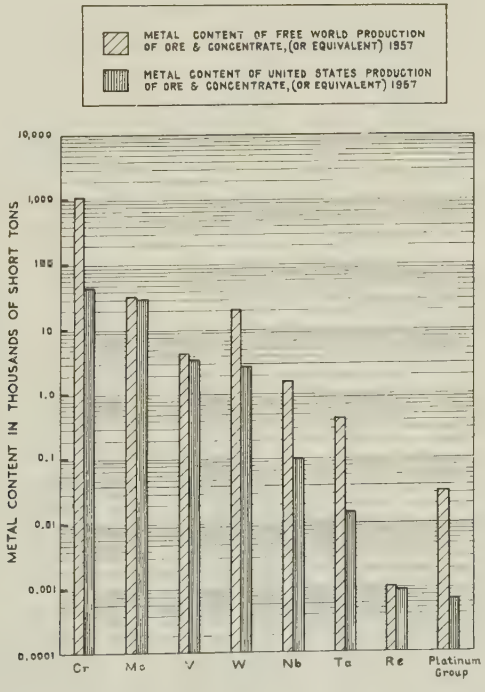

Fig. 4. Free world production and U.S.A. production of Cr, Mo, V, W, Nb, Ta, Re and the Pt group metals in 1957.

On the question of availability Fig. 4[2] is an extract of an MAB graph plotted on log scale of the free world and U.S.A. production of some of these metals. The total availability of the platinum group metals is of the order of 30 tons/year; rhenium is in still

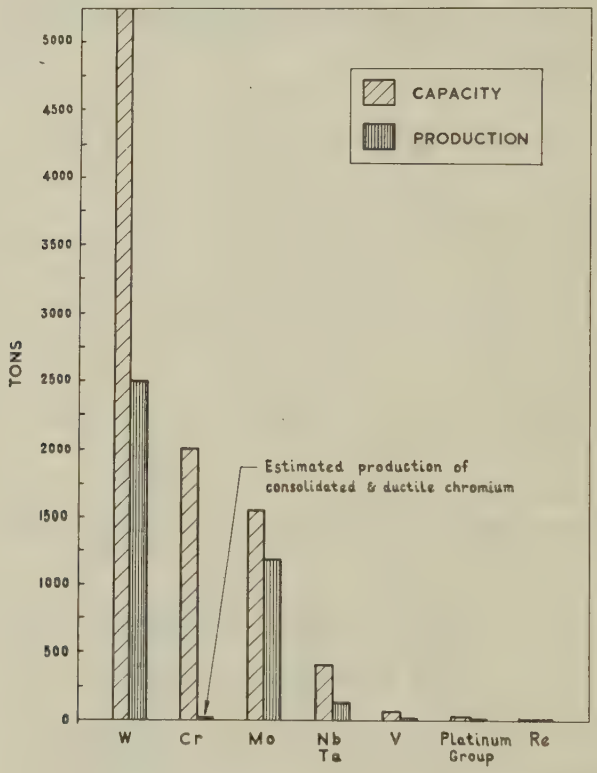

Fig. 5. U.S.A. production and capacity for first reduction metal (tons/year utilising domestic and imported concentrates).

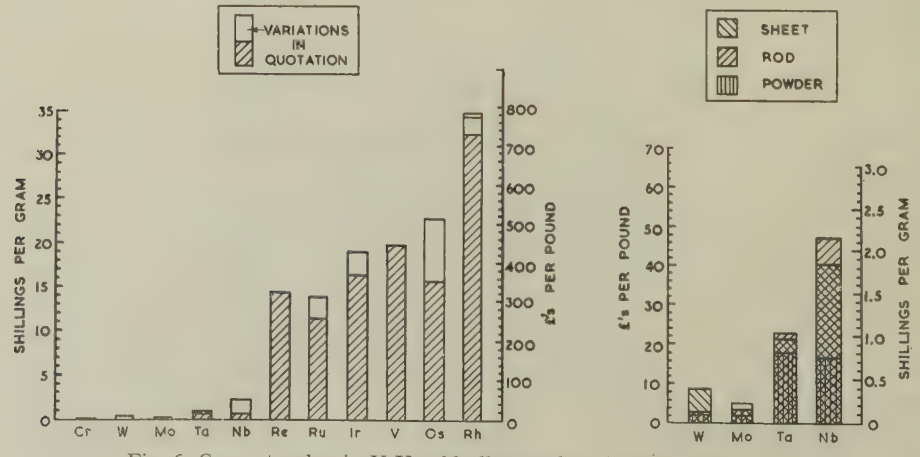

Fig. 6. Current value in U.K. of bulk samples of individual metals.

shorter supply with about 10 tons potential availability, the current production being from half to one ton/year. Fig. 5[3] shows U.S.A. production and capacity. From this it will be seen that the capacity for V and the precious metal group and rhenium tends to rule these out of account where extensive quantities are likely to be required. The current consumption of alloys for gas turbine blades alone runs into thousands of tons/year.

In addition to availability, some account should also be taken of the cost of the different metals and Fig. 6 shows the current value in the U.K. of bulk samples of individual metals. Attention is drawn to the exceptionally high prices for the precious metals, rhenium and vanadium; in addition Nb and Ta, whilst much cheaper, are many times more costly than Mo and W. As far as the future is concerned this picture may be pessimistic for niobium since new deposits of a rich pyrochlore ore which is claimed to be free from tantalum, have recently been found in Brazil. At the present time, however, the main supplies of niobium still come from the Ta–Nb Columbite ores.

Bearing in mind the low availability and exceptionally high cost for engineering applications, there is justification in deleting metals not in groups 5A and 6A, leaving six metals, V, Nb, Ta, Cr, Mo and W and if we delete two of these having melting points much below 2000°C, namely V at 1885°C and Cr at 1875°C, we are left with Nb, Ta, Mo and W; the bulk of the remainder of this paper will be devoted to these four metals only.

DUCTILE AND BRITTLE TRANSITION

The majority of the metallic elements form one of the three lattice structures, face-centred cubic, body-centred cubic or close-packed hexagonal. The refractory metals we are now considering have the body-centred cubic structure.

The difference in behaviour between the body-centred cubic on the one hand and the face-centred cubic metals on the other needs to be emphasised since the consequences of this structural difference form one of the governing factors in determining the extent to which the high temperature metals may be employed for engineering purposes in the high temperature field.

The characteristic behaviour of the body-centred cubic and, to a lesser extent, the close-packed hexagonal metals, as the testing temperature is decreased, is the transition from the ductile to the brittle condition within a narrow temperature range, indicated by a large decrease in energy absorption accompanied by cleavage fracture. The temperature of this transition is not a fixed attribute of the material but is raised by increasing the rate of strain or triaxiality of loading, and is also affected by composition as governed by alloy additions and the presence of impurities as well as by the heat treatment and fabrication history.

The three features of engineering importance of the body-centred cubic metals are:

(a) The proportional increase of the yield point, maximum stress and hardness with drop in temperature is very much greater than that of the face-centred cubic metals, especially at some well defined temperature. Fig. 7 shows the effect of temperature on yield stress; Ni as a f.c.c. metal is included for comparison.

(b) The embrittlement (the reduction in tensile elongation and reduction of area) at low temperature taking place at the same time as (a) (see Fig. 8), here again although the b.c.c. metals undergo a sharp drop in ductility; this does not happen with the f.c.c. metals.

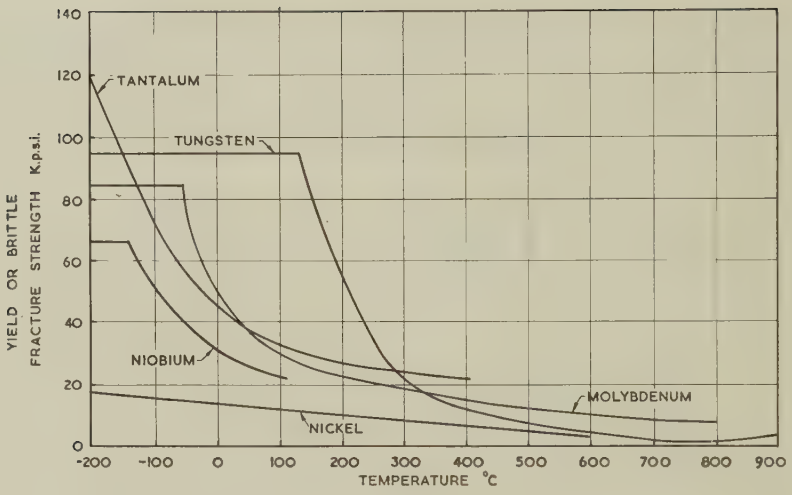

Fig. 7. Effect of temperature on yield strength.

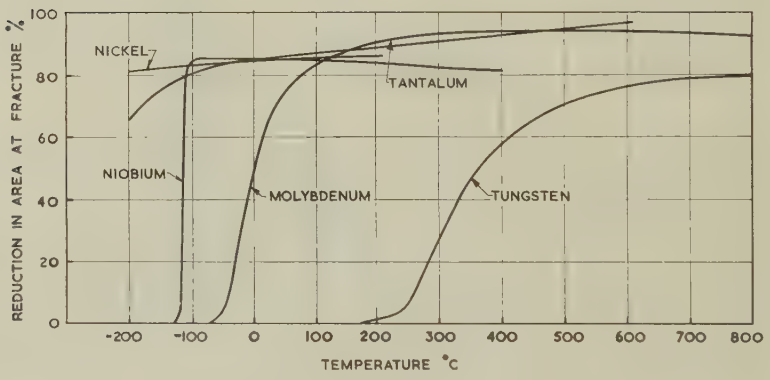

Fig. 8. Effect of temperature on ductility.

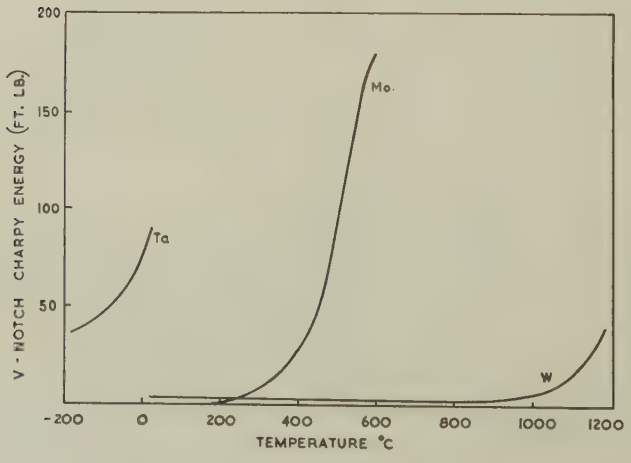

Fig. 9. Effect of temperature of the notch-impact energy of some b.c.c. metals.

(c) The pronounced tough-to-brittle transition in the notched-bar impact test (see Fig. 9). Note that Ta still retains a high impact value even at the lowest temperature but is showing some signs of a drop. In the tensile test whereas the face-centred cubic metals retain their ductility, and the values for yield point and ultimate tensile strength are increased only by about 50% as the temperature drops from say room temperature to −250°C the body-centred cubic metals lose their ductility and their tensile values increase by a factor of from 2 up to as much as 10.

One picturesque way of looking at the behaviour of the b.c.c. as compared with the f.c.c. metals is given by the Ludwig–Davidenkov–Orowan hypothesis shown in Fig. 10. As the b.c.c. metals have their yield point increased so much with drop in

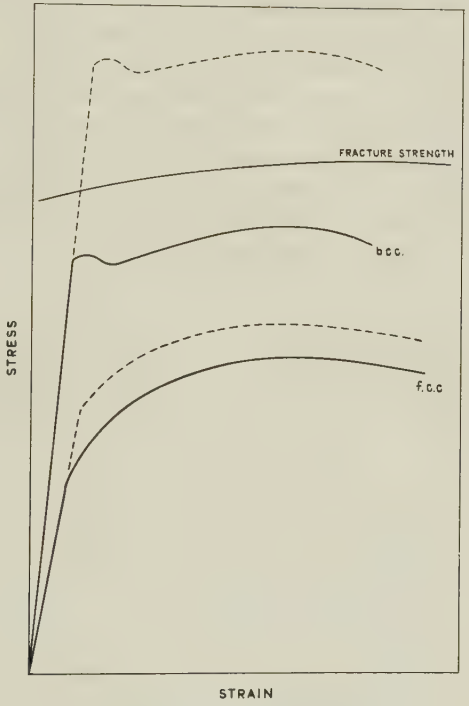

Fig. 10. Ludwig diagram.

temperature, the stage may be reached when the yield point curve cuts the fracture stress curve, in which case brittle fracture with little plastic deformation occurs. It would appear that the increase in yield of the f.c.c. metals with drop in temperature is so slight that it never reaches the fracture strength, so that considerable deformation always occurs before failure takes place.

I still regard the Ludwig theory as a useful concept in arguing about brittle failure effects but it is possible that the fracture stress determined experimentally may no longer be regarded as an inherent characteristic of the material. PETCH and others have demonstrated that the experimental failure stress varies with grain size in precisely the same way as does the yield point and hence both stress characteristics

must be influenced by the same processes. It is now argued that the true fracture stress characteristic of the material is never realised because of internal stresses associated with piled-up dislocations. This argument does not differ from that involving allowances for the stress concentration at the end of Griffith cracks, though it does make it difficult or impossible to estimate the true fracture stress of the material.

Why the sharp increase in yield strength of the b.c.c. metals with drop in temperature? This is generally explainable in terms of the Cottrell locking of impurities. COTTRELL has discussed the interaction of dislocations with impurity atoms and showed that solute atoms, especially interstitial solutes like carbon, nitrogen and oxygen will segregate into the vicinity of dislocations and anchor them. By definition, if the dislocation is difficult to move, the material cannot show ductility even in single crystal form. Since the movement of solute atoms is associated with thermal fluctuations which decrease with reduced temperatures, higher external forces are required to pull the dislocations away from their atmospheres at low temperature; in other words, lowering the temperature results in stronger anchoring forces and results in raising the yield strength. Dislocations pile up at grain boundaries, imperfections, sub-grains and other barriers until the local stress concentration builds up sufficiently to initiate further plastic flow or to initiate micro cracks if the fracture stress is exceeded. Brittle fracture occurs when the energy of propagation of the micro cracks is less than that of plastic deformation.

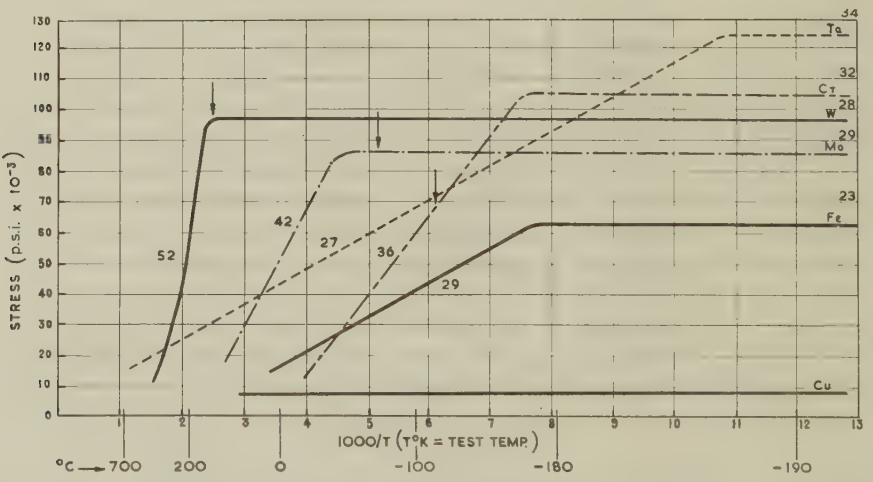

Fig. 11. Curves of stress *vs.* $1/T$ for some b.c.c. metals.

It has also been suggested that the greater tendency to brittle failure in b.c.c. metals arises from the possibility of both screw and edge dislocations interacting simultaneously with solute atoms to form highly condensed atmospheres with correspondingly localised high internal stresses.

In b.c.c. metals the interaction energy, and consequently the temperature range over which the rapid increase in yield strength is observed, depends upon the elastic modulus and the extent of the lattice expansion caused by the solute atoms. LOUAT[4] in a modification of the Cottrell hypothesis, plots yield stress and brittle fracture stress

as appropriate against the reciprocal of the test temperature for those metals in which Cottrell locking has been observed. Fig. 11 shows that the shape of the stress against $1/T$ curves for b.c.c. metals is as predicted by theory. In all cases stress varies linearly with $1/T$ over a range of temperature, whilst at higher and lower temperatures the stress is approximately invariant. Again, in agreement with theory, the slopes of the linear parts of the curve increase with increasing values of Young's Modulus, which are 27, 29, 36, 42 and $52 \cdot 10^6$ p.s.i. for tantalum, iron, chromium, molybdenum and tungsten respectively. A plot for copper is also included and it will be seen that the yield stress of copper is relatively insensitive to changes in temperature over the same range.

The difference in the behaviour of the different metals may be explained on the assumption that the atoms in metallic lattices behave as elastic spheres and that there are thus smaller holes available in b.c.c. lattices for accommodating interstitial impurities, such as carbon, oxygen and nitrogen, than in f.c.c. lattices. B.c.c. metals which show a low transition temperature or none at all, *e.g.* sodium potassium, and to a lesser extent tantalum, are those with large lattice parameters, and thus with the largest holes. The Group Va metals have relatively low transition temperatures because of their relatively high solubility for interstitials. The Group VIa metals have higher transition temperatures, chromium and tungsten being highest and molybdenum lowest. The effect of working the metals below the temperatures at which recrystallisation or rapid diffusion occurs results in a lower transition temperature and a flattening out of the transition curve, as shown in Fig. 12 in the case of molybdenum. Such deformation not only increases the number of dislocations but breaks the original dislocations away from their impurity atmospheres. Needless to say, if the temperature is raised sufficiently to allow rapid diffusion to occur, then the earlier condition is regained.

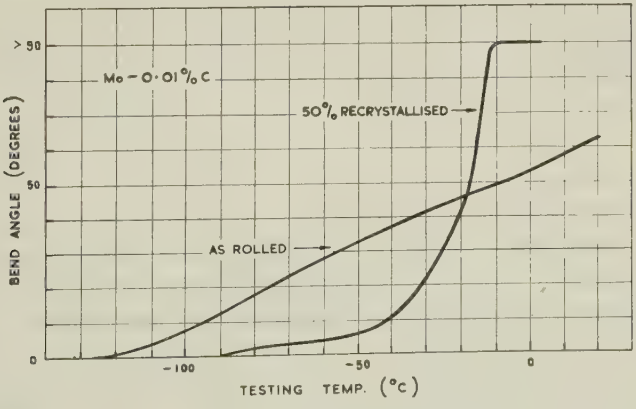

Fig. 12. Transition curves for Mo–0.01% C.

What can be done about lowering the tough–brittle transition in the b.c.c. metals, apart from mechanically working them? Since the interstitial elements play such an important part, an obvious solution to the problem is to remove them and work on these lines as has recently been described. BELK[5] in A.R.D.E. has studied the prop-

erties of purified Mo, using the electron bombardment floating zone melting technique. This yields zone-refined bars of single crystals. The ductility of the purified crystals is such that they can be rolled at room temperature without cracking. The tensile properties of the rods are shown in Fig. 13. The carbon content of the low carbon sample is about 0.001% with no evidence of yield point, whereas the yield point returns at about 0.004% carbon. Impact tests on unnotched as-grown $\frac{1}{4}$ in. diameter rods are shown in Fig. 14 and the pronounced lowering of the transition

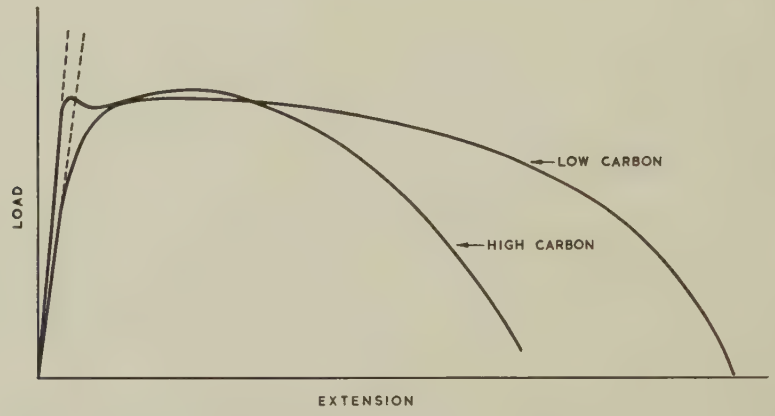

Fig. 13. Stress–strain curves for both ends of a zone-refined crystal.

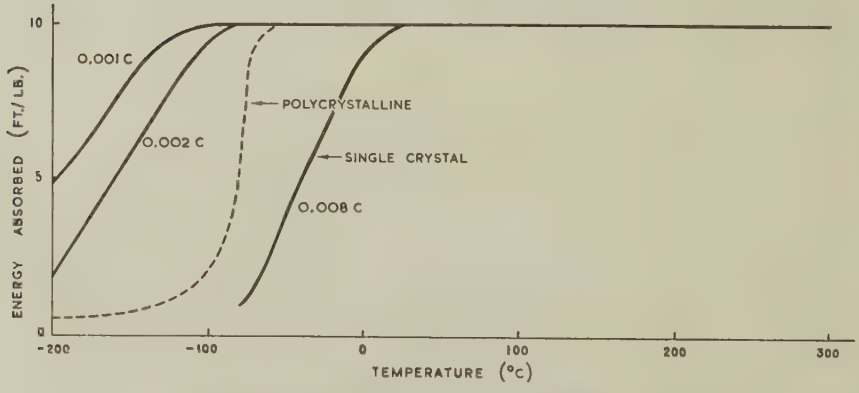

Fig. 14. Impact tests in single and polycrystalline molybdenum.

temperature with a reduction in carbon content will be seen; the full lines represent single crystals, the dotted line polycrystalline samples. Similar results for Nb are shown in Fig. 15[6], it being noted that the powder metallurgy material was machined to a sub-standard size; although it would be expected that the total energy absorbed by the thinner specimen would be lowered, the transition temperature would be relatively unaffected. Results obtained in A.R.D.E. on powder metallurgy samples of Nb are similar, only low values of impact being observed. WULFF[7] has examined the

tensile properties of wire drawn from zone-refined rods of molybdenum and found no discontinuous yielding, nor any semblance of a sharp yield point, and there was substantial ductility in tensile tests at —78° and —196°C.

Extensive work has been carried out, in U.S.A. in particular, to show that oxygen is also detrimental in Mo, and studies of solid state purification and of impregnating purified Mo with oxygen have confirmed that low oxygen samples have much lower

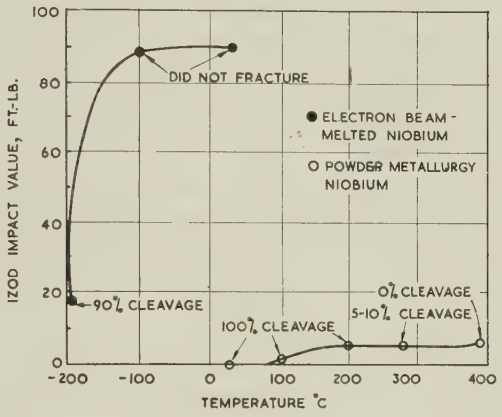

Fig. 15. Effect of temperature on the impact properties of recrystallised Nb: ●, electron beam melted Nb; O, powder metallurgy Nb.

transition temperatures. In this connection it may be worth while pointing out that Mo with as little as 0.0001 wt. % of oxygen contains about $3.8 \cdot 10^{17}$ oxygen atoms/ml and it is interesting to compare this with a possible value of 10^{18} dislocations/ml. Much work has been carried out to nullify the harmful effects of carbon and oxygen by stabilising additions, and significant improvements have been obtained.

All these results point to the fact that the refractory metals we are discussing have an inherent ductility but show an exceptionally high sensitivity to embrittlement by additions of certain impurities.

ALLOYING BEHAVIOUR

The end phases in many binary alloy equilibrium diagrams consist of primary solid solutions which possess the same crystal structure as their respective parent metals and thus constitute the first stage in the promotion of alloys. It has now been established fairly conclusively for the binary systems of certain univalent and divalent metals that the formation of the more common, substitutional type of these phases is dependent on the relative atomic-size, valency and electronegativity of the solute and solvent metals.

These principles (proposed by HUME-ROTHERY and co-workers) have received general recognition for the established alloys of certain normal metals of Groups I and II, but their application to the binary systems of the metals of higher valency and atomic number, in particular to those of the transition metals, has been restricted. This is attributable to the imperfect understanding of both the valency of these complex metals and its effect on solid solubility.

Despite the uncertainty as to the valency factors involved, the principles governing the formation of primary solid solutions in the solvent-rich binary alloys of the refractory metals may be considered.

In the theoretical study of the refractory metals alloys with other metals, the following conclusions may be drawn:

(1) Elements in Groups 1 and 2 are characterised by maximum deficiency of valency electrons, hence irrespective of size factor, negligible solubility may be expected.

(2) The close electron similarity of the transition metals suggests that extensive solubility will be obtained in those systems in which the solute element has a b.c.c. structure. The similarity is greatest for the elements in Groups V and VI, namely V, Nb, Ta, Cr, Mo and W, all of which are b.c.c. and have favourable size factors. These elements form complete solid solutions with each other at all temperatures and Fig. 16[8] shows the variation in lattice parameters. This has the effect of a general increase in hardness towards the middle of the diagram and a decrease in conductivity. Fig. 17 shows the hardness curve for Mo–Ta alloys and Fig. 18 the hardness and conductivity curves for the W–Nb alloys.

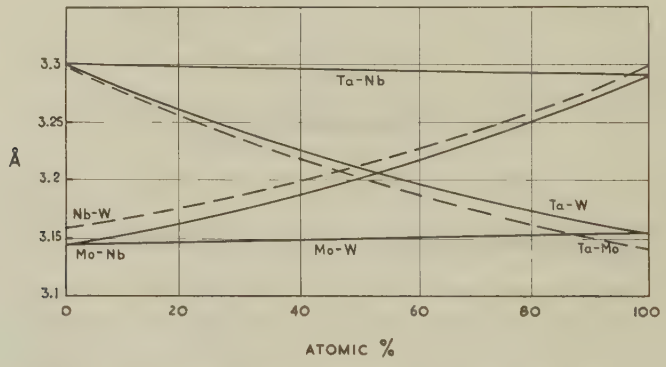

Fig. 16. Lattice parameters of alloys of W, Nb, Ta and Mo[3].

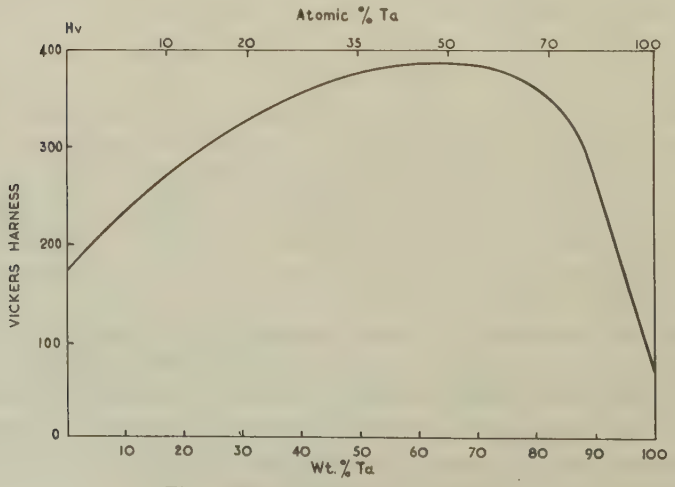

Fig. 17. Hardness of Mo–Ta alloys.

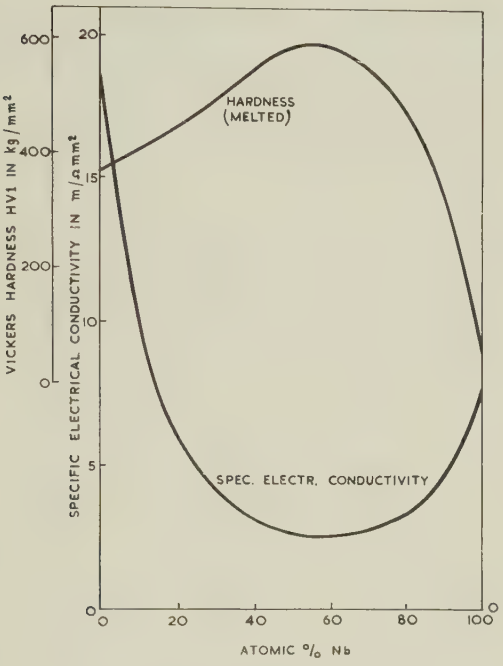

Fig. 18. Hardness and specific electrical conductivity of W–Nb alloys.

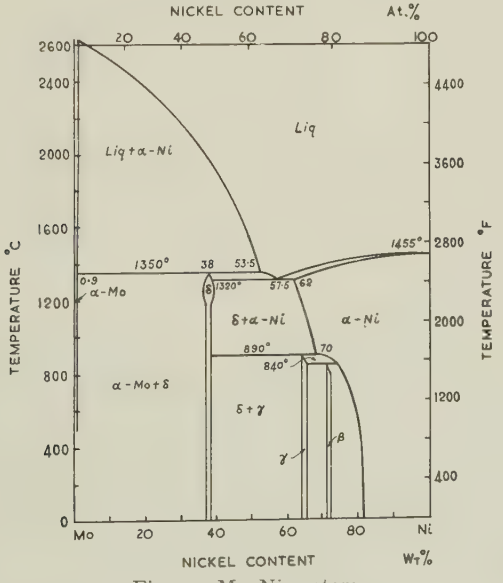

Fig. 19. Mo–Ni system.

(3) The 9 transitional elements of Group 8 have favourable size factors but in each period the difference between the electron structure of the metal and that of the refractory metal increases with increasing atomic number. Accordingly, the solid solubilities of the elements may be expected to diminish with increasing atomic number in

each period and to be greatest in the second long period. In considering the alloys in Mo, for example, the maximum solubility decrease is predicted from about 10% iron, to 3% cobalt and to 0.9% Ni; Fig. 19 shows the Mo–Ni diagram. As would be expected, there is no gradual change in mechanical properties or hardness across the diagram though the compounds show high hardness but are quite brittle.

Mo- or W–rhenium alloys

The effect of large additions of rhenium to molybdenum and to tungsten is quite remarkable. In these two systems the influence of rhenium is similar, though it is more marked with molybdenum and here attention will be concentrated on the Mo–Re system (Fig. 20). The initial discovery of the ductility of the 35 at. % Mo–Re alloy was due to GEACH AND HUGHES[9] and the results have been amply confirmed and

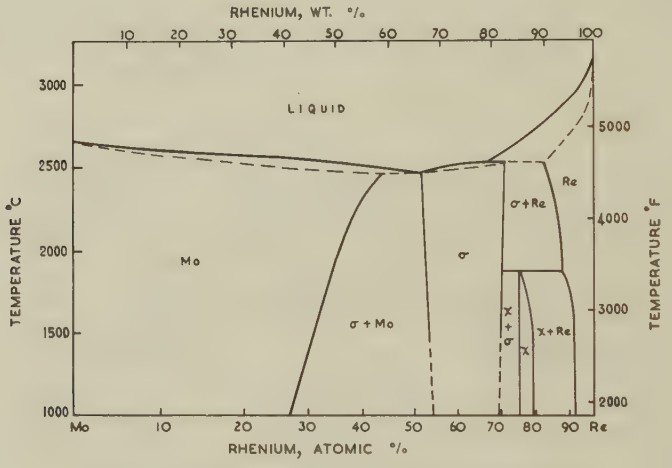

Fig. 20. Equilibrium diagram of Mo–Re system.

extended by others, notably JAFFEE, SIMS AND HARWOOD[10,11]. The alloy is about three times as hard as molybdenum (Fig. 21) and yet is capable of undergoing deformation greater than 90% even at room temperatures. As GEACH AND HUGHES point out, high strength with such ductility is unknown in other materials.

The main reason for this ability to deform is the extensive mechanical twinning of which the alloy is capable. The twinning system is not known, but there is no reason to suppose that it is other than the (112) [111] system characteristic of other body-centred cubic metals and induced in molybdenum by CAHN by compression impact at —196°C. JAFFEE AND SIMS show that twinning, as might be expected, increases with the strain rate and with decrease in temperature from room temperature to —50°C. Increasing the temperature to 250° reduces twinning. The yield point increases sharply as the temperature is dropped from 250°C to room temperature. Such an increase in yield usually signals the onset of brittle fracture but twinning supervenes and the yield again drops with the lowering of the temperature to —50°C.

Thus the twinning characteristic of this system occurs just in the right conditions to extend the ductility when the ordinary slip mechanism is beginning to fail and the ability to twin maintains the ductility over a wide temperature range.

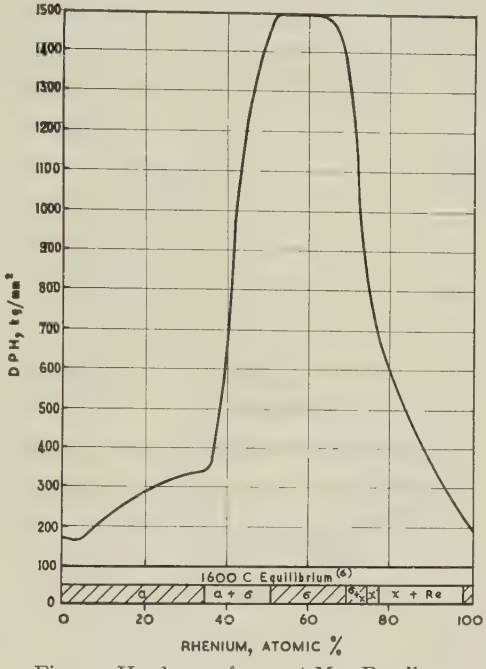

Fig. 21. Hardness of as-cast Mo–Re alloys.

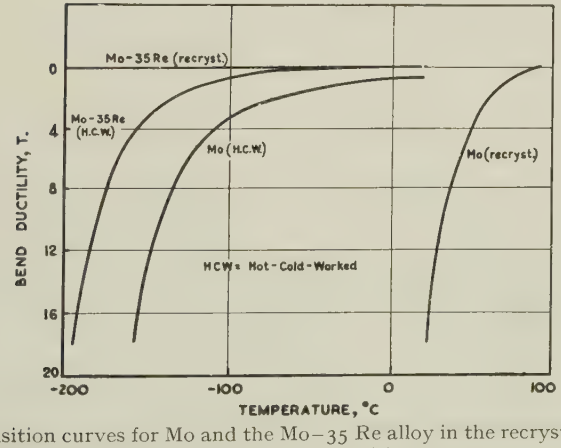

Fig. 22. Bend–transition curves for Mo and the Mo–35 Re alloy in the recrystallised and hot-cold-worked (H.C.W.) conditions.

This is equivalent to saying that the transition temperature is lowered and Fig. 22[11] shows this to be so. Another way of looking at the same picture of the lowering of the transition temperature by rhenium is shown in Fig. 23[11] where the tensile characteristics are plotted against composition. One would not suspect from the elongation

curve, the outstanding ductility of the 35 at. % Re alloy, for the elongation is less than that of pure molybdenum. The reduction of area, however, shows a pronounced increase. Most notable is the drop in yield in spite of the rise in the tensile strength.

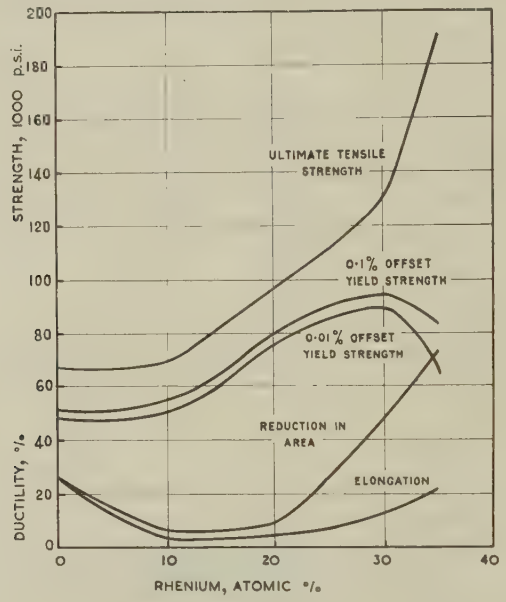

Fig. 23. Room-temperature tensile properties of Mo–Re alloys.

Such a fall in yield ratio is just what is needed on the Ludwig–Orowan–Davidenkov hypothesis already mentioned to ensure a low transition temperature. The extent of the fall in yield ratio (more strictly in this country the proof stress ratio) is shown in Fig. 24.

This picture of the twinning does not exhaust the interest of the Mo–Re system. The twinning is, in fact, only becoming important at comparatively low temperatures. The high strength of the 35 at. % alloy without embrittlement must be largely ascribed to new conditions in the oxide phase. Molybdenum is embrittled by oxygen. The oxide phase accumulates in the grain boundaries where its low dihedral angle promotes the formation of brittle grain boundary films. In the rhenium alloy, however, the picture is changed. The surface tension of the oxide at some critical stage in the cooling is increased. The oxide occurs as globules in the grains as well as at the boundaries and in this condition it has no appreciable embrittling effect.

Jaffee and Sims show that a mixed oxide of molybdenum and rhenium, or a rhenium molybdate, is formed and to this they attribute the high tolerance of the Mo–Re alloy to oxygen. It might perhaps be worth noting that their rhenium contained 0.005% Mg, 0.010% Al and 0.007% Si. These elements in the 35 at. % (50/50 wt. %) alloy would stoichiometrically account for 100 p.p.m. oxygen and could have a considerable influence on the oxide phase.

Even allowing for this effect of the oxide form, the high temperature deformation of the Mo–Re alloy is quite interesting. Niobium and tantalum in Group V are text-

book examples of metals that may be worked extensively without great increase in hardness. Molybdenum and tungsten in Group VI work harden to an appreciable extent while rhenium in Group VII suffers from work hardening to an extent that appears to be greater than that of any other metal. It is surprising, therefore, that the 35 at. % Mo–Re alloy has a work-hardening curve nearer to those of the Group V elements than to either of its constituents. This may be explained by assuming that Re acts in the Mo–Re alloy as a source of extra electrons which are capable of entering

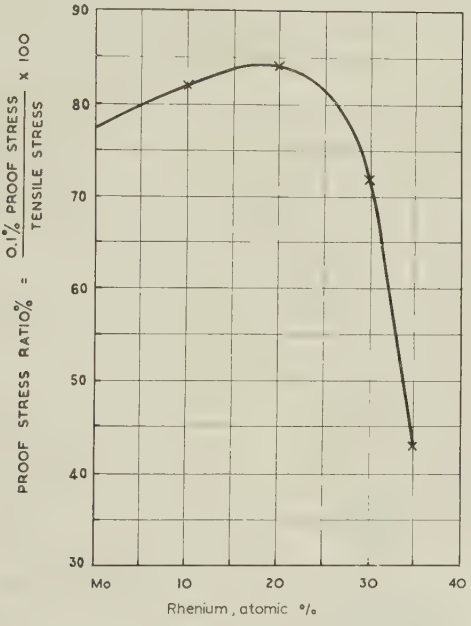

Fig. 24. Proof stress/tensile strength ratio of Mo–Re alloys.

the non-bonding orbitals and coupling with electrons which would otherwise, in pure molybdenum, have contributed to the metallic bonding. The whole complex is thus reduced to a system greatly resembling the Group V elements. This is an interesting example of the ideas of electron structure first discussed by PAULING.

Rhenium is also noteworthy for retaining its strength at high temperatures and this characteristic is passed on to the alloy, which is as strong at high temperatures as the well known molybdenum–$\frac{1}{2}$% titanium alloy and maintains its hardness to even higher temperatures. It might, of course, be argued that this result is to be expected since rhenium melts at 3180°C and the melting point of the Mo–Re alloys is maintained at a high level. Comparisons with other additions, for example nickel, where a 1% addition brings the solidus down to 1350°C, gives the impression that finding adequate substitutes for rhenium would not be easy. It is therefore unfortunate that even if more rhenium were available, the cost of the 35 at. % Mo–Re alloy would be almost prohibitive, being a hundred or more times greater than molybdenum.

As a final word on the Mo–Re and W–Re systems, it should be said that rhenium itself oxidises badly and does nothing to improve the other metals in this respect.

OXIDATION AND PROTECTION

One of the main disadvantages of the refractory metals we are considering is that none of them is sufficiently resistant to oxidation for use in air at high temperatures for any extended period. At 2000°F (about 1100°C) the oxidation rates of Nb, Ta and W are of the same order, whereas Mo is about ten times as bad, with Re and V about the same. Fig. 25[12] shows the relative scaling rates of the 4 metals at 2000°F. In addition, Nb and Ta may absorb oxygen and nitrogen with considerable embrittling effect.

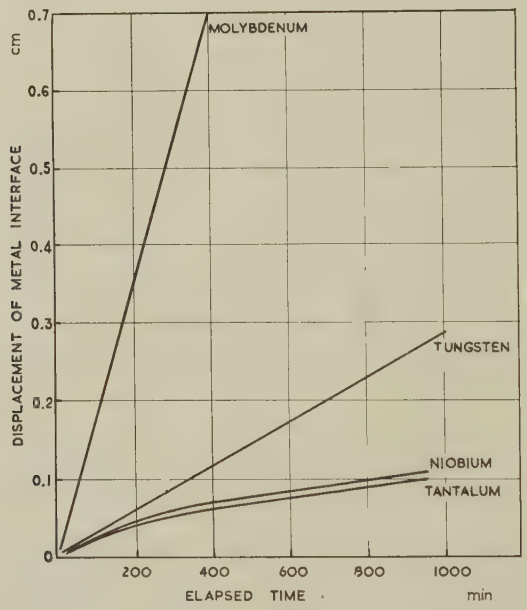

Fig. 25. Scaling of Mo, W, Ta and Nb displacement of metal interface after various times in air at 2000°F.

The metal having the highest oxidation resistance is Rh (see Fig. 26)[13]. This does not, of course, mean that the base metals are unusable. Apart from vacuum or inert gas conditions there is sometimes little free oxygen in combustion products and useful lives may be obtained. Even reducing the partial pressure of oxygen can help; thus it has been shown that at 175,000 ft. Mo would oxidise at only 1/100 of its rate at sea level.

The ideal way of improving the outlook would be to produce oxidation-resistant alloys. Although some success has been obtained by alloying, even to reducing oxidation rates by a factor of 50 or more, there seems to be no prospect of an alloy of any of the four major refractory metals that would not require a coating or other form of protection. The reason for this lies partly in the absence of any general useful theory to guide the development of oxidation-resistant alloys.

The factors that have to be considered are largely the properties of the oxides, *e.g.* melting and boiling points. Mo and, to a lesser extent, W have volatile oxides. Above 450°C an oxide smoke may be seen arising from Mo and this becomes noticeable at 700°C. W follows the same course at a temperature about 200° higher. The oxides of Nb and Ta are adherent but are not very protective. Oxygen can diffuse through

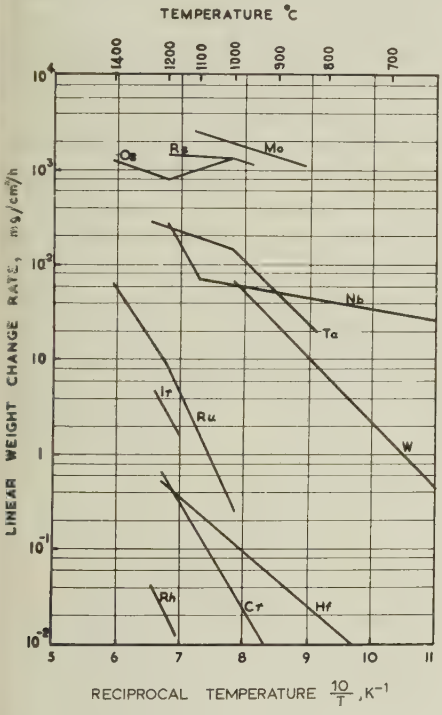

Fig. 26. Oxidation of the refractory metals.

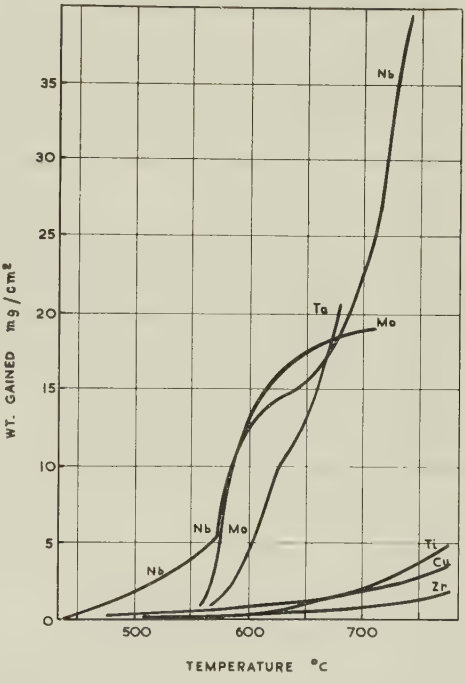

Fig. 27. Oxidation curves for various metals under conditions of a linear temperature increase of 5°C/min and constant oxygen pressure of 100 lb./in.² absolute.

the oxide and become absorbed by the metal for some depth ahead of the oxide front. The hypothesis put forward by PILLING AND BEDWORTH in 1923 is of little use in considering the refractory metals. Although the specific volume of the oxide is greater than that of the metal, it is too much so and the oxide coating that might otherwise offer protection, cracks and spalls while relatively thin. The oxidation therefore follows a linear rather than a parabolic law. Fig. 27[14] shows the oxidation curves under conditions of a linear temperature increase of 5°C/min and constant oxygen pressure of 100 lb./in.² absolute. The curves show the difference in the oxidation behaviour between those metals which oxidise according to linear law (Ta, Nb and Mo) and those (copper, titanium and zirconium) which oxidise according to the parabolic law — those in which a protective film is formed. The main objects in improving oxidation resistance have been to ameliorate these awkward oxide properties. The specific volume of the oxides in the case of Nb and Ta has been reduced by adding small anions such as Mo and V with good effect on the oxidation resistance. The oxides

are semi-conductors of the anion-deficient type and conduction can be reduced by adding ions of higher valency. Attempts to stabilise the volatile oxide of Mo have been only partially successful. It can be converted to a stable Ni molybdate by adding large amounts of Ni to the alloys. However, the effect of Ni in lowering the solidus has already been mentioned, the recrystallisation temperature is badly affected, the high Ni/Mo alloys are very brittle and the Ni molybdate has an allotropic change with a big volume difference and spalls badly when cooled through the change temperature.

Probably the most effective and generally useful method of improving oxidation by alloying is to add a metal with a greater free energy of oxide formation. Such an element would be expected to oxidise preferentially and might form new oxides or complex oxides with better protective properties. This is the theory behind the improvement in the oxidation resistance of Nb by the addition of titanium or zirconium and also accounts for the improvements sometimes found by the addition of silicon, aluminium or chromium. But contradictory results have been obtained and Fig. 28 shows the oxidation rates of binary alloys of W and chromium in dry oxygen at 1200°C. It is probable therefore that the design of oxidation-resistant alloys will always be difficult and will usually have to be related to particular test conditions.

We must consider that the refractory metals will almost always require some form of coating to help them resist oxidation but this need not be considered too terrible

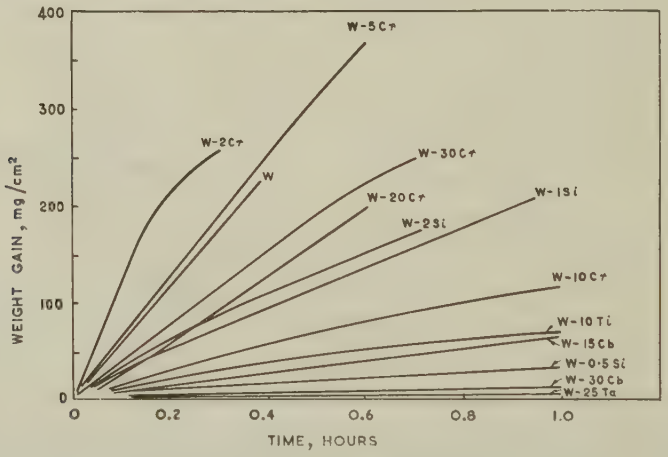

Fig. 28. Oxidation rates of W and some binary alloys in dry oxygen at 2000°C.

a thought because even such alloys as the Nimonics are frequently coated and the practice is becoming more common for high temperature work.

Most of the work on coatings has been carried out on Mo, Nb has received some attention, Ta and W hardly any. Many types of coatings have been studied; clad coatings of the nickel/chromium type have been applied to Mo, and sprayed coatings of the silicon–aluminium–chromium type are used on a number of metals. Vapour phase deposition, particularly of chromium and of silicon have been used. Dipped coatings of aluminium have been investigated and some success has been claimed for zinc coatings on Nb up to 950°C. Complex Ni–Cr plating has given promising results

and ceramic coatings have also been used. It is common, moreover, for more than one of these treatments to be applied. As an indication of the results achieved, alternate Ni–Cr electro-deposits followed by Al_2O_3 have successfully withstood 1100 h at 1100°C with daily cycling. The recent modifications to the W2 Chromalloy silicon diffusion treatment on Mo are said to have overcome its former lack of resistance to thermal shock, making it potentially a most useful coating. Vapour diffusion has the advantage of offering the best possible chance of completely protecting complex shapes. Session III is devoted to the subject so little more need be said here.

An interesting development has been reported in the U.S.A.: Universal Cyclops Steel Co. in co-operation with O.N.R. has built a process laboratory filled entirely with purified argon, in which the refractory metal ingot may be forged, rolled and heat treated without the fear of oxygen or nitrogen pick-up or loss of metal by oxidation.

MECHANICAL PROPERTIES

As there is to be a separate session dealing with the mechanical properties of the individual refractory metals and their alloys, it will suffice here to give the overall picture as I see it. In conformity with the usual patterns, strength falls off as the temperature is raised but all four metals have significant strength at high temperatures and the strength can be more than doubled by the addition of suitable alloying daditions. Most of the work on the development of high strength alloys has been

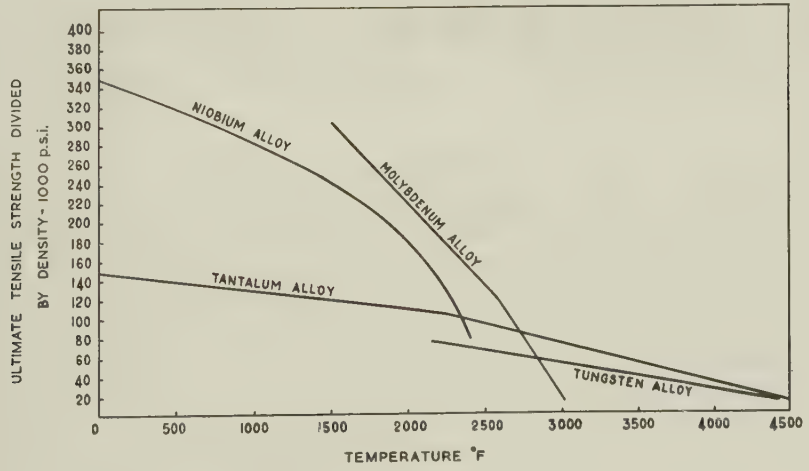

Fig. 29. Tensile strengths of strongest known refractory alloys.

carried out on Mo and Nb, relatively little on Ta and W, and there is plenty of scope here.

Fig. 29[15] shows typical curves for the best of the different base metals alloys, from which it will be seen that at temperatures up to about 2700°F Mo and Nb alloys are much superior to Ta and W, whereas above this temperature W and Ta have higher strengths, so that the choice of material depends upon the temperature of operation. Fig. 30[15] shows the relative strengths of the different metals and alloys at two selected temperatures. The open blocks give the values of tensile strength divided

by the density in lb./in.^{3}. Attention is drawn in particular to the high values for Mo to which quite small alloying additives have been made. The creep properties of the alloys in general follow the same order as tensile strengths.

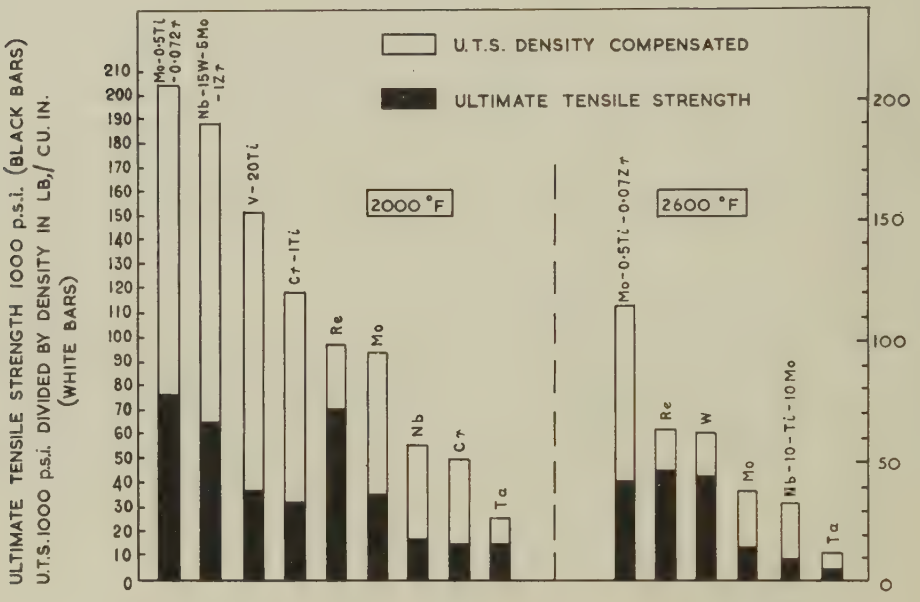

Fig. 30. Tensile strengths of refractory metals at two temperatures.

INGOT PREPARATION

As the melting point of these metals is above the working temperatures of the common refractories, the classical method of obtaining bulk samples was by the powder metallurgy technique. This is still used, particularly for materials in the lamp and electronic fields, and modifications have been introduced to enable larger and larger samples to be obtained. Billets weighing over 100 lb. can be prepared using hydraulic pressing followed by sintering but the capabilities are limited owing to the high pressures and large sintering furnaces required for really large billets. The development of the consumable arc melting process, particularly by Climax for Mo, using a water-cooled copper mould, gave a boost to the melting method and ingots in the ton range are now regularly produced. There is a third method now coming into use known as electron beam melting and equipment is available for melting ingots up to 10 in. diameter. Each process has its advantages and drawbacks and a brief review of these seems desirable in order to provide a background against which to view the papers of the Conference.

For components of small size, strip and wire, the powder metallurgy technique has much to recommend it, as the equipment is relatively simple and inexpensive, the product is fine grained and generally readily workable.

Molybdenum and tungsten are not significantly purified by vacuum sintering and as they are not susceptible to hydrogen embrittlement they are normally sintered in

hydrogen and no substantial purification accompanies the process. Niobium and tantalum on the other hand absorb large quantities of hydrogen and are therefore sintered in vacuum. The sintering is also relied upon for the removal of carbon and oxygen by the carbon monoxide reaction. The two impurities are deliberately balanced in the charge. Because of the long times involved the degassifying reaction can go far towards completion. For niobium and tantalum, in contradistinction to molybdenum and tungsten, the purity of the final product is better than can be produced by arc melting.

A difficulty which obviously arises is that sintering must be controlled to allow time and opportunity for the escape of gases. This can be an important matter when dealing with large pieces. Aside from this degassing problem the other sintering problems are mainly those of attaining adequate pressure for compacting large powder masses and of ensuring adequate and uniform density in the product.

The process next most used industrially is that of arc melting, and for molybdenum especially this is relied upon for the larger pieces, and has some advantage in purity of product over the powder metallurgy method. This is largely because in vacuum arc melting the carbon monoxide reaction although not reducing to equilibrium will reduce oxygen to an acceptable value. Inert atmosphere arc melting, however, must rely on sufficient purity in the initial material.

There are two main types of arc melting furnaces — the first is the Climax type in which powder is fed into the machine and pelleting, sintering and arc melting features are successively conducted, the larger melting units using multiple electrodes. The more conventional arc melting unit starts off with pressed or baled billets which after melting are remelted in a larger furnace. This double melting results in ingots of higher purity but our A.R.D.E. experience with the Climax type furnace is that double melting of Mo is unnecessary.

The chief disadvantage of arc melting is the characteristic crystal structure of the ingots produced in the water-cooled copper moulds. The large grain together with the residual impurities make ingot breakdown an uncertain operation unless extrusion is used.

The third process, only recently coming into prominence, is electron beam melting. With this method there is more elasticity in the time factor than in arc melting and with better vacuum conditions it is the method most easily able to produce a pure product. The high vacuum necessary — better than 10^{-4} mm Hg — has its disadvantages since metal may be lost by evaporation. This is particularly the case with any alloy having a higher vapour pressure than the parent metal. Electron beam melting, even more than arc melting, gives an ingot structure consisting of long columnar grains which cause considerable difficulty in fabrication. It has been reported that in an endeavour to overcome this embarrassment niobium is being electron beam melted to purify the partially sintered pressed powder electrodes and that the electron beam melted ingots are subsequently arc melted with the introduction of alloys.

FUTURE DEVELOPMENTS

Awaiting exploration is a large field in alloy development. Wide ranges of composition in the niobium-base alloys have been investigated; as for molybdenum, excellent properties have been obtained with quite small additions and there is clearly room

for more work here. Relatively little work has been done on the development of Ta-base and W-base alloys. With all the metals, possibly the most urgent requirement lies in the development of improved oxidation-resistant coatings since there are already available alloys having sufficiently good properties to warrant their immediate practical application if only the bogey of oxidation could be laid.

Except for the highest temperatures, there is little to choose between the best of the Mo- or Nb-base alloys, Mo having the advantages of higher strength and modulus of elasticity, niobium being better from the welding standpoint, though the welding and fabrication of some of the complex Nb alloys are more difficult than that of the pure metal.

For the highest temperature ranges, W has the advantage of having the highest melting point but this in itself raises difficulties in melting and alloy preparation and its high transition temperature increases the difficulty of fabrication. From the fabrication standpoint tantalum is to be preferred but its application is likely to be limited owing to its low availability and high cost.

A big step forward would be indicated by a considerable improvement in the supply position of rhenium; while this is in such short supply and the price is so high, advantage cannot be taken of the remarkable properties of the Mo–Re and W–Re alloys, variations of which offer the optimum both in properties and fabrication. It is not to be expected that any one alloy will be suitable for all purposes but the choice will depend upon the particular application and the service to which the component is subjected.

REFERENCES

1 R. Kieffer, K. Sedlatschek and H. Braun, *J. Less-Common Metals*, 1 (1959) 20 (diagram according to Epprecht).
2 *Materials Advisory Board Report of the Committee on Refractory Metals, Washington, D.C.*, (1959).
3 *Materials Advisory Board Report of the Committee on Refractory Metals, Washington, D.C.*, (1959).
4 N. Louat and H. L. Wain, *A.R.L./Met. Rept. 32, Australia*, (1959).
5 J. A. Belk, *J. Less-Common Metals*, 1 (1959) 50; *Nature*, 184 (1959) 897.
6 R. T. Begley, *W.A.D.C. Tech. Rept. 57-344*, (1958).
7 H. S. Spacil and T. Wulff, *The Metal Molybdenum*, American Society for Metals, Cleveland, Ohio, 1958, p. 262.
8 H. Bückle, *Metallforschung*, 1 (1946) 53.
9 G. A. Geach and J. E. Hughes, *Plansee Proc.*, (1955) 245.
10 R. I. Jaffee, C. T. Sims and J. J. Harwood, *Plansee Proc.*, (1958) 380.
11 R. I. Jaffee and C. T. Sims, *Battelle Mem. Inst. Tech. Rept.*, (1958) April.
12 A. B. Michael, *A.I.M.E. Conference, Buffalo*, (1958).
13 R. I. Jaffee, *Battelle Mem. Inst., D.M.I.C. Memorandum, 40* (1959).
14 J. P. Baur, D. W. Bridges and W. M. Fassell, *J. Electrochem. Soc.*, 102 (1955) 490.
15 *Materials Advisory Board Condensed Report*, (1959).

THE AMMONOLYSIS OF SOME HEXACHLOROZIRCONATES

J. E. DRAKE AND G. W. A. FOWLES

Dept. of Chemistry, The University of Southampton (Great Britain)

(Received December 12th, 1960)

SUMMARY

Several hexachlorozirconates (M_2ZrCl_6, M = NH_4, Rb and Cs) have been prepared and allowed to react with liquid ammonia. The ammonolysis resembles that of zirconium(IV) chloride in that the ammonobasic zirconium(IV) chloride $ZrCl_3(NH_2)\cdot xNH_3$ is formed, but the enhanced solubility of the product when made from diammonium hexachlorozirconate is considered to result from complex formation. The tensimetric results suggest the initial formation of complex salts $M_2[ZrCl_5(NH_2)]$.

INTRODUCTION

When halides of the transition metals in their higher valency states are ammonolysed, the ammonobasic metal halide can usually be isolated because of its insolubility in liquid ammonia[1,2]. The product is often soluble in concentrated solutions of ammonium and potassium halides in liquid ammonia, however, and this solubility has been considered to arise through the formation of complex anions, *e.g.*, $TiX_4 \xrightarrow{NH_3} TiX(NH_2)_3 + 3\ NH_4X \longrightarrow (NH_4)_2[TiX_4(NH_2)_3]$.

Further information about the possibility of such complex formation in the titanium(IV) halide–ammonia systems has been obtained by a study of the ammonolysis of hexachloro- and hexabromotitanates[3], and this work has now been extended to some of the analogous zirconium systems.

EXPERIMENTAL

Preparation of hexachlorozirconates

Rubidium and caesium salts. Zirconium(IV) chloride (0.05 g mol) was dissolved in the minimum amount of concentrated hydrochloric acid and the solution saturated with hydrogen chloride gas at 0°C; to this was added a similar solution of the alkali metal chloride (0.1 g mol). The hexachlorozirconate, which precipitated immediately, was filtered, washed with anhydrous ethanol and kept *in vacuo*. Found (for Rb salt): Zr, 19.3; Cl, 44.9%. Calculated for Rb_2ZrCl_6 : Zr, 19.2; Cl, 44.8%. Found (for Cs salt): Zr, 15.9; Cl, 37.4%. Calculated for Cs_2ZrCl_6 : Zr, 16.0; Cl, 37.3%.

Sodium and potassium salts. Attempts to make these salts were unsuccessful. Sodium and potassium chlorides were insufficiently soluble in concentrated hydrochloric acid, and only grossly hydrolysed products were obtained from dilute acid.

Ammonium salt. This was prepared using 8–10 *N* hydrochloric acid, and was washed successively with a 5% solution of thionyl chloride in ether, and ether. Found:

Zr, 26.4; Cl, 62.6; N, 8.4%. Calculated for $(NH_4)_2ZrCl_6$: Zr, 26.8; Cl, 62.6; N, 8.2%.

Miscellaneous salts. The hexachlorozirconates of cobalt(II), copper(II), nickel(II), tin(II) and zinc(II) could not be made either from hydrochloric acid or ethanol saturated with hydrogen chloride[4].

Analyses for zirconium, chlorine and nitrogen were carried out as described previously[5]. Rubidium and caesium were estimated by difference.

Reactions of hexachlorozirconates with liquid ammonia

The reactions of the ammonium, rubidium and caesium salts with liquid ammonia were examined by the standard washing and tensimetric methods[1]. In the washing runs the salt was allowed to react on the filter pad with excess of anhydrous ammonia at —35°C, and the product was then filtered and washed with liquid ammonia until no further soluble material could be extracted — this usually took about six washes of 50 ml each. Excess of ammonia was removed from both the soluble products by prolonged pumping, and the residues were hydrolysed with dilute sulphuric acid and analysed.

All tensimetric experiments were carried out at —36°C, and the products were subsequently decomposed by heating *in vacuo* at regular temperature intervals.

Diammonium hexachlorozirconate. The results of washing experiments are given in Table I, and those of the tensimetric runs are plotted in Figs. 1 and 5.

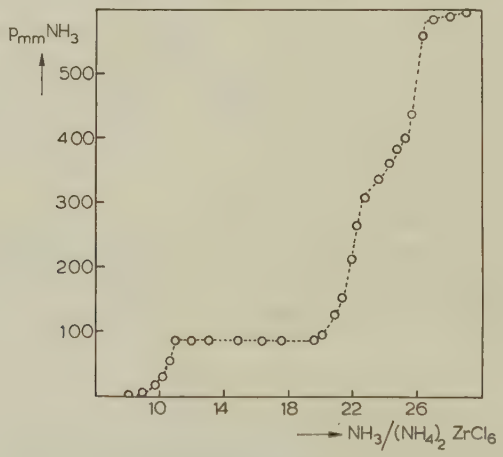

Fig. 1. $(NH_4)_2ZrCl_6$–NH_3.

Dirubidium hexachlorozirconate. Although the insoluble product was washed six times, it was nevertheless contaminated with rubidium chloride, which has only a

TABLE I

PRODUCTS OF THE $(NH_4)_2ZrCl_6$–NH_3 REACTION

Run No.	*Insoluble*				*Soluble*	*Pumping temp. (°C)*	*Soluble Zr / Insoluble Zr*
	%Zr	*%Cl*	*%N*	*Zr : Cl : N*	*Zr : Cl : N*		
1	33.0	38.4	23.1	1.00 : 2.99 : 4.56	1.00 : 9.76 : 11.2	20	0.7
2	39.2	45.5	12.0	1.00 : 2.98 : 1.99	1.00 : 5.31 : 6.90	100	0.9

modest solubility in liquid ammonia. Found (for insoluble): Zr, 24.2; Cl, 37.0; N, 14.2; Rb, 21.5% corresponding to Zr : Cl : N : Rb = 1.00 : 3.93 : 3.83 : 0.95. Assuming all the rubidium is present as the chloride, this gives a ratio Zr : Cl : N = 1.00 : 2.98 : 3.82 + 0.95 RbCl. The soluble portion contained a mixture of ammonium chloride, rubidium chloride and some zirconium compound (about 20% of the total zirconium used initially). In a second experiment the insoluble product was pumped at 20°C for 12 h and then successively at 40°, 100° and 150°C for 2 h, any liberated ammonia being trapped and estimated; from an analysis of the final product the composition of the intermediate stages was determined. Found (for the 150°C product): Zr, 22.8; Cl, 39.7; N, 5.1; Rb, 31.3% corresponding to 1.46 RbCl + Zr : Cl : N = 1.00 : 3.02 : 1.46. The following ratios were evaluated for the intermediate temperatures: 100°C, Zr : Cl : N = 1.00 : 3.02 : 2.18; 40°C, Zr : Cl : N = 1.00 : 3.02 : 4.22; 20°C, Zr : Cl : N = 1.00 : 3.02 : 4.71.

The results of the tensimetric experiments are plotted in Figs. 2 and 5.

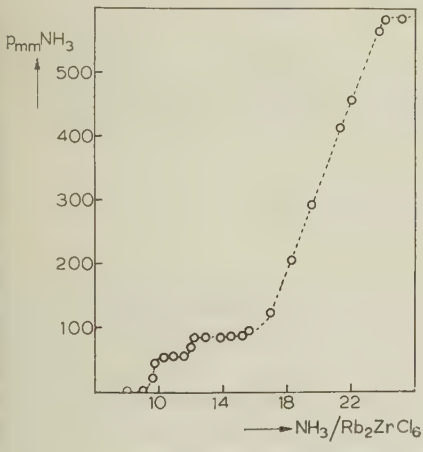

Fig. 2. Rb_2ZrCl_6–NH_3.

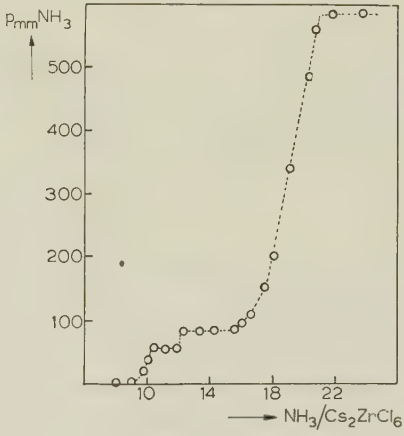

Fig. 3. Cs_2ZrCl_6–NH_3.

Dicaesium hexachlorozirconate. This resembled the rubidium salt in its reaction with ammonia except that almost no zirconium was found in the soluble portion. The results of the washing runs are summarised in Table II, and those of the tensimetric experiments are plotted in Figs. 3 and 5.

TABLE II

PRODUCTS OF THE Cs_2ZrCl_6–NH_3 REACTION

Run No.	*Insoluble*					*Soluble*	*Pumping temp.*	*Pumping time*
	%Zr	*%Cl*	*%N*	*%Cs*	*Zr : Cl : N + xCsCl*	*Zr : Cl : N : Cs*	*(°C)*	*(h)*
1	32.6	40.1	15.8	8.1	1.00 : 3.00 : 3.16 + .17	—	20	20
							60	6
2	32.5	42.4	5.8	17.6	1.00 : 2.99 : 1.24 + .37	0 : 2.00 :	20	20
						1.12 : 1.02	150	6
3*		—			1.00 : 3.15 : 4.59 + .96	—	20	12
		—			1.00 : 3.15 : 3.69 + .96		50	2
	22.8	36.4	7.2	32.0	1.00 : 3.15 : 2.07 + .96		100	2

* Product analysed after final heating to 100°C, and composition of intermediate stages calculated from this analysis and determination of liberated ammonia.

Rubidium and caesium chlorides. Tensimetric experiments confirmed BILTZ's observation[6] that these halides do not form ammoniates.

DISCUSSION

The insoluble product obtained from the ammonolysis of diammonium hexachlorozirconate appears to be identical with that obtained from zirconium(IV) chloride[7], namely $ZrCl_3(NH_2)\cdot xNH_3$; after the products were heated *in vacuo* to 100°C, $x = 1$ in each case. The marked difference in the two reactions is that for the hexachlorozirconate reaction between 70 and 90% of the total zirconium content was found in the soluble products, whereas with zirconium(IV) chloride the figure was around 10%. It is probable that the hexachlorozirconate first dissolves in ammonia and then undergoes a solvolysis similar to that found for reactions with aliphatic amines[4].

$$(NH_4)_2ZrCl_6 \xrightarrow{NH_3} (NH_4)_2[ZrCl_5(NH_2)] + NH_4Cl \qquad (1)$$

The complex should be quite soluble, and most of it will dissolve on washing, but some will remain behind on the filter pad, and when the excess of ammonia is removed this solid complex is likely to break down into ammonium chloride and the ammonobasic zirconium(IV) chloride:

$$(NH_4)_2[ZrCl_5(NH_2)] \longrightarrow 2\ NH_4Cl + ZrCl_3(NH_2) \qquad (2)$$

On addition of further ammonia the ammonium chloride will dissolve, and this solution will take up a small part of the ammonobasic zirconium(IV) chloride (as in the ammonolysis of zirconium(IV) chloride), but some residue will remain. Thus the ammonobasic zirconium(IV) chloride which is formed from zirconium(IV) chloride is likely to be highly polymeric and is broken down into a soluble complex only with difficulty, but the complex is "preformed" from the hexachlorozirconate and comparatively little "insoluble zirconium" is to be expected.

When the hexachlorozirconate–ammonia reaction is examined tensimetrically at —36°C (*cf.* Fig. 1), a univariant step is found corresponding to the characteristic dissociation pressure of ammonium chloride triammoniate. The length of this step shows that three moles of ammonium chloride are present in the ammonolysis mixture, and this can be interpreted in either of two ways. Firstly, we can consider that one zirconium–chlorine bond is ammonolysed as in the washing experiments, but that under the tensimetric conditions (with no excess of liquid ammonia) the complex breaks down giving three moles of ammonium chloride (eqns. 1 and 2). Alternatively, we can suppose that three zirconium–chlorine bonds are ammonolysed (eqn. 3), and that the complex formed is stable under the tensimetric conditions.

$$(NH_4)_2[ZrCl_6] \longrightarrow (NH_4)_2[ZrCl_3(NH_2)_3] + 3\ NH_4Cl \qquad (3)$$

We favour the first postulate, because it is in agreement with the washing runs, and, moreover, fits in nicely with the previously reported results of the ammonolysis of the hexahalogenotitanates[3]. Thus with diammonium hexachlorotitanate two titanium–chlorine bonds were ammonolysed, and some 90% of the product was soluble.

The rubidium and caesium salts appear to be ammonolysed to the same extent as the ammonium salt, although the insoluble ammonobasic zirconium(IV) chloride is contaminated by the rubidium and caesium chlorides. Apart from this contamination, however, the products are identical with that obtained from zirconium(IV) chloride as a comparison of their thermal decompositions shows (Fig. 4). The lower solubility

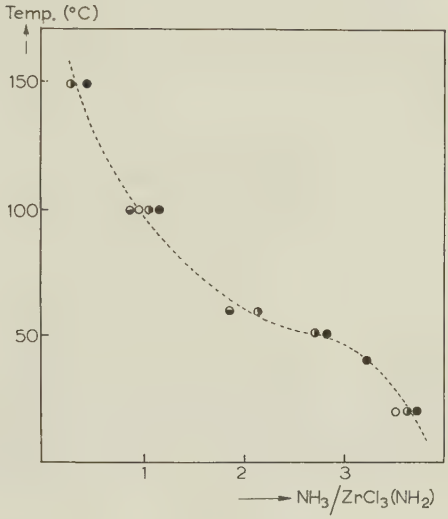

Fig. 4. Thermal decomposition of insoluble products: ○, $(NH_4)_2ZrCl_6$; ●, Rb_2ZrCl_6; ◑, Cs_2ZrCl_6; ◒, $ZrCl_4$.

of the complex salts of these heavier alkali metals is to be expected. In the tensimetric studies one mole of ammonium chloride is found in each case. Rubidium and caesium chlorides do not form ammoniates[6], so that the experiments cannot prove whether or not the simple chlorides are present as a result of the decomposition of the complex. If the product is a mixture of ammonium chloride, the alkali metal chloride, and the ammonobasic zirconium(IV) chloride, however, then the tensimetric curves should be identical with that found for the zirconium(IV) chloride–ammonia system. They differ in that there is a univariant portion at 57 mm, which occurs neither with zirconium(IV) chloride nor with diammonium hexachlorozirconate. Furthermore, there appears to be no trace of the higher metastable ammoniate found with zirconium (IV) chloride around 450 mm; some trace of this is observed in the diammonium hexachlorozirconate–ammonia system. A reasonable explanation for these observations might be that the alkali metal complexes are rather more stable than the ammonium ones, and remain stable at low temperatures, so that the extra ammoniate which is found is associated with the complex (eqn. 4).

$$M_2ZrCl_6 + \text{excess } NH_3 \rightarrow M_2[ZrCl_5(NH_2)] \cdot 2\ NH_3 + NH_4Cl \cdot 3\ NH_3 \qquad (4)$$

These complexes presumably break down on heating, in view of the similarity of their decompositions to those of the products formed by the diammonium salt (*cf.* Fig. 5).

Valuable information on the stability of the complexes would be provided by tensimetric studies on hexachlorozirconates of metals whose chlorides themselves form characteristic ammoniates, but unfortunately we have been unable to prepare such salts.

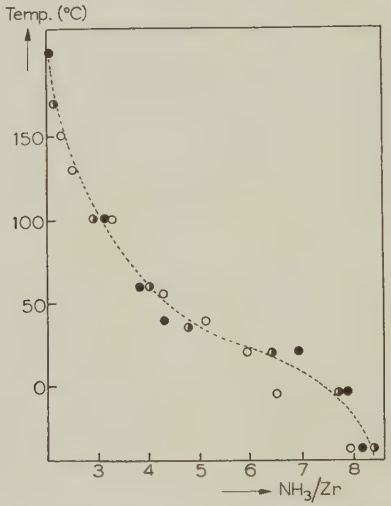

Fig. 5. Thermal decomposition of tensimetric mixtures: ○, $(NH_4)_2ZrCl_6$; ●, Rb_2ZrCl_6; ◑, Cs_2ZrCl_6.

ACKNOWLEDGEMENTS

We thank the Esso Petroleum Company for a maintenance grant (J.E.D.), and the Titanium Manufacturing and Alloy Company for supplying zirconium(IV) chloride.

REFERENCES

1 G. W. A. Fowles and F. H. Pollard, *J. Chem. Soc.*, (1953) 2588.
2 G. W. A. Fowles and D. Nicholls, *J. Chem. Soc.*, (1958) 1687.
3 G. W. A. Fowles and D. Nicholls, *J. Inorg. & Nuclear Chem.*, in the press.
4 J. E. Drake and G. W. A. Fowles, *J. Inorg. & Nuclear Chem.*, in the press.
5 J. E. Drake and G. W. A. Fowles, *J. Chem. Soc.*, (1960) 1498.
6 W. Blitz, *Z. anorg. Chem.*, 130 (1923) 93.
7 J. E. Drake and G. W. A. Fowles, *J. Less-Common Metals*, 2 (1960) 401.

A STUDY OF THE EFFECT OF COOLING RATE ON THE DECOMPOSITION OF THE γ-PHASE IN URANIUM–LOW MOLYBDENUM ALLOYS

R. F. HILLS AND B. R. BUTCHER

Atomic Energy Research Establishment, Harwell, Berks.

AND

J. A. HEYWOOD*

Fulmer Research Institute, Stoke Poges, Bucks. (Great Britain)

(Received December 10th, 1960)

SUMMARY

The transformations that take place when uranium-molybdenum alloys are cooled at various rates from the γ-phase field have been studied for a range of compositions by an end-quenching technique. A number of metastable phases have been observed. A tentative explanation is offered to account for the transformation sequence in each alloy.

INTRODUCTION

Many uranium alloy systems in which there is a high solubility of the solute in the γ-phase, notably uranium–niobium, uranium–molybdenum, uranium–titanium, and uranium–vanadium, exhibit metastable phases at room temperature when quenched from the γ-phase field. These systems have been briefly reviewed by HARDING AND WALDRON[1]. As metastable phases had been observed during earlier work on quenched uranium–molybdenum alloys[2] it was decided to examine the effects of cooling rate and composition on the phases present in uranium-rich alloys of this system. This has been done for alloys containing from 2.5 to 15 at. % molybdenum using an end-quenching apparatus which gave cooling rates varying from direct quenching to radiation cooling. The results have been studied using metallographic, X-ray, and hardness techniques.

EXPERIMENTAL

Materials

The uranium used was Springfields magnesium-reduced billet material, having a total impurity content of approximately 620 p.p.m. Full analysis is given in Table I.

The molybdenum, which was in the form of 0.020 in. sheet, was of 99.98% purity. Throughout the paper at. % refers to the molybdenum contents of the alloys.

Alloy preparation

Alloys were prepared by arc melting under a reduced argon pressure using a tungsten electrode and a water-cooled copper hearth. Each ingot was melted several

* Present address: International Nickel Co. (Mond) Ltd.

times in an attempt to obtain homogeneity. The final ingot was approximately 5 in. long and weighed about 60 g.

TABLE I

URANIUM ANALYSIS

Element	*p.p.m.*	*Element*	*p.p.m.*
C	370	Cu	<5
Fe	85	W	4
Al	11	Ca	<5
Cr	20	Mo	4
Si	10	O	45
Mn	10	N	19
Ni	13	H	4
Zn	6	Cl	2
B	0.04	Co	<2
Cd	<0.02	Li	<0.1
F	15	In	<0.03
Ti	<2	Mg	<2
Pd	<1	Sn	<2
V	<2	Au	<1
P	10	Be	<0.05
Bi	<0.5	Ga	<0.5
Ge	<0.5	Tl	<2
		Rare earths	<0.035

Specimen preparation

All alloys were sealed in evacuated silica tubes and homogenised for 3 days at 950°C, tantalum foil wrapping being used to prevent reaction between the alloys and the silica tubes during heat treatment. They were then swaged at γ-phase temperature to rods of 0.140 in. diameter and cut into 6 in. lengths. One end was then machined to a conical point, whilst the other end was threaded.

Quenching apparatus

The apparatus used was that described by HARDING AND WALDRON[1] wherein the specimen is screwed into a Zircaloy holder, which is suspended by means of a length of Nichrome wire from a short length of fuse wire connected across two terminal points. To drop the specimen, mains voltage is passed through the fuse wire. Two vacuum couplings are employed at either end of the vertical furnace tube, the top one being fitted with the thermocouple and electrical connections in addition to an argon entry tube, and the lower one being fitted with a wire spider which terminates the free fall of the specimen by holding back the Zircaloy block. A positive argon pressure is maintained throughout the experiment, the excess argon being released through a bleed hole in the lower vacuum coupling. All specimens were quenched into mercury at room temperature from 1000°C and the depth of immersion was 0.5 in.

Specimen examination

Metallographic examination. After quenching, the rods were cut into six sections, mounted in cold setting "Marco" resin and ground on silicon carbide papers under lubricant. This was followed first by diamond polishing and then by attack polishing, using rotating terylene cloth pads immersed in a solution of 1 part chromic oxide and 1 part concentrated nitric acid in 2 parts of water containing a suspension of γ-alumina. This treatment gave surfaces suitable for polarised light examination.

Etching was carried out using a 1 : 1 solution of nitric acid and glacial acetic acid.

X-ray examination. All X-ray diffraction work was carried out using a glancing angle technique. A para-focussing 14 cm camera was used, and the solid specimens were positioned so that the low angle diffraction lines were in focus. During the exposure the specimen was rotated about a normal to its surface, and oscillated $\pm 4^\circ$ about an axis in its surface perpendicular to the incident beam. Cobalt $K\alpha$ radiation with an iron filter was used throughout.

Hardness examination. Vickers diamond hardness impressions were made along the length of the rods using a 30 kg load.

RESULTS

2.5 at. % molybdenum–uranium alloy

Metallographic. Under polarised light examination, from the quenched tip to about 2.4 cm along the rod the structure consisted of martensite-like plates showing fine internal markings. These plates were fairly widely spaced and between them there was a finer acicular structure. Polygonal areas of the structure had a different polarising effect and the plates did not cross the polygon boundaries. These polygons presumably show the grain size of the original structure from which the plates had come. Immediately following this was an area wherein fine, ragged α-type grains were observable along the original grain boundaries whilst the matrix was almost irresolvable, as in Fig. 1. The amount of pseudo α rapidly increased until at 2.7 cm from the tip it covered the cross-section completely. No further changes were observed

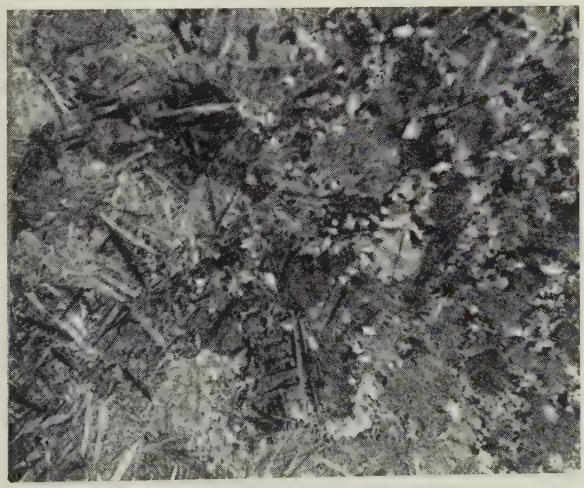

Fig. 1. 2.5 at. % alloy. Transition zone. Polarised light. (× 200)

over the remainder of the specimen length. The structure at the slowly cooled end is illustrated in Fig. 2.

After prolonged etching, structure could be distinguished from 2 cm from the quenched tip to the threaded end of the rod, *i.e.* the structure showing the large plates etched for the last 4 mm of its length, the first 2 cm of the rod being highly resistant

to etching. Under the highest magnification obtainable optically the structure appeared granular, but electron microscopy of replicas taken from this area (Fig. 3) showed that the structure between the plates was of a lamellar nature, although some of the lamellae appeared to be incompletely developed. The structure immediately beyond the last plates was similar to that between the plates although it contained

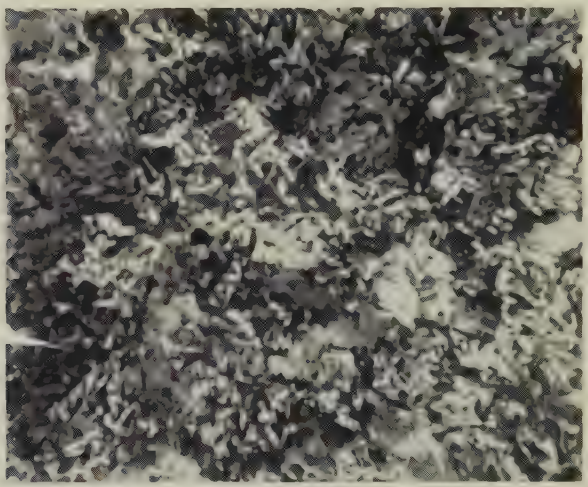

Fig. 2. 2.5 at. % alloy. Slowly cooled end. Polarised light. (× 200)

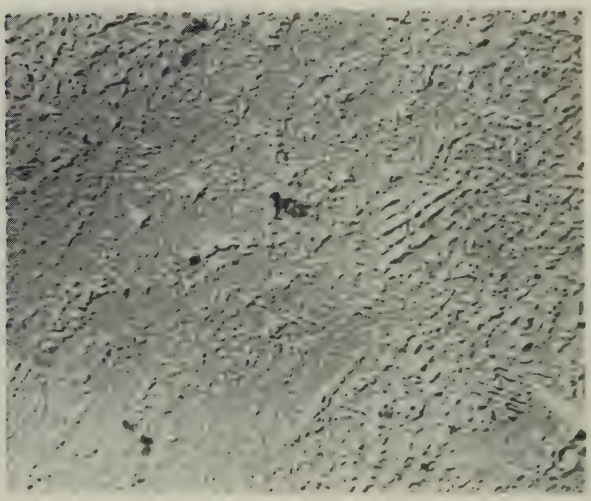

Fig. 3. 2.5 at. % alloy. Structure between plates. (× 8000)

small areas of much coarser lamellae, thought to correspond to the fine pseudo α grains seen in Fig. 1. The coarser lamellar structure increased in extent until it covered the entire specimen. No further changes, other than coarsening of the lamellar structure, were observed over the remainder of the specimen. A typical area at the slowly cooled end is shown in Fig. 4.

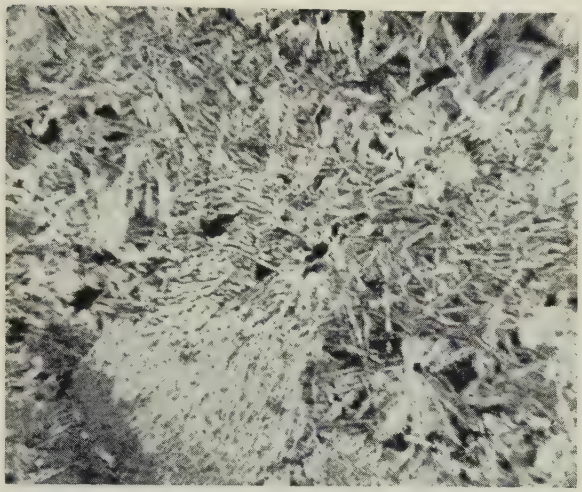

Fig. 4. 2.5 at. % alloy. Etched structure at the slowly cooled end. (× 750)

X-ray and hardness. For ease of reference the X-ray and hardness results have been combined in Fig. 5. At the extreme tip the hardness was 390 V.P.N. increasing fairly rapidly until the transition zone was reached (plate to fine granular structure) and

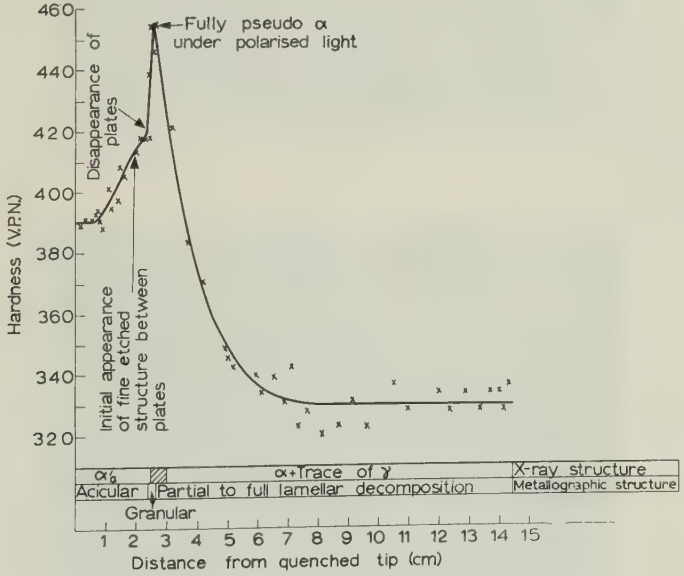

Fig. 5. 2.5 at. % alloy. End-quenched into mercury. Hardness and X-ray results.

thereafter rising rapidly to a maximum of 455 V.P.N. At this point, coincident with the optically detectable lamellar structure, the hardness decreased, reaching a minimum of approximately 330 V.P.N. at 6 cm from the tip, remaining fairly constant for the rest of the length.

X-ray films of the acicular structure showed that the phase in this region was α_a'.

(The terminology used in this report to describe the structures found is that suggested by LEHMANN AND HILLS[3].) The α'-structure although based on the normal orthorhombic α-uranium lattice, had undergone a contraction of the "*b*" parameter compared to the "*a*" and "*c*" parameters*, recognisable by the displacement of the (021) α diffraction line towards the (002) α line. Three cm from the tip the structure was that of α-uranium together with a faint trace of the γ'-phase, the γ'-lines being broad and diffuse. No further changes in the diffraction patterns were detected up to the slowly cooled end of the rod.

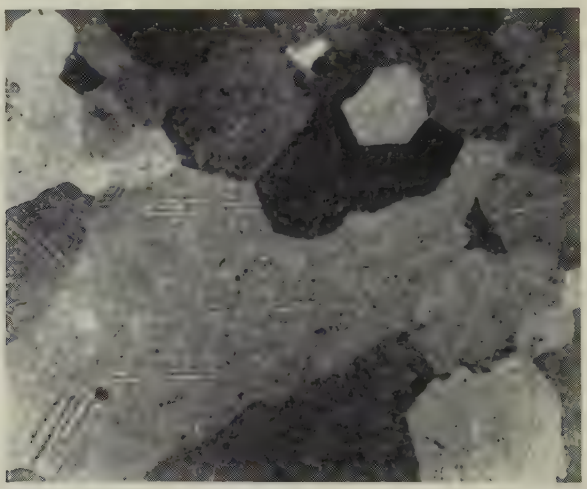

Fig. 6. 5 at. % alloy. Quenched tip. Polarised light. (× 200)

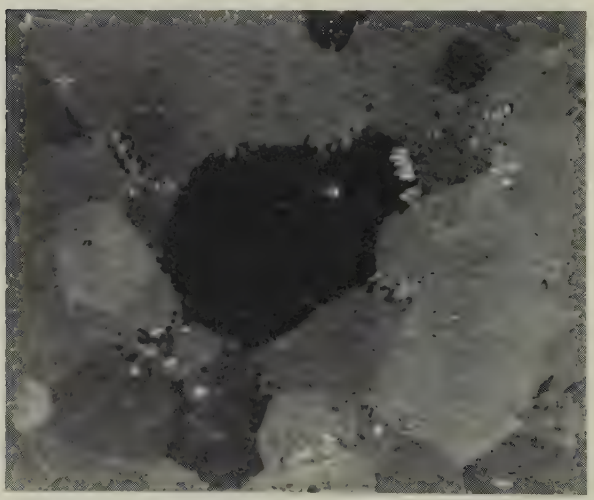

Fig. 7. 5 at. % alloy. Grain boundary decomposition. Polarised light. (× 200)

* No absolute values of the lattice parameters were measured.

5 at. % molybdenum–uranium alloy

Metallographic. Under polarised light the structure for the first 1.5 cm was of polygonal grains exhibiting a banded appearance, characteristic of the α_b'-phase[3] (Fig. 6). Immediately following was a zone in which nucleation and growth of small α-type grains was observed (Fig. 7); this increased until at a point approximately 2.5 cm from the tip no banded areas were detectable. The pseudo α grain structure remained unchanged up to the slowly cooled end of the rod.

After etching, no structural details could be resolved within the banded areas but where α grains could be seen under polarised light decomposition of lamellar nature could be detected. The lamellae were very fine at the position of maximum hardness, being barely resolvable with the optical microscope, but were much coarser at the slowly cooled end.

X-ray and hardness. Fig. 8 shows that the hardness of the quenched end was 390 V.P.N., and this remained fairly constant for the initial 1.5 cm. Coincident with the appearance of the decomposition along the grain boundaries the hardness increased rapidly to reach a maximum of 515 V.P.N. at a position approximately 2.7 cm from the tip, where lamellar decomposition had occurred fully. Over the next 2.7 cm the hardness decreased rapidly to reach a steady state of approximately 400 V.P.N. to the end of the rod.

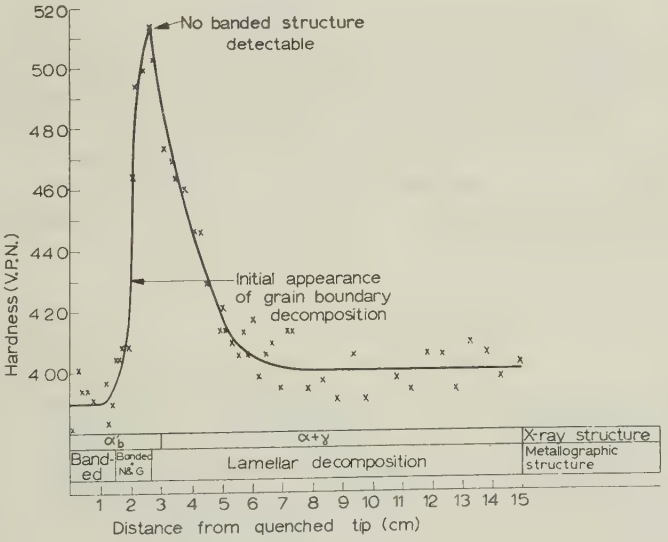

Fig. 8. 5 at. % alloy. End-quenched into mercury. Hardness and X-ray results.

The structure over the first 3 cm as given by X-ray diffraction was that of the α_b'-phase with the b parameter showing a progressive decrease in the amount of relative contraction over this length, *i.e.* there was an increasing tendency for the formation of equilibrium α-phase. At a point 4 cm from the tip the structure was identified as $\alpha + \gamma$, the γ lines being diffuse, and this remained unchanged over the remainder of the rod length.

7.5 at. % molybdenum–uranium alloy

Metallographic. Under polarised light this specimen showed the same structure throughout its length. The appearance of the quenched tip and the slowly cooled end was of polygonal grains exhibiting a distinct form of banding. No structure other than the grain boundaries was brought out by etching.

X-ray and hardness. The results plotted in Fig. 9 indicate that, allowing for the

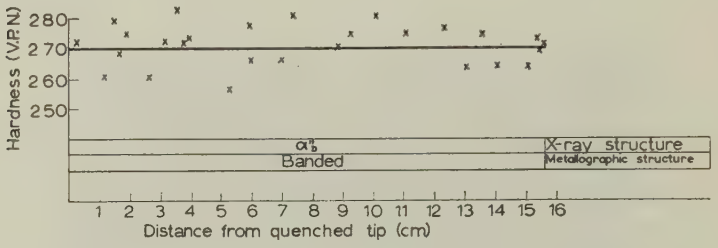

Fig. 9. 7.5 at. % alloy. End-quenched into mercury. Hardness and X-ray results.

scatter, there was practically no variation from the tip hardness of 270 V.P.N. over the complete length of the specimen. X-ray diffraction patterns indicated that the phase retained was α_b'' — this is recognised by an overlapping of the (021) α and (002) α lines and by a systematic splitting of certain α lines. This has been interpreted by LEHMANN[4] as indicative of the formation of a monoclinic cell structure with an angle of approximately 91° between the *a* and *b* axes. From the diffraction films obtained it appeared that the degree of splitting at the slowly cooled end was greater than that at the quenched tip.

10 at. % molybdenum–uranium alloy

Metallographic. As for the previous alloy this specimen had a very similar structure throughout its entire length, consisting of small equiaxed banded grains. At this composition, however, the bands are of a more lenticular nature (Fig. 10) as opposed to the rectilinear form in the 5 and 7.5% alloys and there was a decrease in the observable intensity of the bands between the tip and the slower cooled end. No structure was revealed during subsequent etching, other than grain boundaries.

X-ray and hardness. The hardness (Fig. 11) showed a tendency to decrease from the tip, to the slow cooled end, from 150 to 140 V.P.N. However, in contrast to the metallographic and hardness results, the X-ray diffraction patterns indicated that over the length of the rod there was a distinct crystallographic change. Over the initial 6 cm of the specimen the structure was found to be α_b''; at the slowly cooled end the structure was $\gamma°$, and between the two there was a mixture of α_b'' and some form of γ, the γ lines at this point being too diffuse to index precisely. The diffraction pattern of $\gamma°$ is based on the b.c.c. γ-phase but most of the b.c.c. diffraction lines are split into doublets. This pattern can be indexed as body-centred tetragonal.

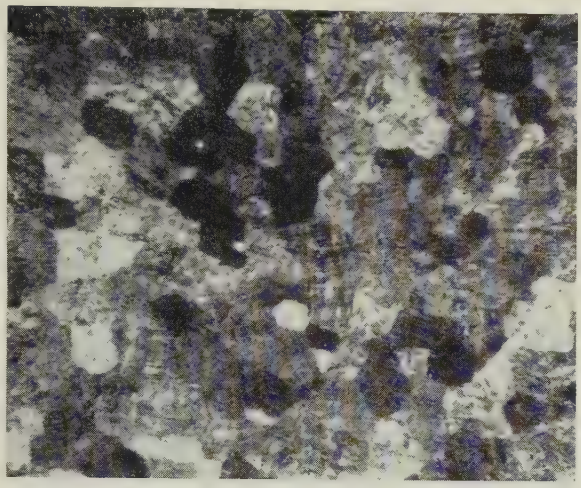

Fig. 10. 10 at. % alloy. Quenched tip. Polarised light. (× 200)

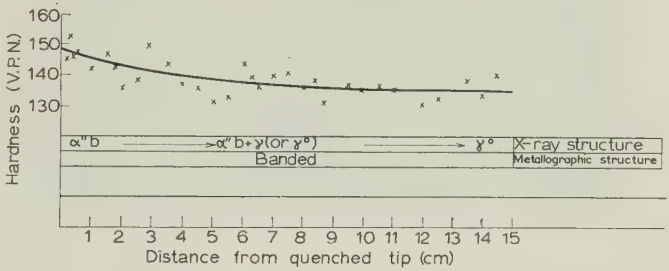

Fig. 11. 10 at. % alloy. End-quenched into mercury. Hardness and X-ray results.

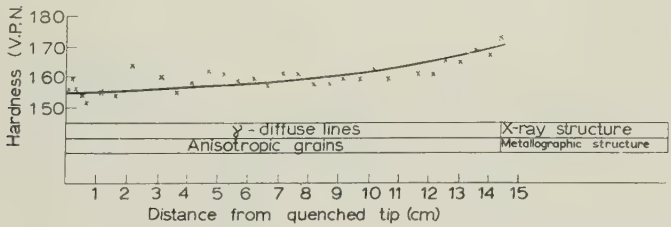

Fig. 12. 12.5 at. % alloy. End-quenched into mercury. Hardness and X-ray results.

12.5 at. % molybdenum–uranium alloy

Metallographic. The structure throughout the length of this specimen was of the γ°-phase, *i.e.* anisotropic equiaxed grains. The grains were free from any internal markings although some striations were produced around hardness indentations. These markings were similar to those within the γ°-grains of the 10% alloy. Etching failed to reveal any sign of decomposition within the grains.

X-ray and hardness. Although all diffraction films from this alloy gave only the b.c.c. γ-pattern all the diffraction lines were broad and diffuse, suggesting a high degree of lattice strain. The hardness curve (Fig. 12) rises slowly from tip hardness 155 V.P.N. to reach approximately 170 V.P.N. at the slowly cooled end.

15 at. % molybdenum–uranium alloy

Metallographic. Metallographically, the structure was found to be of equiaxed grains exhibiting anisotropic properties throughout the length of the specimen. No further information was gained by etching; Fig. 13 shows a typical structure.

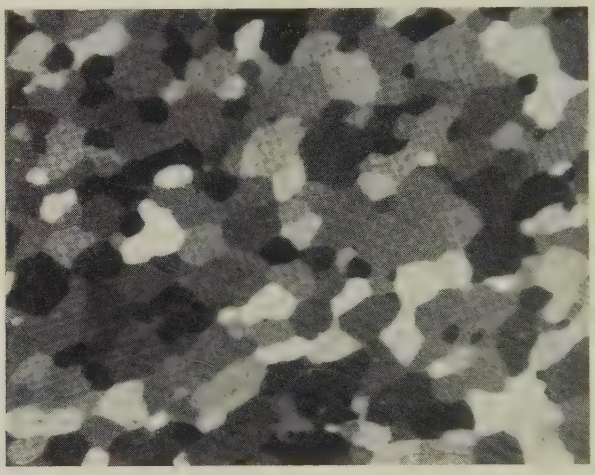

Fig. 13. 15 at. % alloy. Typical structure. Polarised light. (× 200)

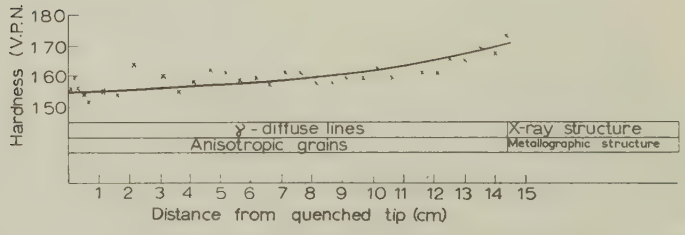

Fig. 14. 15 at. % alloy. End-quenched into mercury. Hardness and X-ray results.

X-ray and hardness. As shown in Fig. 14, the tip hardness for this alloy was about 215 V.P.N. — this increased slowly along the specimen to reach approximately 228 V.P.N. at the slowly cooled end. X-ray diffraction identified only the b.c.c. γ-phase.

SUBSIDIARY EXPERIMENTS

From the foregoing experiments the sequence of transformation in the 2.5 and 10 at. % molybdenum alloys was obscure. These alloys will be discussed later but some clarification of their behaviour was obtained from a few relatively simple experiments.

Effect of quenching rate on the 10 at. % alloy

A section of the slow-cooled end of the rod, which had shown γ_a° on previous examination, was heated to 950°C for 30 min, and quenched into mercury. Metallographic examination revealed a banded structure and X-ray examination showed that this was due to α_b''.

Effect of quenching rate on an 11.5 at. % alloy

To ascertain the cause of the banded microstructure of the γ°-phase in the slowly cooled end of the 10 at. % alloy the effect of cooling rate on the metallographic structure of an 11.5 at. % was studied. It was known that at the latter composition γ° could be retained using a variety of quenching rates.

Accordingly, two pieces of this alloy were prepared in a similar manner to the other alloys. Both were heated at 950°C for $\frac{1}{2}$ h. One was quenched rapidly into mercury while the other was quenched into oil. Under polarised light the former showed a banded microstructure and the latter an equiaxed polygonal structure. Both gave a γ° X-ray pattern.

Effect of deformation on the 10 and 11.5 at. % alloys

It is a common phenomenon in martensitic transformations that if the transformation temperature is just below ambient the application of stress will often cause the transformation to occur. This has been demonstrated by HARDING AND WALDRON for uranium–titanium alloys, where deformation of the metastable γ°-phase induced transformation to α_b'. Accordingly, a piece of the slow-cooled end of the 10 at.% alloy was crushed in a vice. X-ray examination was inconclusive, due to the diffuseness of the lines, but the structure was probably some form of α.

An 11.5% alloy was treated to produce a polygonal strain-free structure of γ° and deformed in various ways, in some cases until rupture occurred. Metallographically, severe deformations were accompanied by heavy banding in the original polygonal grains but X-ray examination showed that only the γ°-phase was present.

Effect of sub-zero quenching on the 10 at. % alloy

A piece from the slow-cooled end of the rod was polished, examined to see that it was flat, and quenched from room temperature into liquid nitrogen. If the M_s for the transformation of $\gamma_a^\circ \rightarrow \alpha_b''$ had been between room temperature and —190°C (approx.) the transformation would have partially or wholly occurred. The reverse transformation may have occurred on reheating to room temperature but strain markings due to the transformation would undoubtedly have been evident. On re-examination after heating to room temperature the surface of the specimen was perfectly smooth.

Effect of tempering on the 2.5 at. % alloy

The variation in hardness and etching characteristics of the acicular structure in this alloy could have been due to a tempering effect. A specimen of this alloy was quenched from the γ-phase into mercury, and then cut in half. One half was tempered at 400°C for 1 min and the cut faces were then polished and etched together. The quenched structure was similar to that in the tip of the quenched rod and did not

etch at all, whereas the tempered structure was similar to that 2 cm from the tip of the end-quenched rod. The hardness of the tempered structure was 20 to 30 points higher than that of the quenched structure. Similar specimens were tempered at 400°C for 2, 4, 8 and 16 min. The structures were all very similar, but the difference in hardness between the quenched and tempered specimens rose to about 50 points after 4 min tempering and then fell to 30 points after 16 min tempering.

Quenching the 2.5 at. % alloy from the $\gamma + \beta$ phase field

A piece of this alloy was polished, heated at 800°C for $\frac{1}{2}$ h, cooled to 700°C and held at this temperature for 2 h, quenched into mercury and immediately electro-polished without further mechanical preparation. Examination under polarised light disclosed that a duplex lamellar structure had been developed and that one of the phases responded weakly to polarised light. After storage for one day the weakly anisotropic phase was found to have partly decomposed to very small grains that responded strongly to polarised light. Thus, immediately after the quench an $\gamma + \beta$ mixture had been retained, the β containing approximately 1.25 at. % molybdenum according to the equilibrium diagram.

DISCUSSION OF RESULTS

Understanding of the transformation of uranium molybdenum alloys can be divided into two parts; the sequence of formation of the phases with cooling rate, and the variation of the phases formed by rapid quenching with composition. At the moment insufficient is known to discuss the latter, since the exact structure and parameters of the phases that form and the phase from which they form, together with the temperatures of formation are largely unknown. The sequence of formation is, however, fairly clear in the alloys containing 5, 7.5, 12.5 and 15 at. % molybdenum and hypotheses can be formed about the 2.5 and 10 at. % molybdenum alloys.

5, 7.5, 12.5 and 15 at. % molybdenum alloys

In the 5 at. % alloy the fastest quenching rate leads to a direct martensitic transformation of γ-phase to a variant of the α-phase, namely α_b'. With somewhat slower cooling rates, nucleation and growth occur at the grain boundaries, and these give a marked hardness increase. The nucleated structure is probably due to a direct $\gamma \rightarrow \alpha + \gamma$ transformation, since LEHMANN[4] states that it is very difficult to form the β-phase at this composition during continuous cooling at rates as low as 2.5°C/min.

The maximum hardness appears to be a function of lamellar spacing, since it occurs when the structure is fully lamellar, but at the fastest cooling rate capable of producing such a structure. At the slowly cooled end the lamellae of $\alpha + \gamma$ are coarser and the hardness is less. For the 7.5 at. % alloy, the cooling rate over the whole specimen was sufficient to produce a martensitic transformation throughout, giving an α_b'' structure and practically constant hardness over the whole length.

The metallographic appearance of both the 12.5 and 15 at. % alloys suggests that they have similar structures. From the diffraction films there is definite evidence of tetragonality for the 12.5 at. % alloy, but not for the 15 at. %. Even so, the structure in both alloys has been referred to as γ^o, since they both respond to polarised light. The reason for the response to polarised light of the b.c.c. structure is not known.

It could be due to an epitaxial oxide film, but the epitaxial nature would have to depend strongly on film thickness, since the best response was obtained with a freshly polished surface. Both these alloys show little variation in hardness over the specimen length, commensurate with the structure. The 15 at. % alloy is harder than the 12.5 at. % alloy, due probably to solid solution hardening.

10 at. % molybdenum alloy

In the 10 at. % alloy, α_b'' was formed at the quenched tip and γ_d° at the slowly cooled end. This was not an effect of large scale segregation, since a specimen from the slowly cooled end subsequently quenched gave α_b'', but must have been an effect of the quenching rate. The latter could have been due to at least two causes; the thermal stresses in the quenched tip could have assisted in the transformation of γ_d° to α_b'', or the slower cooling rate at the other end could have allowed atomic movements preventing the formation of α_b''.

When stress was applied to γ_d° in an attempt to produce α_b'' the results were inconclusive and sub-zero quenching of γ_d° gave no indication of the formation of α_b''. On the other hand, experiments on the 11.5 at.% alloy have shown that the markings in γ° can be formed either by thermal or mechanical stresses, and when the mechanical stresses were in some cases the ultimate no α_b'' formed. The formation of α_b'' from γ_d° would seem to be very difficult. In this connection, however, LEHMANN[4] demonstrated that α_b'' could form isothermally when the γ-phase of a 9.4 at. % alloy was quenched to 350°C, whereas if it was quenched in oil to room temperature γ_d° resulted. Attempts by the authors to repeat this work on the 10 at. % alloy have given very inconclusive results; a banded microstructure was produced by this type of isothermal treatment, but the X-ray examination gave films with vague blurs rather than lines on them, rendering identification impossible. TANGRI AND WILLIAMS[5] have shown that the axial ratio of the γ°-phase in a uranium–16 at. % niobium alloy* increases from 0.96 at room temperature to approximately 0.985 at 300°C, and thus at 300°C the γ-phase which transforms to α_b'' in uranium–molybdenum alloys may not be structurally the same as the γ°-phase at room temperature.

At this stage in the research then the second alternative given above seems more likely, *i.e.* the γ°-phase and the α_b''-phase are alternative phases both forming from the γ-phase. The structural changes which lead to the formation of γ° in the 10 at. % alloy are conjectural. Moreover, they must be existing or able to form very rapidly in the 12.5 at. % alloy, where mercury quenching from the γ-phase gives γ°. One guess would be that a super-lattice forms, since this could explain the time dependence of the γ°-phase formation in the 10 at. % alloy, and the tetragonality of the phase. A big objection to this, however, is that if the super lattice forms on cooling, the domains of ordering would be quite small, and it is possible to obtain the γ°-phase as large crystals which respond uniformly to polarised light in alloys containing above 10 at. % molybdenum.

2.5 at. % molybdenum alloy

Rapid quenching results in an acicular structure being formed in the 2.5 at. % alloy. This is presumably formed by a martensitic process but it is difficult to decide

* The uranium–niobium system exhibits α_b'–, α_b''–, and γ°-phases in the γ-quenched alloys analogous to those in the uranium–molybdenum system.

whether this is a direct $\gamma \rightarrow \alpha$ or a $\gamma \rightarrow \beta \rightarrow \alpha$ transformation. From the fine markings within the individual plates this structure appears similar to the typical α_b'-phase but its lenticular appearance is more characteristic of the athermal $\beta \rightarrow \alpha$ transformation. LEHMANN obtained a much finer acicular product on quenching in oil from 950°C and, in the main, only obtained coarser needles when quenching from a $(\gamma + \beta)$-field. She attributed the fine structure to a $\gamma \rightarrow \alpha$ martensitic transformation, and the coarse to a $\beta \rightarrow \alpha$ martensitic transformation where the β was of equilibrium composition.

DELAPLACE[6] has reported that with a uranium alloy containing 2.8 at. % molybdenum it was impossible to suppress the $\gamma \rightarrow \beta$ transformation at cooling rates up to 2000°C/sec. The form of the product varied with the cooling rate but at 700°C/sec it was very similar to the acicular structure found by the authors at the tip of the 2.5 at. % molybdenum alloy. However, during the present work traces of some original grains from which the α forms can be seen. This grain size is large with straight boundaries and would seem more typical of high temperature γ than of β formed during quenching unless the β- and γ-grains corresponded in size and position. Again, since β of almost equilibrium composition is retained on mercury quenching from the $\gamma + \beta$ field (see p. 165), supersaturated β formed in very rapid cooling might well be retained since it is present to some extent in the 1.5 at. % molybdenum alloy[7]. In fact, no retained β was observed after γ-quenching the 2.5 at. % alloy. This slight evidence seems to favour the $\gamma \rightarrow \alpha$ martensitic transformation with the very rapid quench used.

Although the hardness begins to increase 1 cm along the rod, the first metallographic change is noticeable approximately 1.9–2.0 cm from the tip where the matrix between the needles etches to reveal a fine decomposition product. Over the following 2 or 3 mm whilst the hardness is still increasing the structure changes rapidly. The number of needles decreases and a new structure appears, consisting of small pseudo α-grains at the original grain boundaries, which etch to give a fine lamellar structure. The remanent matrix looks similar to the fine decomposition product observed between the needles. A rapid increase in the number of pseudo α-grains occurs until they cover the entire original γ-grains, to the exclusion of both needles and the fine matrix. Since the plates or needles are large they are presumably formed first and since pseudo α grains are found at grain boundaries they are also presumably formed first. Therefore the fine decomposition product, if it is the same between the needles and pseudo α-grains, cannot be a product formed prior to the needles, otherwise it would restrict needle size. On the other hand, it must have formed after the small pseudo α-grains. In other words, the sequence of formation with decreasing temperature must have been pseudo α-grains, martensitic needles, and then the fine decomposed structure. This sequence is possible only if the fine decomposed structure is a result of the breakdown of the fine acicular structure, *i.e.* a tempering process. This could occur if the M_s for the $\gamma \rightarrow \alpha$ transformation were above 400°C, since as has been shown (p. 165) tempering can give this type of decomposition product in very short times at 400°C. The maximum hardness is achieved in the region where decomposition to pseudo α-grains is complete. This area etches to show a fine lamellar structure. Over the next 2 cm a rapid fall in hardness (120 V.P.N.) occurs, accompanied by little change other than a slight coarsening in the size of the pseudo α-grains and the lamellae. Thereafter, both structure and hardness remain fairly constant. It is con-

sidered that the formation of the pseudo α-grains is a result of direct $\gamma \rightarrow \alpha + \gamma$ transformation. LEHMANN did not succeed in suppressing the $\gamma \rightarrow \gamma + \beta$ reaction, but the cooling rate she observed never exceeded 180°C/min, while in the present work, over the relevant temperature range the rate of cooling was approximately 400°C/min.

CONCLUSION

This work has established the relationship between the hardness and the microstructure of uranium–molybdenum alloys of various compositions quenched at various rates. It has also gone some way towards establishing the sequence of transformation in these alloys although more work is required to determine the nature of the process at which the $\gamma \rightarrow \alpha$ martensitic transformation takes over from the $\gamma \rightarrow \beta \rightarrow \alpha$ decomposition, where the $\beta \rightarrow \alpha$ transformation is martensitic.

ACKNOWLEDGEMENTS

The authors would like to thank Dr. M. B. WALDRON, Dr. G. I. WILLIAMS and Dr. K. TANGRI for many useful discussions of the work reported here.

REFERENCES

1 A. G. HARDING AND M. B. WALDRON, *A.E.R.E. Rept. M/R. 2673*, (1958).
2 R. F. HILLS, D. R. HARRIES, D. J. HODKIN AND M. B. WALDRON, *A.E.R.E. Rept. M/R. 2840*, (1959).
3 J. LEHMANN AND R. F. HILLS, *J. Nuclear Materials*, 2 (1960) 261.
4 J. LEHMANN, *Thesis*, University of Paris, June, 1959.
5 K. K. TANGRI AND G. I. WILLIAMS, Fulmer Research Inst., personal communication.
6 J. DELAPLACE, *Centre d'Études Nucléaires de Saclay Rapport no. C.E.A. 1399*, (1960).
7 R. F. HILLS, unpublished work.

HOT HARDNESS TESTING APPLIED TO THE AGEING AND HEAT TREATMENT OF BERYLLIUM

R. THOMSON*

Babcock & Wilcox, Ltd., Renfrew (Scotland)

B. BEGLEY AND A. J. MARTIN

Atomic Weapons Research Establishment, Aldermaston, Berks. (England)

(Received December 15th, 1960)

SUMMARY

This account describes work at A.W.R.E., Aldermaston, on the hot hardness testing of beryllium; a brief description of the apparatus is included. Sections from extruded rod, produced from thermally reduced pebble metal ingot, and from electrolytically reduced flake metal ingot, have been tested at temperatures up to 600°C.

The results show that pebble metal exhibits both strain and precipitation ageing mechanisms, these being removed by precipitation annealing between 600°C and 800°C with consequent improvement in high temperature ductility characteristics. No such phenomena have been detected in flake material.

INTRODUCTION

One of the chief subjects of interest in beryllium metallurgy has been the investigation of the cause of the brittle behaviour of the commercial metal, and the influence of temperature and impurity content on the ductility characteristics. As part of a general study of these last two aspects, an investigation of ageing phenomena in beryllium was initiated using a hot hardness device as a means of detecting and recording the deformation characteristics of polycrystalline material and, therefore, by inference, the disposition and movement of impurity atoms. The examination was aimed at analysing the time–temperature parameters of quench-ageing, and evaluating from these treatments that could possibly affect the tensile ductility. During the course of the work, a parallel study of the effects of heat treatment on the hot tensility of beryllium at elevated temperatures revealed the importance of heat treatment designed to establish equilibrium constitutions in the particular grades of metal under consideration. It was in this field particularly that the hot hardness apparatus proved of great value in providing a rapid means of interpreting the effects of heat treatment on the mechanical properties, once the relationship between the latter and hardness results had been understood.

The work reported here is divided, therefore, into:

(1) A section dealing with ageing.

(2) A section concerned with more general aspects of the heat treatment of beryllium.

*Present address: Dept. of Mines and Technical Surveys, Ottawa, Ontario, Canada.

Throughout the investigation, the metal used was extruded ingot, *viz.*, thermally reduced metal and electrolytically reduced flake. An extrusion ratio of 44 : 1 at 1050°C was employed in all cases to produce 0.6 in. diameter bars.

EXPERIMENTAL DETAILS

The thin "temper" film of oxide formed on beryllium after a short time in air at 650°C was not found to affect hardness appreciably, and a minimum load of 10 kg produced reasonably sized impressions (0.3–0.7 mm diagonal length) over the temperature range 25–650°C. Thus neglecting the protective atmosphere and low loading features of hot hardness testing, it was possible to modify a Rockwell machine for high temperature use by simply adding a furnace assembly to the existing specimen table, and by replacing the ball indentor by a Vickers diamond attachment. A sectional diagram of the modification is shown in Fig. 1, from which it will be noticed that the furnace assembly is attached to a compound table, thus allowing the entire surface of the specimen to be indented during a single experiment. The minor load of the Rockwell

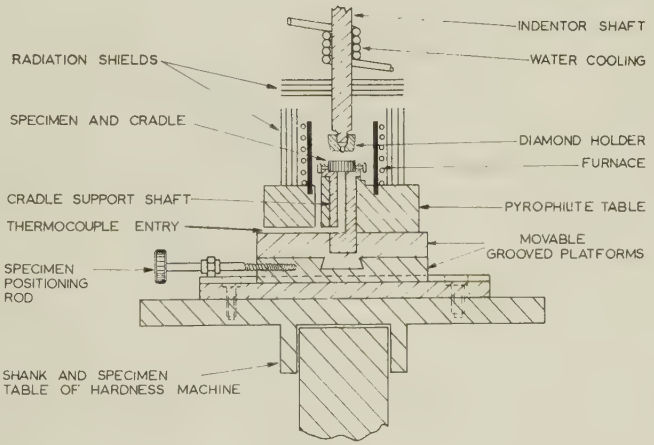

Fig. 1. Detail of hot hardness assembly.

tester, 10 kg, was applied in 5 sec and maintained for 30 sec at all temperatures. Cylindrical test specimens cut from extruded bar were prepared by acid etching and manual wet grinding to '000' grade emery paper.

Indentations were measured by a Vickers ocular attachment, no correction being made for thermal contraction of the diagonal lengths. In practice, successive indentations on a transverse surface were accurate to within 5%, except where the grain size is large, and the anisotropy factor[1] produces a greater deviation from the average. All heat treatments mentioned were carried out *in vacuo*.

AGEING

In the following text, the terms "ageing" and "age-hardening" refer to both strain and precipitation ageing. Evidence of both mechanisms being operative in beryllium is found in the work of MASH[2], BROWN[3], and HARTREE[4]. The first two workers were

concerned with strain ageing effects detected during tensile tests, whereas HARTREE has made a direct examination of precipitation ageing. The objects of the present study were to investigate these observations more fully and to attempt to evaluate heat treatments to improve the range of mechanical properties of beryllium.

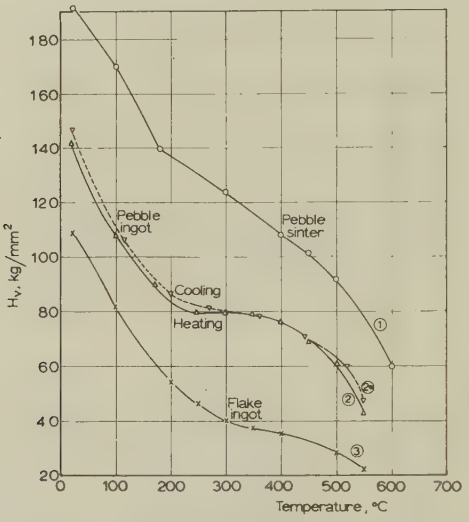

Fig. 2. Hardness *versus* temperature for different grades of beryllium. Curve 1, pebble sinter extruded; curve 2, pebble ingot extrude tested on heating; curve 2a, pebble ingot extrude tested on cooling; curve 3, flake ingot extruded.

TABLE I

CHEMICAL ANALYSIS – FIGURES FOR MATERIALS EXAMINED

(All figures in wt.%)

Impurity	*Extrusions of*	
	1 *Flake ingot*	*2* *Pebble ingot*
Fe	0.041	0.248
Si	0.061	0.237
Al	0.065	0.060
Mg	0.002	0.001
Mn	0.0008	0.004
Cu	0.005	0.001
Ni	0.018	0.022
Cr	0.007	0.011
BeO	0.011	0.025
BeC	0.006	0.023
Total Impurity		
1. Metallic	0.197	0.494
2. Non-metallic	0.017	0.048
Total	0.214	0.542

Results

Preliminary work established the variation of hardness with temperature on heating for extruded pebble ingot and extruded flake ingot (chemical analyses figures appear in Table I). Both materials were air-cooled from the extrusion temperature of 1050°C.

From Fig. 2, the relative order of hardness is quite consistent with tensile strength/temperature characteristics. It should be noted that, although grain sizes are the same (100 μ), both the absolute values and the shapes of the hardness curves differ. The marked inflection on the pebble ingot curve between 200°C and 400°C, when compared with the smooth curve of flake ingot, indicates the operation of a hardening mechanism which was not removed when the specimen was annealed 12 h at 550°C and hardness-tested on cooling.

A series of isothermal ageing experiments were completed in the hot hardness assembly, the specimens having been solution-treated at 950°C for one hour, to minimise grain growth, then quenched to room temperature and aged at 250°C, 350°C and 450°C to yield the hardness at temperature/time relationships shown in

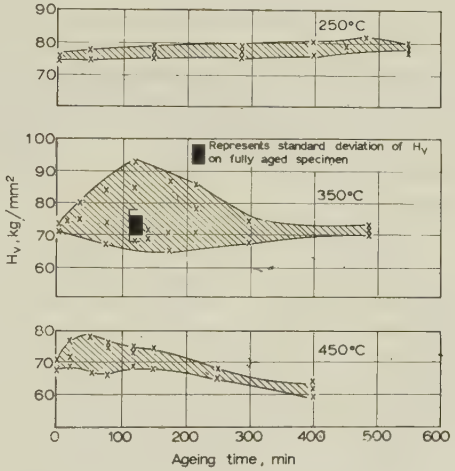

Fig. 3. Hardness *versus* time at ageing temperature. Material: extruded pebble ingot. Solution treatment at 950°C for 1 h, water-quenched.

Fig. 3. From the 250°C isothermal a very slight hardening tendency can be inferred, with a maximum scatter of 4 VPN units. The 350°C isothermal, on the other hand, shows a maximum scatter of 25 VPN units localised between 1.5 and 2.5 h on the time axis, with an initial and final scatter of 4 VPN units. The H_v values revealed a maximum in hardening tendency of 73 to 93 VPN after 2 h ageing, followed by a softening back to 73 VPN after 6 h ageing.

Similar observations can be made on the 450°C isothermal, where the maximum occurs more rapidly and is less marked than in the 350°C ageing treatment.

Isothermal tests on as-extruded pebble ingot, and solutionised and quenched flake ingot showed no dependence of hardness on time.

The specimen, aged for 6 h at 350°C, was re-heated and tested after 2 h at 350°C. 20 indentations were made in as many minutes, and the average hardness, maximum and standard deviations evaluated. These were respectively 73 VPN, $\pm$ 5 VPN and 6 VPN, and represent the *experimental* scatter of results under the test conditions described.

Discussion

The anomalous hardness characteristics of pebble ingot material (see Fig. 2) can only be ascribed to the interference of impurity atoms with the normal deformation behaviour of beryllium as exemplified by the H_v/T°C curve for the purer flake ingot. This suggests an ageing phenomena whose mechanism may be:

(a) precipitation hardening of the matrix as the input of thermal energy is increased, or

(b) strain-age hardening in the volume of metal affected by an indentation; that is to say, the Cottrell theory of strain ageing is applicable during the process of indentation.

The main difference between the two mechanisms, *viz.*, the irreversibility of precipitation and the dynamic, reversible nature of strain ageing, has been exploited to indicate which is operative in curve (2) of Fig. 2. The coincidence of the curves 2 and 2(a) shows, in fact, that the impurities have not been lost from solution in beryllium by simulated "over-ageing" treatment at 550°C, and that there exists a temperature range below 550°C in which solute atoms have sufficient mobility to interfere with the process of deformation.

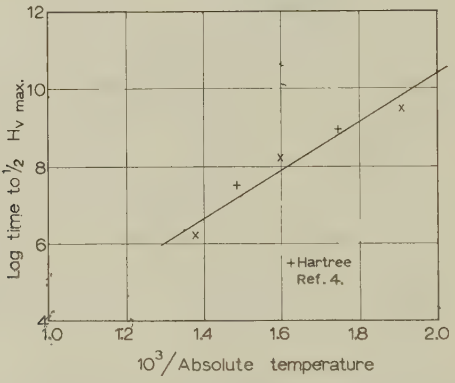

Fig. 4. Rate of hardening *versus* $1/T$.

Though isothermal hardness tests on as extruded ingot materials gave no evidence of precipitation ageing, it was found that by increasing the solute content of pebble ingot by solutionising heat treatments, a dependence of hardness on time was detectable at 250°C, 350°C and 450°C. Control of the errors involved in these tests permit the inference that the results reflect the operation of precipitation age-hardening in the temperature range examined. A reciprocal rate plot yielded an activation energy of 11,500 cal/mole (Fig. 4). Although this figure is, at this stage, of no absolute significance, the fact that it could be obtained suggests that the time dependence of hardness resulted from the diffusion of one species of solute in the beryllium lattice. The large scatter of hardness figures at peak ageing conditions may reflect (expected) anisotropic precipitation.

The present results (Fig. 4) are in good agreement with those of HARTREE.

Conclusions

(1) The hot hardness curves of two grades of cast and extruded beryllium differed in absolute values and shape. It was found that pebble ingot material, with the greater solute content, gave evidence of strain age hardening during indentation of the as-extruded metal, and precipitation age hardening in the annealed and quenched condition.

(2) Since medium temperature annealing (550°C) of as-extruded pebble ingot did not remove the strain ageing effect, it must be inferred that the solute element(s) responsible were in "stable" solid solution up to 550°C at least, or that, if the solution was, in fact, metastable, then their disposition in the metal would only be altered by heat treatment above 550°C.

(3) Finally, it can be argued that both ageing effects may be caused by the same solute element.

HEAT TREATMENT

The work described below is complementary to the study by BROWN *et al.*[3] on the effects of heat treatment on the hot tensility of beryllium, in which it was shown that:

(1) The multiple yielding associated with strain ageing in pebble ingot extrude was

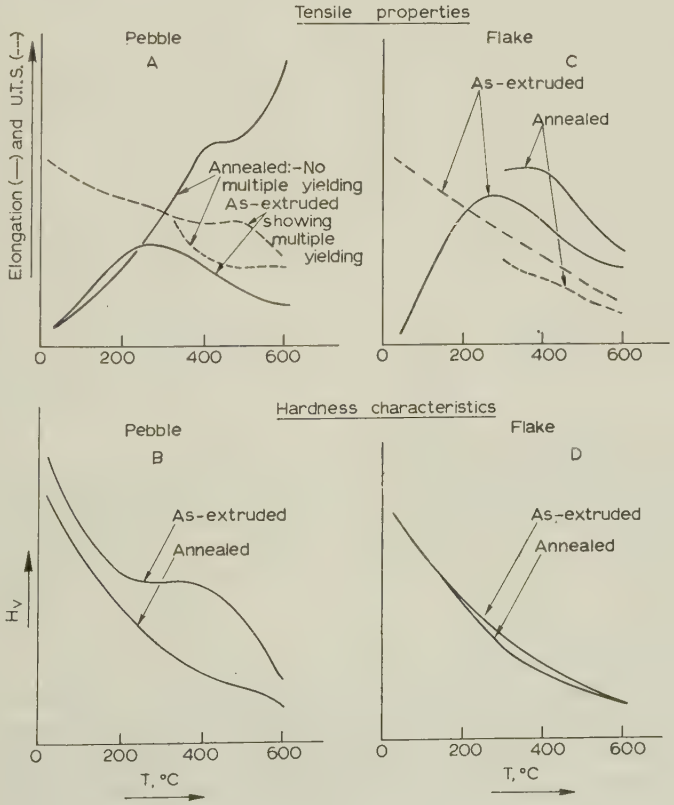

Fig. 5.

still in evidence after annealing at 500°C, but disappeared after annealing at 780°C.

(2) This latter heat treatment altered the hot ductility characteristics of pebble ingot without affecting grain size, etc.

(3) Flake ingot extrude was only slightly susceptible to heat treatment. These findings, illustrated in Figs. 5A and C, could be explained by the theory that heat treatment at 780°C induces the precipitation of impurities from metastable solid solution, so altering the constitution of the material to permit greater possible deformation at elevated temperatures.

Results

A preliminary comparison of H_v/T°C curves for the pebble material in the as-extruded and heat-treated states (see Fig. 5B) showed that the latter was softer and gave no evidence of a hardening arrest between 250°C and 450°C. From the conclusions of the section on AGEING therefore, regarding the cause of the plateau, it was assumed that the 780°C anneal had removed the strain ageing effect, presumably by precipitating out solute elements that were present in metastable equilibrium. It was considered, therefore, that if the relative softening illustrated in Fig. 5B was caused by precipitation, then the effect of the heat treatment could be reversed by re-solution of the precipitated phases at higher temperatures. This was, in fact, achieved, as a scrutiny of Fig. 6 will reveal, and the precipitation hypothesis has therefore been verified.

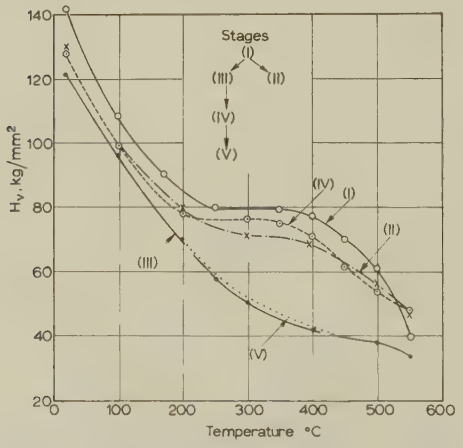

Fig. 6. Hardness *versus* temperature of heat-treated pebble ingot extrude. (I), As-extruded; (II), solutionised 1050°C 1½ h and quenched; (III), annealed 780°C 100 h; (IV), specimen III solutionised 1050°C and quenched; (V), specimen IV re-annealed 780°C.

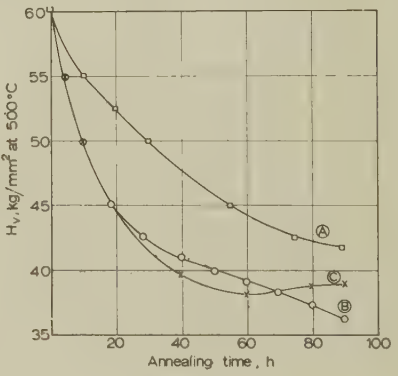

Fig. 7. Hardness *versus* annealing time for pebble ingot extrude. Curve A, annealed 600°C; curve B, annealed 700°C; curve C, annealed 800°C. Standard deviation of hardness values at 500°C ≯ 1.5 kg/mm².

The slight effect of precipitation heat treatment on flake material is illustrated in Figs. 5C and D. To establish the kinetics of precipitation, tests were carried out on pebble ingot specimens annealed at 600, 700 and 800°C for periods up to 80 h. The progress of precipitation softening was detected by interrupting the anneal, quenching, and measuring hardness values at 500°C. Fig. 7 shows the results obtained from this examination, each point plotted being the average of 5 measurements of H_v at 500°C.

Discussion

The general nature of the mechanism involved, and the effects of time and temperature on the heat treatment of pebble ingot extrude are elucidated by the data on Figs. 5 and 6. Following the legend on Fig. 5, it is evident that the initial hardness plateau of the as-extruded material can be removed by medium temperature, long term annealing, and replaced again by high temperature, short term treatment and quenching. Since the inflexion is caused by strain-ageing, then its removal and replacement is tantamount to the precipitating and solutionising of the solutes responsible for the effect. This argument is an important one in support of the theory that precipitation of impurities endows hot ductility, because no new phases have been detected metallographically in heat-treated pebble material. It may be that the scale of matrix and grain boundary precipitation is sub-microscopic with the parameters used.

The results of the examination of the rates of softening (see Fig. 6), are interesting in the following respects:

(1) Considerable precipitation softening occurs at all three annealing temperatures.

(2) The rate of attainment of equilibrium and the hardness values at equilibrium would appear to suggest that the diffusion rate of the solutes is low at 600 °C; that rapid precipitation occurs at 800°C although the equilibrium solute content may be higher than at 700°C.

(3) Optimum parameters to induce maximum precipitation appear to be around 700–750°C for 100 h.

If these experiments were repeated and extended, and hardness testing done during annealing, it might be possible to evaluate diffusion data for the precipitation process.

With regard to the mode of precipitation and the effect of this on high temperature deformation, the following points are of interest:

(1) Precipitation of the solutes in pebble ingot affected only that region of the ductility/temperature curve where grain boundary properties were of paramount importance (Fig. 5A).

(2) The H_v/T°C characteristics of annealed pebble ingot material were identical to those of both as-extruded and annealed flake material (Figs. 5B and 5D). This infers identical resistance to deformation of matrices, in spite of the large differences in hot ductility.

(3) Long diffusion times were required at precipitation temperatures to produce any changes in strain ageing or hot ductility effects. It seems likely, therefore, that the diffusion of impurities to, and their dispersed precipitation at the grain boundaries in ingot beryllium, will alter high temperature deformation mechanisms to permit larger tensile elongations.

Conclusions

(1) Long term annealing treatments of relatively impure extruded pebble ingot beryllium induced the precipitation of metastable solute impurities in the region of grain boundaries. The deformation mechanism of the resultant constitution is such that high tensile elongations are attainable above 400°C.

(2) Flake ingot extrude did not show this precipitation susceptibility.

(3) The optimum parameters for precipitation heat treatment of pebble ingot

extrude are around 100 h at temperatures between 700°C and 750°C. This process is reversible by solutionising at 1050°C for 1½ h and quenching.

(4) It is conceivable that the solute or solutes responsible for strain and precipitation ageing around 400°C in a metastable solid solution of pebble beryllium are identical to those precipitated by heat treating such material around 700°C.

REFERENCES

[1] G. L. TUER AND A. R. KAUFMANN, in *The Metal Beryllium*, American Society for Metals, Cleveland, Ohio, 1955, p. 373.
[2] D. R. MASH, *Trans. A.I.M.E.*, 203 (1955) 1235.
[3] A. B. BROWN, F. MORROW AND A. J. MARTIN, Unpublished work.
[4] D. P. HARTREE, *A.E.I. Report No. A858*, November 1958.

Short Communication

The system thorium–ytterbium: its alloy properties

In connection with work in progress on the alloying properties of thorium, the thorium–ytterbium system has been examined, for comparison with the thorium–cerium system, in which there is evidence, in the form of a marked contraction of the lattice spacings relative to that expected from the atomic diameters of the components, for electronic changes in the solid solution[1]. As raw materials, iodide thorium and ytterbium as supplied by Messrs. Johnson, Matthey and Co., Limited, were employed; the ytterbium, which was supplied as a coarse powder, was melted prior to use in preparing alloys. In this condition, and after stress relief of filings at 675°C, the spacing of the face-centred cubic structure was 5.4750 ± 0.0005 kX, in good agreement with that reported by SPEDDING, DAANE AND HERRMAN[2] for material of 99.9% purity (5.4751 ± 0.0004 kX).

Attempts to make alloys of thorium and ytterbium by arc-melting were unsuccessful; the two metals appeared to be virtually immiscible even at the melting point of thorium. At this temperature the volatility of ytterbium is serious, resulting in heavy losses of the metal which, when deposited in the form of a thin film on the inside of equipment, proved to be pyrophoric on subsequent exposure to air. However, several specimens were obtained after complete melting; these consisted of distinct volumes of thorium-rich and ytterbium-rich material with no evidence of bulk alloying. One such specimen was annealed for several days at 675°C; filings were taken from the interface region between the thorium-rich and ytterbium-rich material, and exposed to copper Kα radiation. The resulting diffraction patterns showed that the α-thorium spacing had increased from 5.0745 kX for pure thorium to 5.0761 ± 0.0002 kX. The spacing for ytterbium had at the same time decreased from 5.4750 kX to 5.4740 ± 0.0003 kX. There is thus evidence of some slight mutual solid solubility at 675°C. If it is assumed that the lattice spacings of these solid solutions vary linearly with composition along the line joining that of face-centred cubic thorium to that of face-centred cubic ytterbium, the measured spacings are consistent with approximate solid solubilities of 0.4 at. % ytterbium in thorium, and 0.25 at. % thorium in ytterbium. No diffraction lines corresponding to the presence of an intermediate phase were observed, while metallographic examination of the diffusion interface also failed to reveal any evidence of such a phase.

The atomic size-factor of ytterbium with respect to thorium is approximately 8%, so that the very limited mutual solid solubility, and the immiscibility at temperatures up to approximately 1700°C, are surprising. The restriction of solubility does not appear to be due to differences in electrochemical character, since no compound is formed; it is more likely to be connected with differences in electronic constitution.

In the case of thorium–cerium alloys, the lattice spacing of thorium is contracted by additions of cerium up to approximately 30 at.% in spite of the larger atomic

diameter of cerium; this has been interpreted in terms of the ionization of a 4*f* electron to give effectively 4-valent cerium in solution. Similar explanations have been advanced for the relatively high compressibility of cerium as compared with that of lanthanum, praseodymium and neodymium. Since the overall* compressibility of ytterbium is comparable with that of cerium[3], it is possible that there may be a similar tendency for the partial ionization of a 4*f* electron to give rise to a valency state exceeding the chemical valency of 2, which is characteristic of metallic ytterbium, when the metal is dissolved in thorium. The present experiments, however, provide no evidence for such a valency adjustment. With the transfer, or partial transfer, of a 4*f* electron to the conduction band, ytterbium would be expected to take on the characteristics of the trivalent metals of the rare-earth type, which are extensively soluble in thorium (*e.g.* lanthanum, yttrium), and would at the same time decrease the magnitude of its atomic size-factor with respect to thorium. In these circumstances, extensive solubility of ytterbium in solid thorium might be expected; the present experiments show that this does not occur.

Grateful acknowledgement is made to the United Kingdom Atomic Energy Authority for general support given to the programme of which this work forms a part, and to the General Electric Company, Limited, (U.K.), for the award of a research scholarship to one of us (D.S.E.).

Department of Physical Metallurgy,
The University of Birmingham,
Edgbaston, Birmingham (Great Britain)

D. S. EVANS
G. V. RAYNOR

[1] R. T. WEINER, W. E. FREETH AND G. V. RAYNOR, *J. Inst. Metals*, 86 (1958–59) 185.
[2] F. H. SPEDDING, A. H. DAANE AND K. W. HERRMAN, *Acta Cryst.*, 2 (1956) 559.
[3] P. W. BRIDGMAN, *Proc. Am. Acad. Arts Sci.*, 76 (1948) 71.

Received January 3rd, 1961

* At low pressures, the compressibility of cerium is somewhat less than that of ytterbium.

J. Less-Common Metals, 3 (1961) 179–180

ERRATUM

J. Less-Common Metals, Vol. 3 (1961) p. 24, lines 2–3 of the text below Fig. 2 should read:

"found, by the method of least squares, to be $7.6 \cdot 10^7$ c.g.s. units. The standard error was $1.19 \cdot 10^9$ c.g.s. units and thus it has little significance. K_y is thus less than that obtained by CHURCHMAN[6] ($3–5 \cdot 10^6$ . . ."

CONTENTS

Oxidation of titanium in the temperature range 800–1200°C
by P. KOFSTAD, P. B. ANDERSON AND O. J. KRUDTAA (Oslo) 89

The pilot plant production of electrolytic uranium dioxide
by J. R. CHALKLEY (Gloucester) 98

High temperature allotropy and thermal expansion of the rare-earth metals
by F. H. SPEDDING, J. J. HANAK AND A. H. DAANE (Iowa) 110

Some features of the refractory metals
by L. NORTHCOTT (Fort Halstead) 125

The ammonolysis of some hexachlorozirconates
by J. E. DRAKE AND G. W. A. FOWLES (Southampton) 149

A study of the effect of cooling rate on the decomposition of the γ-phase in uranium-low molybdenum alloys
by R. F. HILLS, B. R. BUTCHER AND J. A. HEYWOOD (Stoke Poges, Bucks.) 155

Hot hardness testing applied to the ageing and heat treatment of beryllium
by R. THOMSON, B. BEGLEY AND A. J. MARTIN (Renfrew, Scotland and Berks., England) 170

Short Communication
The system thorium–ytterbium: its alloy properties
by D. S. EVANS AND G. V. RAYNOR (Birmingham) 179

All rights reserved

ELSEVIER PUBLISHING COMPANY, AMSTERDAM
Printed in The Netherlands by
NEDERLANDSE BOEKDRUK INRICHTING N.V., 'S-HERTOGENBOSCH

FILED IN STACKS

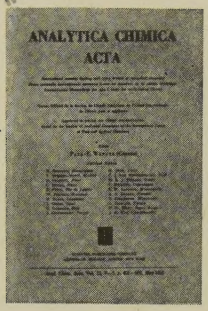

SOME ELSEVIER SCIENTIFIC JOURNALS

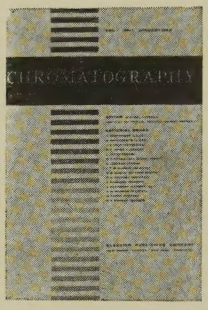

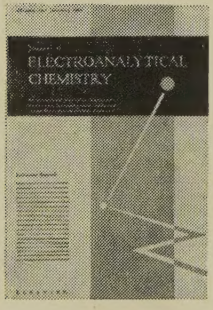

Analytica Chimica Acta

Journal of Chromatography

Journal of Electroanalytical Chemistry

Abstracts Section of the Journal of Electroanalytical Chemistry

ICSU Review

Journal of the Less-Common Metals

Wear - Usure - Verschleiss

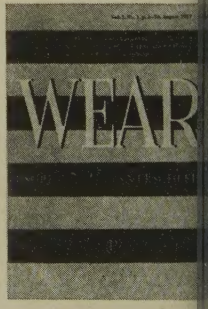

ELSEVIER PUBLISHING COMPANY
AMSTERDAM

221 E